Atomic Layer Deposited Coatings for Corrosion Protection of Metals

Emma Salmi
(née Härkönen)

Laboratory of Inorganic Chemistry
Department of Chemistry
Faculty of Science
University of Helsinki
Finland

ACADEMIC DISSERTATION

To be presented, with the permission of the Faculty of Science of the University of Helsinki, for public examination in Auditorium A110 of the Department of Chemistry, A.I. Virtasen aukio 1, on October 30th, 2015, at 12 o'clock noon.

Helsinki 2015

Supervisor

Professor Mikko Ritala
Laboratory of Inorganic Chemistry
Department of Chemistry
University of Helsinki
Finland

Reviewers

Professor Jari Koskinen
Physical Characteristics of Surfaces and Interfaces
Department of Materials Science and Engineering
Aalto University of Technology
Finland

Associate professor Ola Nilsen
Inorganic Materials Chemistry
Department of Chemistry
University of Oslo
Norway

Opponent

Professor Erkki Levänen
Materials Science
Tampere University of Technology
Finland

ISBN 978-951-51-1561-4 (paperback)
ISBN 978-951-51-1562-1 (PDF)
http://ethesis.helsinki.fi
Helsinki University Printing House
Helsinki 2015

Abstract

Corrosion is a major global challenge with both economical and technological impacts. The total world-wide costs of corrosion have been evaluated to rise to over 2 000 000 million euros annually. While several methods exist for corrosion protection, atomic layer deposited (ALD) coatings have an advantage in applications where thin, fully conformal, highly precise and well-defined coatings both in composition and thickness are needed. In this work the corrosion protection properties of ALD Al_2O_3 and Ta_2O_5 based coatings on low alloy steel were studied. The aim was to increase the general understanding on factors affecting the protective properties and failure mechanisms of the ALD coatings.

The protective performance of ALD coatings on steel was improved by focusing on three topics: substrate pre-treatment, optimisation of the ALD coating architecture, and combination of the optimised ALD coatings with layers deposited by other methods.

The substrate surface was found to significantly influence the ALD coating performance. Improved protective properties were found on steel samples that were mechanically polished to a lower surface roughness, and efficiently cleaned with H_2-Ar plasma in addition to the traditional degreasing with an organic solvent. The smoother surface finish was concluded to be beneficial due to decreased defect formation after the coating deposition upon detachment of loose particles or mechanically fragile sites. The H_2-Ar plasma removed organic residues from the steel surface, therefore improving the quality of the first layers of the ALD coating.

The performance of the ALD coatings themselves was found to improve when Al_2O_3 and Ta_2O_5 were combined to produce Al_2O_3-Ta_2O_5 nanolaminate and $Al_xTa_yO_z$ mixture coatings. In these coatings Al_2O_3 provided sealing properties and Ta_2O_5 the chemical stability, therefore resulting in coatings with better long-term performance than could be achieved with either material alone. Optimisation of the Al_2O_3-Ta_2O_5 nanolaminate and $Al_xTa_yO_z$ mixture coating architectures further enhanced the protective properties.

To further improve the coating-steel interface and to widen the application areas for the ALD based protective coatings, the optimised ALD coating processes were combined with layers deposited with other methods. Firstly, thin filtered cathodic arc sublayers were used to separate the ALD process from the steel surface. This enabled a more precise control of the coating-steel interface and led to improved durability of the ALD coatings. Secondly, pinhole defects in physical vapour and plasma-enhanced chemical vapour deposited hard coatings were sealed with ALD to afford coatings with both good corrosion protection performance and resistance against mechanical wear.

Preface

The research and experimental work included in this dissertation were conducted in the Laboratory of Inorganic Chemistry at the Department of Chemistry of the University of Helsinki.

I would like to thank Professors Markku Leskelä and Mikko Ritala for giving me the opportunity to work in the thin film group of the Laboratory of Inorganic Chemistry. Furthermore, my supervisor Professor Mikko Ritala is additionally thanked for guidance and advice. It has been a privilege to learn about ALD from you.

The reviewers of this thesis, Professor Jari Koskinen and Associate professor Ola Nilsen, are thanked for the timely review process and criticism. The work was greatly improved through your contribution.

The contribution from my co-authors is humbly acknowledged. Thank you Dr Belén Díaz, Dr Jolanta Światowska, Dr Vincent Maurice, Dr Antoine Seyeux, and Professor Philippe Marcus for the electrochemical and failure mode analysis. Thank you Dr Martin Fenker for the NSS testing. Thank you Dr Lajos Tóth and Dr György Radnóczi for the TEM imaging, and Dr Marko Vehkamäki for the TEM and EDS analysis. Thank you Mrs Maarit Mäkelä and Dr Jaakko Niinistö for helping with the plasma pre-treatments. Thank you Mrs Sanna Tervakangas, Mr Jukka Kolehmainen, and Dr Ivan Kolev for the deposition of the PVD and PECVD coatings for the duplex-coating studies. Thank you Dr Marianna Kemell for guidance with FESEM imaging and EDS analysis, and for teaching me to use the Picosun ALD reactor. I could not have completed this work without you. Also all the former and present colleagues at the Laboratory of Inorganic Chemistry are thanked for their help with the practical and scholarly aspects of research, and creating an enjoyable working atmosphere.

The research leading to this thesis received funding from the European Community's Seventh Framework Program (FP/2007–2013) under grant agreement no. CP-FP 213996-1, and was also supported by the Academy of Finland (Finnish Centre of Excellence in Atomic Layer Deposition).

I am deeply grateful to my parents, Aimo and Pirkko, and to my sisters, Eeva, Iida, and Hanna, for always supporting me. My friends are thanked for the numerous pressure-relieving laughs and talks over the years. Finally, I would like to express my special gratitude to my husband Leo, daughter Ella, and dog Tera for their love, patience, understanding, and motivation.

Helsinki, June 2015

Emma Salmi

Contents

List of original publications

The thesis is based on the following publications, which will hereafter be referred to by the roman numerals.

I E. Härkönen, S. Potts, W.W.M. Kessels, B. Díaz, A. Seyeux, J. Światowska, V. Maurice, P. Marcus, G. Radnóczi, L. Tóth, M. Kariniemi, J. Niinistö and M. Ritala
Hydrogen-argon plasma pre-treatment for improving the anti-corrosion properties of thin Al_2O_3 films deposited using atomic layer deposition on steel
Thin Solid Films, 2013, **534**, 384-393

II B. Díaz, E. Härkönen, J. Światowska, V. Maurice, A. Seyeux, P. Marcus and M. Ritala
Low-temperature atomic layer deposition of Al_2O_3 thin coatings for corrosion protection of steel: Surface and electrochemical analysis
Corrosion Science, 2011, **53**, 2168-2175

III B. Díaz, E. Härkönen, V. Maurice, J. Światowska, A. Seyeux, M. Ritala and P. Marcus
Failure mechanism of thin Al_2O_3 coatings grown by atomic layer deposition for corrosion protection of carbon steel
Electrochimica Acta, 2011, **56**, 9609-9618

IV B. Díaz, J. Światowska, V. Maurice, A. Seyeux, E. Härkönen, M. Ritala, S. Tervakangas, J. Kolehmainen and P. Marcus
Tantalum oxide nanocoatings prepared by atomic layer and filtered cathodic arc deposition for corrosion protection of steel: Comparative surface and electrochemical analysis
Electrochimica Acta, 2013, **90**, 232-245

V E. Härkönen, B. Díaz, J. Światowska, V. Maurice, A. Seyeux, M. Vehkamäki, T. Sajavaara, M. Fenker, P. Marcus and M. Ritala
Corrosion protection of steel with oxide nanolaminates grown by atomic layer deposition
Journal of the Electrochemical Society, 2011, **158**, C369-C378

VI E. Härkönen, B. Díaz, J. Światowska, V. Maurice, A. Seyeux, M. Fenker, L. Tóth, G. Radnóczi, P. Marcus and M. Ritala
$Al_xTa_yO_z$ mixture coatings prepared using atomic layer deposition for corrosion protection of steel
Chemical Vapor Deposition, 2013, **19**, 194-203

VII B. Díaz, E. Härkönen, J. Światowska, A. Seyeux, V. Maurice, M. Ritala and P. Marcus
Corrosion properties of steel protected by nanometre-thick oxide coatings
Corrosion Science, 2014, **82**, 208-217

VIII E. Härkönen, S. Tervakangas, J. Kolehmainen, B. Díaz, J. Światowska, V. Maurice, A. Seyeux, P. Marcus, M. Fenker, L. Tóth, G. Radnóczi and M. Ritala
Interface control of atomic layer deposited oxide coatings by filtered cathodic arc deposited sublayers for improved corrosion protection
Materials Chemistry and Physics, 2014, **147**, 895-907

IX E. Härkönen, I. Kolev, B. Díaz, J. Światowska, V. Maurice, A. Seyeux, P. Marcus, M. Fenker, L. Tóth, G. Radnóczi, M. Vehkamäki and M. Ritala
Sealing of hard CrN and DLC coatings with atomic layer deposition
ACS Applied Materials & Interfaces, 2014, **6**, 1893-1901

The author has actively participated in planning the research, written papers I, V, VI, VIII and IX and participated in writing papers II, III, IV and VII. The author has prepared all the ALD coatings in papers II-IX and half of the coatings in I. Out of the coating characterisation the UV-Vis, XRR and FESEM imaging were made by the author.

Abbreviations and acronyms

ALD	atomic layer deposition
cf.	confer
CIGS	copper indium gallium selenide
CVD	chemical vapour deposition
DLC	diamond like carbon
DSSC	dye-sensitised solar cell
EDS	energy dispersive X-ray spectrometry
e.g.	exempli gratia
EIS	electrochemical impedance spectroscopy
FCAD	filtered cathodic arc deposition
FESEM	field emission scanning electron microscope
FIB	focused ion beam
i.e.	id est
LSV	linear sweep voltammetry
MCFC	molten carbonate fuel cell
NSS	neutral salt spray
OCP	open circuit potential
OLED	organic light-emitting diode
OPV	organic photovoltaics
OTFT	organic thin film transistor
O_2TR	oxygen transmission rate
PEALD	plasma-enhanced atomic layer deposition
PECVD	plasma-enhanced chemical vapour deposition
PEC	photoelectrochemical cell
PEN	polyethylene naphthalate
PET	polyethylene terephthalate
PLA	polylactic acid
PP	polypropylene
PVD	physical vapour deposition
SERS	surface-enhanced Raman scattering
TEM	transmission electron microscope
TFEL	thin film electroluminescent
ToF-ERDA	time-of-flight elastic recoil detection analysis
ToF-SIMS	time-of-flight secondary ion mass spectrometry
UBM	unbalanced magnetron
UV-Vis	ultraviolet-visible
vs.	versus
WVTR	water vapour transmission rate
XRR	X-ray reflection

1 Introduction

Corrosion can be classified as the degradation of a material and its properties in a chemical or electrochemical reaction with the surrounding environment.[1] Corrosion drives materials towards their lowest energy composition. In the most traditional sense, corrosion corresponds to the electrochemical oxidation of metals in reactions with the surrounding liquid or atmosphere, but also environmental degradation of for instance polymers, ceramics, plastics and concrete are considered corrosion. Today, the total costs of corrosion world-wide have been estimated to be 3–4 % of the gross domestic product.[2] Thus in 2014 the costs amounted to ~600 000 million euros in the European Union, and ~9 000 million euros in Finland.[3]

Complete prevention of corrosion is difficult and can only be accomplished in a limited number of cases.[1] Therefore, the aim of corrosion prevention is usually to decrease the corrosion rate to a tolerable level that allows for maintaining the operative properties of a material. Several methods exist for preventing or slowing down corrosion. The system should be planned in a way that the risk of local corrosion is minimised. The decision on the material to be used should be made on the basis that it has sufficient durability in the service conditions. If a corroding material is used, it must be protected. The protection can be accomplished by controlling the electrochemical potential of the material, introducing inhibitors into the corrosive environment, or modifying the material surface by alloying or coating with a more durable material.

The variety of different coating methods includes processes from simple techniques like painting and varnishing to highly sophisticated vacuum techniques like physical (PVD) and chemical vapour deposition (CVD).[4] The aim is to separate the vulnerable material from the environment as completely as possible. This work is focused on corrosion protection with a CVD-based technique, atomic layer deposition (ALD). In ALD the coatings are grown in a surface-reaction limited manner sub-monolayer of atoms at a time.[5,6] The technique is known for enabling growth of films with low defect densities, high conformality and high controllability even on demanding three-dimensional features. This opens up new possibilities for applications in which extreme precision (conformality, thickness, composition) is needed.

The objective of this work was to create basic understanding on the possibilities of ALD in growing corrosion protection coatings. Firstly, the effect of the substrate pre-treatment to the protective properties of the ALD coatings was studied. The focus was on mechanical conditioning and cleaning with H_2-Ar plasma. Secondly, the ALD coatings themselves were optimised in both composition and structure. Coatings combining a material with good nucleation and insulation properties, like Al_2O_3, with a material with good chemical stability, like Ta_2O_5, were targeted. Also the optimum architecture of these coatings was considered. Thirdly, the combination of ALD with other coating techniques was studied to further control the coating-substrate interface and to widen the spectrum of possible applications for the ALD-based protection. In Chapter 2, the existing literature on

ALD corrosion protection coatings on metals is reviewed. Specific attention is given to the differences between ALD materials and influence of coating parameters. In addition, some applications for which ALD coatings have already been considered are presented. The main emphasis was in corrosion protection of metals, metal alloys and metallic constituents in material stacks. In Chapter 3, the conducted experimental work is overviewed. The results are presented and discussed in Chapter 4, and the work is concluded in Chapter 5.

2 Background

2.1 Atomic layer deposition

ALD is a CVD based method for growing thin films with high precision. Numerous excellent reviews have been written on ALD generally,[5-11] and on the potential of ALD in specific applications including thin film electroluminescent (TFEL) displays,[12] microelectronics,[13] energy applications (photovoltaics, fuel cells, batteries),[14-18] and corrosion protection.[19]

ALD film growth occurs through self-limiting and saturating chemical reactions of two or more gaseous precursors on a substrate surface.[5,6] The precursors are introduced on the substrate alternately and separated by inert gas purging. Thus all contact between the precursors is restricted to the surface. A simplified schematic of one ALD cycle is given in Figure 1. The growth mechanism enables deposition of thin films with thickness and composition controlled down to the atomic level.[5] The films follow even challenging surface morphologies conformally.[20]

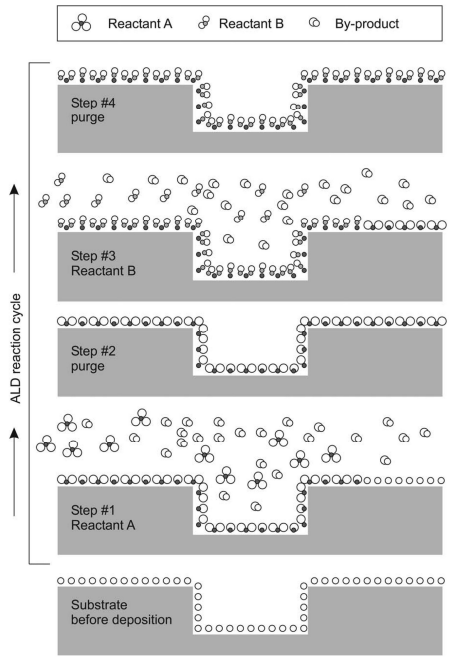

Figure 1 *Schematic presentation of one ALD cycle. Reprinted with permissions from [9]. Copyright [2005] AIP Publishing LLC.*

A variety of materials have been deposited with ALD. The most common ones include oxides, nitrides, sulphides, and metals.[8] Recently also organic materials and inorganic-organic hybrids have been grown with a related technology called molecular layer deposition.[7] In thermal ALD, the activation of the chemical reactions is achieved with

heat.[5,6] However, additional energy can be introduced through activation of the precursors as in plasma-enhanced ALD (PEALD), radical-enhanced ALD and photo-induced ALD.[10,21]

Both the main benefits and challenges of ALD in growing corrosion protection coatings can be derived from the unique growth mechanism. Conformal and precise layers can be grown in regards of structure and composition.[5,6,20] Therefore, the coatings can be tailored for the needs of a specific application. Compared to many methods like painting, sol-gel, PVD, and CVD the conformality of ALD ensures that surfaces with complex shapes can be equally encapsulated, and therefore burial of surface features under thick layers is not necessary. Also post-deposition treatments like annealing, which are needed for instance with sol-gel coatings, are rarely needed for ALD corrosion protection coatings. Furthermore, the defect density of ALD films is known to be very low,[22,23] enabling complete sealing of surfaces with very thin layers. Therefore, the dimensions and morphology of the original surface can be maintained.

The main challenge of ALD is the low growth rate leading to economical infeasibility of thick coatings.[6] Although chemical protection from the environment can be achieved already with thin coatings, protection against mechanical wear might be limited. Furthermore, as the growth occurs through chemical reactions on the substrate surface, the properties of ALD films are affected by the substrate.[22-25] Most applications utilizing ALD films are on highly defined substrates like silicon or previously deposited layers.[6,13-18] In these systems the composition of the substrate surface is known and can be modified to ensure better ALD growth, if deemed necessary. In corrosion protection, heterogeneous surfaces with unknown and varying composition are common. In addition, the surfaces of bulk metals and metal alloys can be rough and contain particles that may upon detachment form defected sites that expose the protected material. Often the substrates have been machined at workshops, and may be protected with oils to prevent corrosion during handling and/or storing. These issues can lead to unideal ALD nucleation, poor adhesion and insufficient protection with ultra-thin layers.

2.2 Corrosion protection with atomic layer deposited coatings

In this chapter the properties ALD films as corrosion protection coatings are reviewed. Main emphasis is given to the protection of metals and metallic constituents in multimaterial structures. However, some general references are also made to the most studied applications utilizing protective ALD coatings on non-metallic surfaces. In the first section the most common ALD materials in protective applications are presented with some process and general material related details. The second section is focused on protection of surfaces against gaseous corrosives. The permeation barrier properties of ALD films for common corrosive gases in the atmosphere are mainly recounted, but improvement of durability at elevated temperatures is also considered. In the third section protection against liquid corrosives is reviewed. The sealing properties and chemical

durability of the ALD coatings are especially focused on. The final section gives a short review on preventing out-diffusion of metals from the substrate into active device layers and inter-diffusion of metals from one active layer to another causing performance degradation.

2.2.1 Materials

2.2.1.1 Oxides

By far the most frequently used ALD corrosion protection coating is Al_2O_3 and it is almost always deposited from trimethyl aluminium ($Al(CH_3)_3$) and water.[19,26-30] The main reason for this is that the process is almost ideal,[9] can be successfully used in a wide temperature range of 33–500 °C,[9,31,32] the films are amorphous as deposited and do not crystallise below 800 °C,[8,33] and the precursors are relatively cheap. The films are quite pure, and the purity is improved with increasing deposition temperature.[9,31,32] For instance, the hydrogen impurity content decreases from 21.7 at.% at 33 °C to 1.0 at.% at 250 °C.[31,32] Low carbon impurity contents have been reported at all deposition temperatures (<0.2 at.% at 250 °C). The decrease of the impurity content with deposition temperature is attributed to more complete surface reactions afforded by the increased energy budget.[5] Although ALD Al_2O_3 growth on a variety of different substrates has been shown, the substrate has also been shown to have an influence on the film properties.[22-25] Problems in the growth are often suggested to relate to the shortage of appropriate reactive groups (–OH) on the substrate surface. In the case of Pt, Cu, and stainless steel foils also the substrate roughness has been claimed to impede proper nucleation.[24] Some recent work has shown that the hardness, Young´s modulus and residual stress of ALD Al_2O_3 are dependent on the deposition temperature.[34] The film thickness did not appear to have a significant influence on the mechanical properties. Bulk Al_2O_3 is stable in neutral solutions, but is dissolved in acidic and basic solutions.[35] However, some susceptibility of ALD Al_2O_3 thin films even to deionised water has been reported.[36]

Some studies use ALD Al_2O_3 grown from $Al(CH_3)_3$ and O_3 or PEALD Al_2O_3 grown from $Al(CH_3)_3$ and O_2 plasma as protective coatings.[37,38] The main differences of those processes from the $Al(CH_3)_3$-H_2O process are that better quality films can be deposited at low deposition temperatures,[10] and better nucleation and adhesion to challenging surfaces with unideal chemical species for nucleation can be achieved.[37,39] These differences arise from the higher reactivity of O_3 and O_2 plasma compared to H_2O.[10] However, possible damage to the substrate during the coating process should also be considered for each application. Furthermore, Al_2O_3 films deposited using O_3 or especially O_2 plasma may not have the same level of conformality on complex surface morphologies that can be achieved with the H_2O-based process.[40]

Another frequently used ALD material for corrosion protection coatings is TiO_2.[19,26,41,42] For protective applications TiO_2 is commonly deposited from titanium tetrachloride ($TiCl_4$) or titanium isopropoxide ($Ti[OCH(CH_3)_2]_4$) with H_2O.[19,26,42,43] Sometimes more reactive oxygen sources (e.g. H_2O_2 or O_3) are used.[41,44] The main characteristics of these processes are well documented and especially the $TiCl_4$-H_2O process can also be used in a wide temperature range.[8,45,46] Different from Al_2O_3, ALD TiO_2 films can be polycrystalline as deposited.[8] Besides the deposition temperature, the crystallisation is dependent on the precursors, substrate and film thickness. Generally, anatase formation can be observed around 125–680 °C from $TiCl_4$-H_2O and 150–350 °C from $Ti[OCH(CH_3)_2)_4]$-H_2O.[8,45,46] Rutile formation can start at ≥275 °C depending on the process. Similar to Al_2O_3, the film purity can be improved by increasing the deposition temperature. For instance, TiO_2 deposited with the $TiCl_4$-H_2O process contained 0.3 at.% hydrogen when deposited at 150 °C and 0.1 at.% at 500 °C.[46] The chloride content decreased from 2 at.% at 150 °C to below the detection limit of Rutherford backscattering spectrometry at 500 °C. Bulk TiO_2 is chemically more stable than Al_2O_3,[35] and is thus expected to withstand aggressive solutions better also in the thin film form. Polycrystalline ALD TiO_2 on silicon has been observed to resist etching in H_2SO_4 solutions better than a corresponding amorphous TiO_2 film.[47] However, the grain boundaries in polycrystalline films may act as preferential routes for corrosives to the protected surface.[48]

Other ALD oxides used for corrosion protection include Ta_2O_5,[26] SiO_2,[30,49] ZrO_2,[50,51] ZnO,[52,53] and HfO_2.[51] A variety of ALD processes exist for these materials,[8] but in corrosion protection the most commonly used precursors are H_2O with tantalum pentaethoxide ($Ta[OCH_2CH_3]_5$) for Ta_2O_5,[26] tetrakis(dimethylamino)zirconium ($Zr[N(CH_3)_2]_4$) or tetrakis(ethylmethylamino)zirconium ($Zr[N(CH_3)(C_2H_5)]_4$) for ZrO_2,[50,51] diethyl zinc ($Zn(C_2H_5)_3$) for ZnO,[52,53] and tetrakis(dimethylamino)hafnium ($Hf[N(CH_3)_2]_4$) for HfO_2.[51] SiO_2 is usually deposited with the rapid ALD process from tris(tert-butoxy)silanol ($[(CH_3)_3CO]_3SiOH$) or tris(tert-pentoxy)silanol ($[CH_3CH_2C(CH_3)_2O]_3SiOH$) with $Al(CH_3)_3$ as the catalyst.[30,49] General properties of all the processes are well documented in the literature.[8] The Ta_2O_5 and SiO_2 films are amorphous as deposited, but polycrystalline films of ZrO_2, ZnO, and HfO_2 can be grown from the above-mentioned precursors in appropriate conditions. The chemical durabilities of Ta_2O_5, SiO_2, ZrO_2 and HfO_2 are known to be better than those of Al_2O_3.[35,47]

2.2.1.2 Nitrides

ALD and PEALD nitrides are used mainly as diffusion barriers rather than corrosion protection coatings.[54-57] A number of materials and ALD processes have been studied,[8] but within this work only some general trends are presented. The two most commonly studied diffusion barrier nitrides are TiN and TaN, others including WN, NbN, MoN and VN. The most widely used precursors are halides like $TiCl_4$ and $TaCl_5$ with NH_3 in ALD and with N_2, H_2 or NH_3 plasmas in PEALD.[54-57] For TiN the processes are relatively straightforward,[46,56-58] but for TaN the reduction of Ta(V) to Ta(III), as required for the

formation of the desired phase, is challenging.[59] For instance, the ALD halide processes with NH_3 usually result in Ta_3N_5, which has a high resistivity. TaN can be formed when an additional reducing agent like Zn or $Al(CH_3)_3$ is used,[58,59] or with a more reducing nitrogen precursor instead of NH_3.[60] However, the additional or more complex precursors may also result in incorporation of additional impurities in the films. Commonly studied metalorganic precursors in diffusion barrier studies are alkylamides like tetrakis(dimethylamino)titanium ($Ti[N(CH_3)_2]_4$), and tetrakis(ethylmethylamino)titanium ($Ti[N(CH_3)(C_2H_5)]_4$).[56,61] The main benefits compared to the halide processes are the less aggressive by-products, which do not degrade the substrate or the growing film, and avoidance of halide impurities from the films.[62] However, the thermal stability of the amide precursors is poor.[63]

Similar to the ALD oxides, impurity contents in the nitride films are decreased with increasing deposition temperatures. For instance, Ta(Al)N(C) deposited with the $TaCl_5$-$Al(CH_3)_3$-NH_3 process contain 14 at.% chloride at 250 °C and 4 at.% at 400 °C.[54] The hydrogen impurity content is similarly reduced from 14 to 7 at.%. The nitride films are usually crystalline as deposited.[8] However, with the metalorganic precursors like $Ti[N(CH_3)_2]_4$ amorphous films can be grown at low temperatures. The resistivities of the ALD nitrides are dependent on the impurity contents and crystallinity of the films.[54,57,58,64,65] The Cl impurities in particular have been shown to increase the resistivities.[54,58] Low resistivities (~200 μΩcm) have been reported for TiN.[56-58,61] Also for TaN low resistivities (<500 μΩcm) can be achieved,[55,62] but only if the correct phase is obtained and the films are pure enough. The Ta_3N_5 phase is semiconducting,[59] and TaN films with high impurity contents have resistivities of >1000 μΩcm.[54,66] Resistivities ranging from a few hundred to over thousand μΩcm have been reported for the other ALD nitrides.[65,67-69]

2.2.2 Protection against gaseous corrosives

ALD thin films have been shown to provide protection against the most common corrosives in the atmosphere. The main focus has been in inhibiting exposure of functional materials to O_2 and moisture. ALD gas permeation barriers have been widely considered on polymers for food packaging[44] and organic devices like light-emitting diodes (OLED),[29,30,38,42,50,70-73] thin film transistors (OTFT),[74] and photovoltaics (OPV).[15,16] Permeation barriers are also needed in fully inorganic structures like $Cu(In,Ga)Se_2$ (copper indium gallium selenide, CIGS) solar cells,[15,16] zinc-tin-oxide based thin film transistors,[75] and TFEL displays.[5,12] The most actively studied application areas for protecting metals from gaseous corrosives with ALD are nanoparticles in general,[28,41,76-78] and silver and copper nanostructures used for plasmon-enhanced analysis techniques.[27,79-87] Single papers have also been published on a variety of other applications.[52,88-95] In addition to increased ambient durability, also improvement of the oxidation resistance during annealing has been shown.[76-78,88,90,92,94-96] Silver tarnishing due to sulphur containing compounds has

been slowed down in applications where the visual appearance is of great importance. Some examples include jewels and historical artefacts.[97-100]

2.2.2.1 Applications

Studies on protective ALD coatings on metals and metal nanostructures against gaseous corrosives are very varied and scattered in regards of applications. They include for instance protection of copper rollers used as molds in hot emboss patterning of polymeric components,[88] molybdenum walls in a microreactor,[90] plasmonic silver and copper nanostructures on substrates for analysis devices like biosensors, surface-enhanced Raman scattering (SERS) and femtosecond laser excitation,[27,79-87] and copper nanowires aimed as transparent electrodes.[52] In addition, prevention of spontaneous combustion of metallic nanoparticles,[28,76,77] and preparation of functionalised nanoparticles with ambient durability[41,78] have been studied. The most studied protective material is Al_2O_3,[28,41,76,77,79,81-93,95] but also TiO_2, SiO_2 and HfO_2 single layers, Al_2O_3-ZnS and AlN-TiO_2 nanolaminates and Al_2O_3 doped ZnO have been considered.[41,52,77,78,80,94-96] Because the applications are so varied, drawing general requirements for the coatings or restrictions for the deposition conditions is challenging. However, usually the properties of the underlying metals should be preserved during the ALD process, and in some applications, like when protecting plasmonic nanoparticles, the ALD coating should be thin enough to maintain the intended functionality of the underlying metal.

For silver jewels and historical artefacts the protective ALD coatings are already in use.[97-100] In research, the aim has been to afford the maximum protection with a minimum effect on the visual appearance. Also the other properties of the substrates should be carefully maintained, and the coatings on historical artefacts should preferably be easily removable. Thus, so far the only studied ALD coating materials have been Al_2O_3 and Al_2O_3-TiO_2 nanolaminate. The thicknesses of the coatings have been tailored to maintain the original visual appearance.

Encapsulation of polymers used for food packaging and organic and inorganic devices is widely studied with ALD permeation barriers.[15,16,29,30,38,42,44,50,70-75,101-109] The performance of the layers is commonly evaluated by water vapour transmission (WVTR) and oxygen transmission (O_2TR) rates. WVTRs and O_2TRs in the order of 0.01–100 g/(m^2 day) and 0.01–100 cm^3/(m^2 day) are required for sensitive food products.[44] However, the requirements for organic and inorganic electronic devices are more stringent. The suggested limits for WVTR and O_2TR are in the order of 10^{-6} g/(m^2 day) and 10^{-5}–10^{-3} cm^3/(m^2 day) for stable long-term performance.[50,105,110] In addition, process restrictions like temperature and precursors must be considered, as the functionality of the previously deposited layers should not be compromised.[38,109] The most actively studied ALD permeation barrier materials are Al_2O_3, TiO_2, SiO_2 and ZrO_2.[29,30,38,42,44,50,70-74,105,106,108]

2.2.2.2 Influence of deposition parameters

Systematic research on the influence of deposition parameters on the permeation resistance of ALD coatings is quite limited on plain metallic substrates. Thus some general guidelines are borrowed from the numerous permeation barrier studies on polymers and device structures for OLEDs, OTFTs and OPVs. However, as the substrate has an influence on the ALD thin film properties,[24,25] straightforward analogy of the results cannot be assumed.

In addition to the intrinsic properties of the ALD materials, the deposition temperature,[38,44,70] coating thickness[38,44,70-73] and reactivity of the oxygen precursor[38,44,50,73] have been shown to be critical for the permeation barrier properties on polymers. The steady-state permeation of water and oxygen through good barrier oxides has been suggested to occur through pinholes,[30,70,72,111,112] or along –OH groups existing due to hydrogen impurities.[31,70] The impurity content of ALD films significantly decreases with increasing deposition temperature.[5] The increasing deposition temperature is thus assumed to have a positive effect on the permeation barrier properties. For instance, the barrier properties of Al_2O_3 on polyethylene terephtalate significantly increased with increasing deposition temperature from 50 to 100 °C.[70] However, on heat sensitive substrates, like polymers, the upper temperature limit is usually set by the durability and stability of the substrate. Furthermore, if the deposition temperature is too high, film cracking can occur upon cooling after the deposition due to differences in the thermal expansion coefficients of the substrate and the film.[35] Most permeation barrier studies have been done at deposition temperatures of ≤150 °C.

With bulk metal substrates higher deposition temperatures can be used than with polymers. The responses of the ALD oxide coatings and the substrate to heating are closer to each other, and generally metals themselves are not as sensitive to heat as polymers.[35] On Cu plates an increase of the Al_2O_3 deposition temperature from 100 to 200 °C has been shown to improve the oxidation resistance and adhesion of the coatings.[88] However, nanostructured and highly oxidizing metals might induce similar temperature restrictions as polymers due to sintering or oxidation during the first ALD cycles. For instance, on Fe, Co and Ag nanoparticles and -columns ALD oxide coatings have been deposited at 50–180 °C to restrict morphological and compositional changes during the depositions.[76,78,86,87,93] Additionally, at high deposition temperatures the possible crystallisation of the protective ALD film must be considered. Upon crystallisation grain boundaries, which offer an easier passage for corrosives to the protected surface, are introduced into the coating.[48]

The impurity contents of ALD coatings deposited at low temperatures can be decreased by using reactive oxygen precursors. Replacing H_2O with O_3, H_2O_2 or O_2 plasma has been shown to be beneficial for Al_2O_3, TiO_2 and ZrO_2 coatings on polymers and metals.[38,41,44,50,73,78] However, when choosing the ALD process, care should be taken also to ensure that the precursors themselves do not change properties of the substrate. For

instance, O_2 plasma has been observed to degrade the functional layers of an OLED structure,[109] and H_2O_2 to oxidise the surface of Fe nanoparticles.[78]

Increasing the coating thickness significantly improves the protective properties of ALD films against gaseous corrosives. On polymers a critical thickness has been reported for several materials including Al_2O_3, TiO_2, ZrO_2 and SiO_2.[30,38,42,44,50,70,71,73] Below the critical thickness the permeation barrier properties are highly thickness dependent (Figure 2). This has been attributed to a completion of a continuous ALD coating and exponential decrease of defects with increasing thickness.[70,72] Some further decrease of O_2 and moisture permeation with increasing thickness above the critical thickness can be achieved, but the dependence on the ALD barrier thickness is less drastic. Klumbies et al.[72] have shown that with Al_2O_3 on evaporated copper the number of defects exponentially decreases with thickness at least until 100 nm. However, the permeation barrier properties of the same Al_2O_3 on C_{60}-covered Ca test and OLED structures improved exponentially with thickness only until 25 nm. The decreasing dependence between the permeation barrier properties and thickness was suggested to correlate with defects remaining at these thicknesses being harder to close or forming after the deposition. On the other hand, the fracture toughness and critical strain for crack propagation of ALD Al_2O_3 have been shown to increase with decreasing coating thickness.[106] Therefore, the differences in the thermal expansion coefficient and elasticity of the coating and polymer substrate can result in decreasing protective properties if the thickness is too large (>100 nm).[44,72]

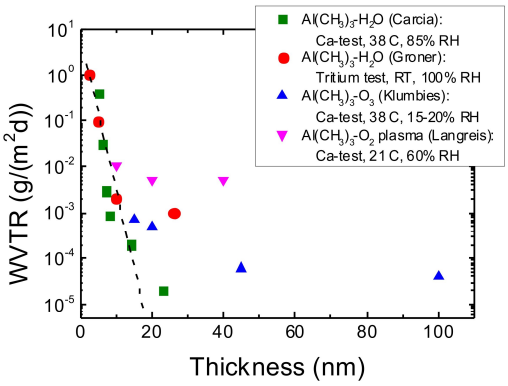

Figure 2 *The influence of ALD Al_2O_3 film thickness on WVTR on polymers. The dashed line represents the approximate decrease of WVTR with thickness below the critical thickness. The data is collected from papers by Carcia et al.[70], Groner et al.[71], Klumbies et al.[72] and Langereis et al.[73]*

Also on metals clear improvements of protective properties with increasing thickness have been reported both at ambient and high temperature exposures.[28,76,77,83,85-88,90,92] For instance, on Fe particles the oxidation resistance during annealing in air has been shown to improve with increasing coating thickness.[77] The failure temperature was increased from 327 to 527 °C by increasing the Al_2O_3 thickness from 2 to 11 nm. On metallic substrates no upper limit is usually observed for the thickness. However, few studies report

protective coatings thicker than 100 nm.[90] On the other hand, ultra-thin coatings are needed in some applications to minimise the influence of the protective layers on the functionality of the protected material.[27,79-81,83-87] For instance, the intensity of the electromagnetic waves from a Ag nanoparticle surface plasmon show an exponential decay with increasing distance from the silver surface.[87] Thus ≤1 nm thick protective layers are preferred in the ALD protected SERS substrates, and ultra-thin Al_2O_3 coatings were shown to afford ambient durability up to 9 months.

2.2.2.3 Comparison of coating materials

The most actively studied protective ALD material against gaseous corrosives on polymers is Al_2O_3.[29,30,38,42,44,70-74] Also TiO_2, ZrO_2 and SiO_2 have gained attention.[30,42,44,50] The WVTR and critical thickness of Al_2O_3 have been found to be lower than the corresponding values for the other oxides (Table 1).[30,38,42,44,50,70-73] Possible reasons are the ideal nature of the ALD Al_2O_3 process ($Al(CH_3)_3$-H_2O)[9] and the better nucleation of Al_2O_3 on polymers.[25] The best reported WVTR values for ALD Al_2O_3 are generally in the order of 10^{-3}–10^{-6} g/(m^2 day) for 20–100 nm thick coatings.[29,38,70-73] The high variability is probably due to differences in the reactive groups of the polymer substrates, ALD processes, and sensitivity of the testing methods. WVTRs in the order of ~10^{-4} g/(m^2 day) have been reported for TiO_2 and ZrO_2 with coating thickness between 50–80 nm.[42,50] The reported permeation barrier properties of SiO_2 coatings are poor.[30] The WVTR of a 60 nm coating was 1×10^{-1} g/(m^2 day).

Table 1. *WVTRs of selected ALD thin films.*

Substrate	**ALD coating** (material (oxygen precursor) / deposition temperature / thickness)	**Testing** (method / temperature / air moisture)	**WVTR** (g/(m^2 day)	**Ref**
PEN	Al_2O_3 (H_2O) / 120 °C / 25 nm	Ca test / 38 °C / 85 %RH	1.7×10^{-5}	29
PET	Al_2O_3 (H_2O) / 100 °C / 10 nm	Ca test / 38 °C / 85 %RH	$<5\times10^{-5}$	70
Glass, Ca and Al electrodes	Al_2O_3 (H_2O) / 80 °C / 60 nm Al_2O_3 (O_3) / 80 °C / 60 nm	Ca test / 20 °C / 60 %RH	4.9×10^{-4} 8.7×10^{-6}	38
PP coated paper PLA coated paper	Al_2O_3 (O_3) / 122 °C / 65 nm Al_2O_3 (O_3) / 108 °C / 65 nm	SCAN P22:68 / 23 °C / 50 %RH	0.3 4.1	44
PEN	Al_2O_3 (O_2 plasma) / 25 °C / 20 nm	Ca test / 21 °C / 60 %RH	5×10^{-3}	73
PET	Al_2O_3 (H_2O)[a] / 50 °C / 15–40 nm	MOCON / 38 °C / 100 %RH	$\sim6\times10^{-3}$	101
Kapton®	Al_2O_3 (H_2O) / 175 °C / 26 nm SiO_2/175 °C / 60 nm Al_2O_3-SiO_2 / 175 °C / 172 nm	Tritium test / 25 °C / 100 %RH	$\sim1\times10^{-3}$ $\sim1\times10^{-1}$ 4.2×10^{-5}	30
PET	TiO_2 / 150 °C / 60 nm	Ca test / 60 °C / 85 %RH	6×10^{-4}	42
Glass, Ca and Al electrode	ZrO_2 / 80 °C / 80 nm	Ca test / 20 °C / 60 %RH	6×10^{-4}	50
PEN	Hf:ZnO /150 °C / ~180 nm	Ca test / 85 °C / 85 %RH	6.3×10^{-6}	103
Glass, Ca and Ag electrodes	Al_2O_3-ZrO_2 / 80 °C / 130 nm	Ca test / 70 °C / 70 %RH	4.7×10^{-5}	105
Kapton®	Al_2O_3-alucone / 135 °C / 25 nm	MOCON / 38 °C / 85 %RH	$<1\times10^{-4}$	104
PET	TiO_2-OTS / 150 °C / 97 nm	Ca test / 60 °C / 85 %RH	7.0×10^{-4}	107

[a]The permeation barrier was grown with spatial ALD.

The greatest challenge in regards of using ALD Al_2O_3 coatings for protection against gaseous corrosives is its chemical stability. Even though it is known to be chemically unstable in acidic and basic conditions,[35] no corrosion was expected in water vapour. However, Dameron et al.[30] showed that the permeation barrier properties of a 26 nm ALD Al_2O_3 grown from $Al(CH_3)_3$ and H_2O on Kapton at 175 °C started degrading after 130 h when the coating was in direct contact with water vapour. When the same Al_2O_3 coating was tested so that the water exposure was on the polymer side and thus the water dose experienced by the Al_2O_3 coating was decreased, stable WVTRs for over 400 h were measured. This indicated that ALD Al_2O_3 is corroded by water vapour and thus cannot be used for long-term encapsulation as a single layer. Although higher WVTRs have been reported for TiO_2, SiO_2 and ZrO_2 than Al_2O_3, degradation of these oxides due to water vapour has not been observed,[30,42,50] and is not expected.

A number of papers report protection of metals with ALD Al_2O_3 coatings during storage in ambient and exposure to high temperatures.[28,41,76,77,79,81-93,95] All these protective Al_2O_3 layers have been deposited with the $Al(CH_3)_3$-H_2O process,[28,41,76,77,79,81,83-89,91-93,95] or the process has not been specified.[82,90] Improved ambient durability has been shown for cobalt nanopillars,[93] nickel-chromium-copper-aluminium-germanium alloy resistors,[89] silver nanoparticles,[87] gold and silver pyramids,[82] and chromium-gold electrodes.[91] Increased high temperature durability has been reported for iron nanoparticles,[28,76,77] copper,[88] niobium,[92] molybdenum,[90,95] and silver nanoparticles.[79,86] Results on high temperature durability of ALD Al_2O_3 coated metals are presented in Table 2. Drawing conclusions from the reported values is challenging. In addition to the different deposition temperatures and properties of the substrates themselves (intrinsic material properties, size of structures), also the testing methods vary. Furthermore, in most cases only the operative performance after storing or annealing is reported, and thus oxidation might have occurred without being noticed if the effect on the operative performance was not significant. However, it would appear that on average the failure temperature of the metals could be increased by some hundreds of degrees with the ALD Al_2O_3 coatings.

Table 2. *Results on oxidation resistance of metals coated with ALD Al_2O_3 coatings.*

Substrate	**ALD coating** (material / deposition temperature / thickness)	**Atmosphere**	**Failure temperature (°C)**		**Ref**
			Uncoated	**Coated**	
Fe particles	Al_2O_3 / 227 °C / 2 nm Al_2O_3 / 227 °C / 11 nm	21 % O_2	276	367 527	77
Fe particles	Al_2O_3 / 180 °C / ~5 nm Al_2O_3 / 180 °C / 8 nm	21 % O_2	RT	> 427	76
Cu	Al_2O_3 / 200 °C / 20 nm Al_2O_3 / 200 °C / 100 nm	21 % O_2	< 200	> 200	88
Cu particles	Al_2O_3 / NA °C / ~5 nm	21 % O_2	RT	~ 300	84
Nb	Al_2O_3 / 150 °C / 1.5 nm Al_2O_3 / 150 °C / 2.5 nm	21 % O_2	< 200	< 200 > 200	92
Mo	Al_2O_3 / NA °C / 200 nm Al_2O_3 / NA °C / 300 nm	21 % O_2 + H_2O	NA	600 550	90
Mo	Al_2O_3 / NA °C / 170 nm	21 % O_2 + H_2O	> 350	> 550	95
Ag particles	Al_2O_3 / 50 °C / 1 nm	10 Torr propane	NA	200	86
Ag wires	Al_2O_3 / 67 °C / 1 nm	21 % O_2	NA	~ 400	79

The failure modes of protective ALD coatings on metals are rarely reported. However, in a molybdenum based microreactor the Al_2O_3 layers were remarked to detach from the substrate at the failure temperature.[90] No further analysis was done and no suggestions were made on the cause. On iron particles a distinctive failure temperature was reported for each ALD Al_2O_3 layer thickness.[28,76,77] Above this temperature the Al_2O_3 coating was

observed to crack (Figure 3), which was attributed to a difference between the thermal expansion coefficients of iron and Al_2O_3.

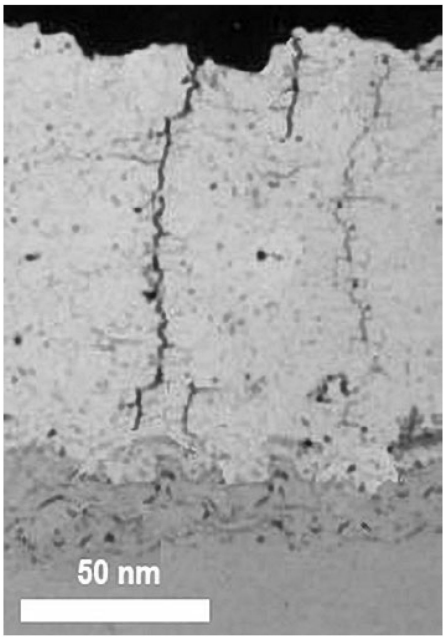

Figure 3 *Cracking of an ALD Al_2O_3 film on a Fe particle after annealing in air. Reprinted with permissions from [77]. Copyright John Wiley and Sons.*

Comparison of the protective properties of ALD Al_2O_3 to other ALD materials on metals is challenging because the number of published papers is limited. TiO_2 coatings have been grown on iron and nickel nanoparticles.[41,78] On iron the depositions were done from $TiCl_4$ or $Ti[OCH(CH_3)_2]_4$ and H_2O_2 at 100 °C.[41,78] The aim was to prepare functionalised magnetic nanoparticles. However, H_2O_2 was so reactive that Fe_3O_4 formation was observed during the ALD film growth. Some improvement could be achieved by a 5 nm thick AlN interface layer deposited by ALD from TMA and NH_3 at 250 °C.[78] Unfortunately, as the main purpose of the TiO_2 coating was to induce photoactivity, the improved stability afforded by the ALD coatings was only suggested and not monitored during exposure to ambient or high temperatures. On nickel the TiO_2 coatings were grown from $Ti[OCH(CH_3)_2]_4$ with H_2O_2 at 100 °C.[41] Different from iron, no NiO was found at the interface after the deposition. During annealing to 700 °C in air the nickel particles reacted with the TiO_2 coating forming nickel titanate and NiO. No testing was done at lower temperatures, and thus the on-set temperature for the reaction is unknown.

Protection of nickel with ALD HfO_2 at high temperatures has been studied. The coatings were grown from $Hf[N(CH_3)_2]_4$ and H_2O at 200 °C.[94] A 30 nm HfO_2 coating completely prevented oxidation during subsequent $Pb(Zr,Ti)O_3$ film deposition by sol-gel, which required repeated thermal cycling from room temperature to 700 °C in air.

ALD SiO_2 coatings were used to protect silver nanohole arrays for surface plasmon resonance biosensing.[80] Coatings of 15 nm thickness deposited from $[(CH_3)_3CO]_3SiOH$ with $Al(CH_3)_3$ catalyst at 100 °C prevented silver oxidation during a 5 min exposure to O_2 plasma under ultraviolet light.

2.2.2.4 Multilayer and mixture coatings

Enhanced permeation barrier properties on polymers have been reported for ALD layers combining two or more materials.[30,102,105,108] Usually Al_2O_3 as an excellent permeation barrier is combined with another chemically more durable material. Examples include Al_2O_3-SiO_2,[30] Al_2O_3-TiO_2,[108], Al_2O_3-HfO_2,[102] and Al_2O_3-ZrO_2 nanolaminates.[105] WVTR and O_2TRs in the order of 10^{-4}–10^{-5} g/(m^2 day) and 10^{-2} cm^3/(m^2 day) have been reported,[30,102,105,108] and the performance can be maintained for extensive time periods up to 10 000 h.[102] In addition to combining good barrier properties with chemical durability, another suggested reason for the improved behaviour is disruption of through-coating defects by separation of crystallised layers with amorphous ones.[105] Also inorganic-organic nanolaminates have been studied with the aim of improving the elasticity of the coatings.[104,107]

The publications on ALD nanolaminate or mixture coatings for preventing degradation due to gaseous corrosives are significantly scarcer on plain metals than on polymers.[52,77,97] On Fe nanoparticles Al_2O_3-ZnS nanolaminates were used to reduce the coating cracking observed at high temperatures due to differences in thermal expansion coefficients between the substrate and an ALD Al_2O_3 film.[77] The coatings were deposited from $Al(CH_3)_3$ with H_2O and $Zn(CH_2CH_3)_2$ with H_2S at 227 °C. With 10 nm coatings the failure temperature in air could be increased from 527 °C for a single Al_2O_3 to 727 °C for the Al_2O_3-ZnS nanolaminate (Figure 4). Improved protective properties were achieved with increasing ZnS content. The highest percentage of ZnS cycles incorporated in the laminates was 30 %.

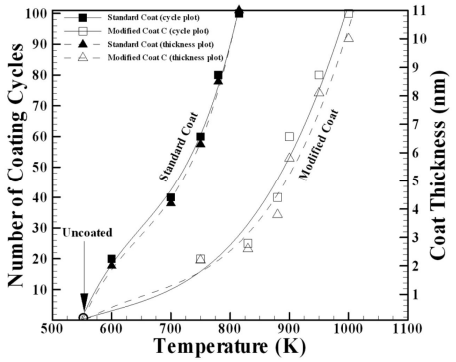

Figure 4 *Correlation between the ALD Al_2O coating thickness (and number of coating cycles) to the failure temperature without (standard coat) and with ZnS layers (modified coat) during exposure to high temperatures in air. Reprinted with permissions from [77]. Copyright John Wiley and Sons.*

Al_2O_3-TiO_2 nanolaminates (90 nm) have been used to prevent tarnishing of silver.[97,100] The precursors, deposition temperature and single layer thicknesses were not disclosed. In accelerated tioacetamide corrosion test (ISO 4538:1978) the bare silver showed significant degradation already after 1 hour, but the ALD coated samples remained almost Ag_2S free for 48 h. The aim of using nanolaminates instead of single layers of Al_2O_3 or TiO_2 was not given, but possibly the combination of the barrier properties of Al_2O_3 with the chemical stability of TiO_2 was attempted. Additionally thicker protective coatings could be made invisible to the naked eye when the nanolaminate structure was adopted instead of single layers. No comparison was made to the protective properties of single layers of Al_2O_3 or TiO_2.

Electrospun Cu nanowires intended to be used as a low cost transparent electrode were protected with ALD ZnO coatings doped with Al_2O_3.[52] $Zn(CH_2CH_3)_3$, $Al(CH_3)_3$ and H_2O were used as precursors and the deposition temperature was 150 °C. The material was chosen due to its transparency and conductivity. A 1 nm ALD Al_2O_3 layer was used as a nucleation layer. The Al_2O_3 nucleation layer was also anticipated to improve the acid resistance of the coating. The oxidation resistance of the nanowires during annealing at 160 °C in dry air was significantly improved by the coating. The bare wires were completely oxidised and turned insulating in 40 min while the 25 nm coated wires showed only a 10 % increase in resistance after 8 h. The afforded protection was even more apparent in humid conditions. Because the conductivity of the protective coating was vital for the application, no comparison in regards of protective properties was made to single layers of Al_2O_3 or ZnO.

2.2.3 Protection against liquid corrosives

Matero et al.[26] were the first to consider the general corrosion protection properties of ALD coatings against liquid corrosives on metallurgical substrates. They studied the protection of stainless steel. Similar studies have since been done on stainless steel,[19,43,113-118] steel,[37] aluminium alloy,[19,37] magnesium alloy,[19,119-121] copper,[19,53,122,123] and silver and sterling silver.[19,97] In addition to the fundamental research on metallic substrates also ALD protection of metals in applications like plasmon-enhanced dye-sensitised solar cells (DSSC),[124,125] nanoparticles used for heterogeneous catalysis,[126-129] biomedical devices,[51,130-132] proteomics based on nanonewton dielectrophoretic forces[133-135] and optical components[49,136] have been considered. Furthermore, combination of ALD with coatings deposited by other methods has opened a pathway to utilise ALD coatings in applications in which ALD layers alone might not offer sufficient protection for instance due to limited mechanical durability.[137-140] Hereafter these combination coatings are referred to as duplex coatings. Protection of non-metallic surfaces from liquid corrosives for instance in lithium-ion batteries,[14,141,142] molten carbonate fuel cells (MCFC),[143-145] and photoelectrochemical cells (PEC) for water splitting[17] have also been widely studied with ALD coatings.

2.2.3.1 Applications

Fundamental research on the electrochemical corrosion protection properties of ALD coatings on metals has gained significant attention.[19,26,37,43,53,97,113-123] Because no single application is specifically considered, there have been no additional requirements for the coatings. The general aim has been to produce as good sealing properties as possible to isolate the protected surface completely from the corrosive liquids. Additionally, the long-term stability and chemical durability should be optimised. The restrictions to the ALD processes are usually determined by the substrate. The most commonly studied protective materials have been Al_2O_3 and TiO_2.[19,26,37,43,53,113,114,116-123] In addition, Ta_2O_5 and AlN single layers and Al_2O_3-TiO_2 nanolaminates have been considered.[19,26,97,113-115,117-119]

Several types of applications have gained attention in protecting metallic components in liquids by ALD. Silver nanoparticles can be incorporated in DSSCs to enhance the energy absorption.[124,125] However, the nanoparticles are easily corroded in the I^-/I_3^- redox shuttle, and their stabilisation with ALD TiO_2 and Al_2O_3-TiO_2 nanolaminate coatings has been studied. The protective coating should be as thin as possible to minimise the exponentially distance dependent extinction of the electromagnetic waves of the surface plasmons. This requirement is similar to the one discussed in the previous chapter in regards of plasmon-enhanced analysis tools.

Copper and cobalt nanoparticles can be used in liquid-phase heterogeneous catalysis for converting biomass to fuels and chemicals.[126-129] The main challenge is to prevent leaching and sintering of the metals during the process operation. ALD Al_2O_3 and TiO_2 coatings have been studied. To enable catalysis on the particles, the protective ALD layers must contain pores. This can be achieved by annealing ultrathin films at 500–700 °C.

Surfaces of several biomedical devices have been protected with ALD. In addition to protecting the surfaces from degradation, in biomedical devices complete sealing is vital also to prevent exposure of living organisms to harmful substances. SiO_2 has been used to protect stainless steel implants.[132] Al_2O_3 has been used to protect nickel-titanium alloys aimed for instance for stents.[130] Al_2O_3 and Al_2O_3-HfO_2 nanolaminates have been used to protect aluminium contacts in complementary metal oxide semiconductor devices aimed for biosensing.[131] Al_2O_3, HfO_2, ZrO_2 and Al_2O_3-HfO_2 nanolaminates have been tested for microelectromechanical systems aimed generally for biomedical applications.[51]

Nanonewton dielectrophoretic forces can be used to selectively attach and detach proteins to a surface for monitoring genetic and protein biomarkers.[133-135] However, the currently used gold-chromium electrodes corrode in the required electric fields. Protection with ALD SiO_2 has been attempted. The coating should be quite thin to avoid unnecessary voltage loss across the protective layer.

Aluminium and silver reflectors in optical components are prone to corrode in the atmosphere and during exposure to corrosive liquids.[49,136] Protection abilities of ALD

SiO_2 and Al_2O_3 coatings have been considered. The main requirement is that the reflective properties of the metal substrates must be maintained. Although specific applications are aimed for, the research has been quite fundamental.

Protective ALD coatings against liquid corrosives on non-metallic surfaces have been also used in several applications. Some actively studied areas include electrodes in Li-ion batteries, MCFCs and PEC water splitting. In Li-ion batteries the electrode materials suffer from chemical and mechanical degradation.[14] Protective ALD coatings have been most actively studied on carbon, silicon, metal oxide, and their hybrid combination anodes. Correspondingly the protection of $LiCoO_2$, $LiMn_2O_4$, and more complex lithium metal oxide cathodes has been studied. Al_2O_3 is the most common protective ALD coating material, but in addition TiO_2, ZnO, ZrO_2 and TiN have been considered.[14,146] The protective layer should be very thin to minimise its influence to the ion and electron transport to the electrodes.

In MCFCs the state-of-the-art nickel oxide cathode is prone to dissolve in the carbonate melt (electrolyte).[143-145] ALD TiO_2, CeO_2, and Co_3O_4 have been suggested as the protective layers. The active nickel oxide phase is formed through electrochemical oxidation/lithiation of nickel in the Li_2CO_3-K_2CO_3 electrolyte. The protective layer should allow the formation of the active layer or a layer with different composition but similar functional properties.

In PEC water splitting the semiconductor electrodes with sufficiently narrow band gaps to harvest energy from the visible light are susceptible to corrosion in the aggressive aqueous electrolytes.[17] Both anodes like Si, ZnO, GaAs and GaP,[17,147,148] and cathodes like Si, Cu_2O and InP[17,149] have been protected with ALD coatings. Bulk of the research has focused on TiO_2 coatings, but other studied materials include MnO and Al_2O_2:ZnO-TiO_2 nanolaminates.[17,147-149]

2.2.3.2 Influence of deposition parameters

In chapter 2.2.2.2 it was elaborated that the ALD process, deposition temperature and coating thickness significantly influence the performance of protective coatings against gaseous corrosives. In liquids, the role of the substrate pre-treatment has been additionally raised. Marin et al.[115] considered the influence of two industrial surface finishes, pickling in HNO_3 and HF (ASTM A480-2D) and skinpassing (ASTM A480-2B), on the protective properties of ALD coatings on stainless steel. The pickling treatment produced a rough surface (RMS 368 nm) with grain boundaries clearly visible while the skinpassing resulted in a smoother finish (RMS 52 nm) with oriented grooves along the direction of the skinpass. A 400 nm ALD Al_2O_3-TiO_2 nanolaminate clearly improved the durability of substrates pre-treated either way. No clear difference between the electrochemical behaviours of the coated samples with different pre-treatments could be observed. This implies that the surface finish did not significantly influence the ALD coating

performance. However, it is possible that the 400 nm coating was too thick to adequately evaluate the influence of the pre-treatment. Furthermore, thus far no consideration has been given to the influence of heterogeneous surface composition like segregated carbides on the surface of steels, or cleanliness. Potts et al.[37] have shown that PEALD Al_2O_3 coatings adhere to steel better than thermal ALD coatings. The suggested cause was a cleaning effect from the highly reactive O_2 plasma in the beginning of the film deposition.

The most common process used in depositing ALD Al_2O_3 corrosion protection coatings against liquid corrosives is $Al(CH_3)_3$–H_2O.[26,37,51,53,113,114,116-120,122-124,128-130,136] Only Potts et al.[37] have used O_2 plasma as the oxidizing precursor in addition to H_2O. They compared the protective properties of thermal and PEALD Al_2O_3 coatings deposited at 150 °C on low alloy steel and aluminium alloy. Thin 10 nm PEALD coatings were observed to perform significantly better than the corresponding thermal ALD coatings. This was attributed to the lower amount of impurities observed in the PEALD coatings. However, already at 50 nm thickness the performance of the coatings was similar or even reversed.

ALD TiO_2 corrosion protection coatings are usually deposited from $TiCl_4$ and H_2O,[19,26,53,114,117-119] but also $Ti(OCH(CH)_2)_4$ and H_2O have been used.[43,124,125] Generally, non-chloride containing precursors would seem more appealing in depositing corrosion protection coatings. Indeed, some microblistering has been observed under TiO_2 coatings deposited from $TiCl_4$ on stainless steel.[114] Furthermore, the electrochemical barrier properties have been observed to be similar for a 100 nm TiO_2 deposited from $TiCl_4$[114] and a thinner 50 nm TiO_2 deposited from $Ti(OCH(CH)_2)_4$[43] on stainless steel. This implies that better results can be achieved with the non-chloride containing precursor. However, direct comparison is challenging due to differences in substrate materials, coating thicknesses, deposition temperatures and testing methods.

For Ta_2O_5 and SiO_2, similar considerations on the effect of the ALD process are challenging. Either only single process has been studied or the testing methods are so different that any comparison would be pointless.[26,113,132-135]

The amount of impurities in ALD films decrease with increasing deposition temperature.[5] This leads to better quality films with higher density and lower defect density. For amorphous ALD coatings, this has indeed been shown to improve the protective properties against liquid corrosives.[26,37,113,116] Diaz et al.[113] showed clear improvement of electrochemical corrosion protection properties of Al_2O_3 coatings with increasing deposition temperature (Figure 5). On stainless steel the passive current density in linear sweep voltammetry (LSV) measurements was decreased by one order of magnitude when increasing the temperature from 160 to 250 °C. Potts et al.[37] observed an almost linear decrease in coating porosities from 4.5 to 0.5 % with increasing deposition temperature from 50 to 150 °C for Al_2O_3 films deposited with PEALD on low alloy steel. The porosities were calculated from corrosion current densities determined from LSV results. However, on aluminium alloy an increase of porosities with deposition temperature was reported for PEALD Al_2O_3 without any clear indication on the cause.

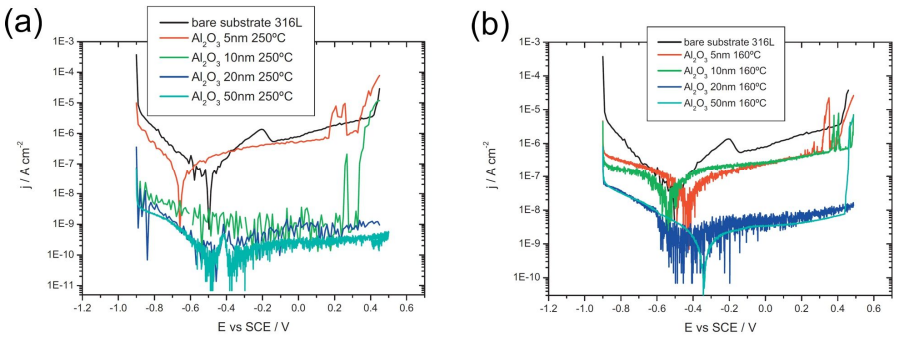

Figure 5 *Influence of deposition temperature and coating thickness on the protective properties of ALD Al_2O_3 on 316L stainless steel in LSV measurements in 0.8 M NaCl solution at pH 7. Reprinted from [113] with permissions from Elsevier.*

The influence of the deposition temperature on the corrosion protection properties of ALD coatings is more complicated for materials that can be deposited either in amorphous or polycrystalline form. For instance, the deposition temperatures for TiO_2 coatings from $TiCl_4$ and H_2O have been varied between 120 and 400 °C.[26,53,114,117-119] Usually the coatings are deposited at low enough temperatures to results in amorphous films to avoid the grain boundary defects.[43,53,114,117-119] However, the afforded sealing properties are limited, probably at least partly due to the impurity content. Matero et al.[26] showed that even though the chemical durability of the TiO_2 coatings was improved with increasing deposition temperature, the optimum temperature for corrosion protection coatings was 200–300 °C. This was a compromise between the effects of coating purity and crystallinity. The impurity content of the coatings deposited at ≤150 °C was so high that the coating quality was poor. On the other hand, the polycrystalline films formed at ≥200 °C contained grain boundaries. Especially the rutile phase formed above 300 °C resulted in rough and defected coatings. TiO_2 coatings deposited from $Ti(OCH(CH)_2)_4$ and H_2O have only been studied at a single deposition temperature of 150 or 200 °C.[43,124,125] At 150 °C, the coatings were amorphous and at 200 °C, anatase was formed. However, comparison of the results is not possible because the substrates and testing methods differ too much. It is expected that, as with the $TiCl_4$-H_2O process, the optimum temperature is a compromise between the degree of crystallinity and purity of the coatings.

Marin et al.[116] have attempted to improve the protective properties of a single material coating by varying the deposition temperature. The idea was that the ´thermal multilayer´ coatings would result in a similar decrease of through-coating pinholes as is observed in multilayer coatings using two or more materials. Three types of coatings were studied. An Al_2O_3 coating was grown on stainless steel by depositing the whole coating isothermally at 120 °C, first layer at 120 °C and the second at 300 °C, or the first layer at 300 °C and the second at 120 °C. The 'thermal multilayers' had lower corrosion and passive current densities than the 'one-layered' Al_2O_3 coatings deposited at 120 °C.[114,116] Furthermore, the coatings with the outer layer deposited at 300 °C were found to have better protective properties than those with the outer layer deposited at 120 °C. However, coatings deposited isothermally at 300 °C were not studied for comparison. Also the possibility that

the lower initial deposition temperature might protect the stainless steel during the subsequent deposition at the higher temperature was not considered.

As was observed with gaseous corrosives, increasing the coating thickness significantly improved the corrosion protection properties of ALD coatings.[26,37,49,53,113,114,116,117,119,120,122-124,136] Compared to the gas environment, more systematic research has been done on metals in corrosive liquids. On stainless steel, a three orders of magnitude decrease in passive current density could be achieved by increasing the ALD Al_2O_3 coating thickness from 10 to 50 nm (Figure 5).[113] With Ta_2O_5, complete blocking of metastable and stable pitting was observed only with 50 nm coatings while the results obtained with thinner coatings were inconsistent.[113] The improvement with the coating thickness was attributed to a decrease in the number of through-coating defects due to increasing coverage of the coating and decreased amount of impurities.[37,113] In ToF-SIMS depth profiles the content of carbon impurities was shown to increase close to the coating-substrate interface. The contamination was suggested to originate from growth on the substrate surface from which hydrocarbon contamination had been incompletely removed by the pre-treatment. The outermost region of the coating was shown to contain more hydroxyl impurities, probably from surface hydroxylation through defects when the samples were exposed to ambient.[150] Therefore, in average the thinner coatings contained more carbon and hydroxyl impurities than the thicker coatings, thus making their density and barrier properties worse.

Chai et al.[123] showed that the improvement of protective properties with increasing thickness level off already for ≥8 nm ALD Al_2O_3 coatings on copper. The effective protective properties at 8 nm thickness were attributed to a thorough surface preparation. The high purity copper plates were fine polished (RMS <1 nm) and washed in an ultrasonic bath in deionised water for 2 min. In other studies on machined metal plates, the substrates were polished by varying methods to a higher RMS roughness (≥20 nm) and thereafter degreased in an ultrasonic bath in either ethanol or isopropanol.[37,49,113,114,116-119,130] However, the surface roughness might not have been the only cause for the difference. It is possible that the surfaces of the ultrapure copper plates contained less chemical heterogeneity, which could help in achieving very low defect densities already with 8 nm thick coatings. Most probably both the decreased roughness and chemical heterogeneity contributed to the excellent protective properties.

The dependence of protective properties with coating thickness is complicated by the observation that the adhesion of ALD coatings decreases with increasing thickness. Marin et al.[114] have shown that a 30 nm Al_2O_3 has better adhesion to a stainless steel than a 100 nm layer. This implies that a compromise between the sealing properties and adhesion should be considered.

In some applications like plasmon-enhanced DSSCs,[124,125] Li-ion batteries,[14,141,142] and nanoparticles for heterogeneous catalysis,[126-129] the protective coatings have to be very thin to maintain the functional properties of the protected materials. For instance, in Li-ion

batteries the protection of electrodes is optimised with 1–5 nm thick coatings.[14,141,142] Thinner coatings offered insufficient chemical and mechanical protection, and thicker coatings hindered electron and ion transportation across the electrode-electrolyte interface and thereby led to reduced capacities. Remarkably, copper and cobalt nanoparticles used in heterogeneous catalysis have been protected from leaching and sintering by ultra-thin coatings, which have been made intentionally porous.[126-129] The ALD Al_2O_3 was shown to grow preferentially on under-coordinated atoms in step edges and defects, i.e. the same sites that were especially vulnerable to leaching. Uncoated areas could be found on the terrace sites and they allowed the catalytic processes to proceed.

2.2.3.3 Comparison of coating materials

The sealing properties of Al_2O_3 have been found significantly better than those of TiO_2, Ta_2O_5 and AlN in electrochemical tests (Table 3).[26,113,114,117-119] For instance, on stainless steel the corrosion current density was decreased three orders of magnitude with a 50 nm Al_2O_3 coating.[113] With TiO_2 and Ta_2O_5, the corresponding decreases were only one and two orders of magnitude.[43,113] This can be attributed to the intrinsically better insulating properties[151,152] and better nucleation on challenging substrates of ALD Al_2O_3 compared to the other materials.[53] Furthermore, TiO_2 and other materials that can be crystalline as deposited suffer from the easier access of corrosives to the protected surface due to the grain boundaries.[26,48,118]

Table 3. *Overview of electrochemically (LSV measurements) determined porosities of ALD coatings on various metals and metal alloys.*

Substrate	**Coating** (material / deposition temperature / thickness)	**Testing solution**	**Porosity** (%)	**Ref**
Stainless steel	Al_2O_3 / 250 °C / 5 nm Al_2O_3 / 250 °C / 50 nm Ta_2O_5 / 250 °C / 5 nm Ta_2O_5 / 250 °C / 50 nm	0.2 M NaCl	15 0.03 14 0.14	113
Stainless steel	TiO_2 / 150 °C / 50 nm	3wt.% NaCl	~9[a]	43
Stainless steel	Al_2O_3 / 120 °C / 107 nm TiO_2 / 120 °C / 102 nm	0.15M NaCl	~0.02[a] ~20[a]	114
Stainless steel	Al_2O_3 / 120 °C / 20 nm TiO_2 / 120 °C / 20 nm AlN / 300 °C / 20 nm	0.2 M NaCl	~0.2[a] ~50[a] ~0.1[a]	118
Steel	Al_2O_3 / 150 °C / 10 nm Al_2O_3 / 150 °C / 50 nm Al_2O_3 (PEALD) / 150 °C / 10 nm Al_2O_3 (PEALD) / 150 °C / 50 nm	0.2 M NaCl	~3.6 ~0.02 ~0.6 ~0.06	37
Magnesium alloy	Al_2O_3 / 120 °C / 109 nm TiO_2 / 120 °C / 104 nm	0.05 M NaCl	~0.33[a] ~0.33[a]	119
Aluminium alloy	Al_2O_3 / 150 °C / 10 nm Al_2O_3 / 150 °C / 50 nm Al_2O_3 (PEALD) / 150 °C / 10 nm Al_2O_3 (PEALD) / 150 °C / 50 nm	0.5 M NaCl	~55 ~10 ~30 ~10	37
Nickel-titanium alloy	Al_2O_3 / 150 °C / 9.8 nm Al_2O_3 / 150 °C / 50 nm	Hanks´solution	59[a] 20[a]	130
Copper	Al_2O_3 / 150 °C / 4.5 nm Al_2O_3 / 150 °C / 7.8 nm Al_2O_3 / 150 °C / 29 nm	0.1 M NaCl	~78 ~3 ~2	122
Silver	Al_2O_3 / 120 °C / 18 nm Al_2O_3 / 120 °C / 86 nm	0.3wt.% Na_2SO_4	~40 ~30	136

[a]The porosity (P) has been calculated from $P=(i_{coat}/i_{subs})\times 100\%$[153] from the reported corrosion current densities of the bare (i_{subs}) and coated (i_{coat}) substrate.

Marin et al.[114,117] have also shown significantly worse adhesion of TiO_2 to stainless steel compared to Al_2O_3. This was most probably due to undesirable reactions between the TiO_2 precursor $TiCl_4$ or the by-product HCl and the stainless steel surface, which resulted in microblistering of the TiO_2 coating. Microblisters were not observed between the TiO_2 coatings and stainless steel when the coatings were deposited using $Ti(OCH(CH)_2)_4$ as the precursor.[43] However, their adhesion was not tested.

As already discussed in chapter 2.2.2.3, the main limitation of Al_2O_3 is the chemical stability. Any problems observed with gaseous corrosives are expected to be more pronounced with the liquids, and thus the possible applications for protective ALD Al_2O_3 coatings are certainly restricted close to neutral solutions.[35] Marin et al.[118] have shown complete stability of 20 nm Al_2O_3 on stainless steel for 2000 h immersion in 0.2 M NaCl at pH 7. However, Abdulagatov et al.[53] observed very severe corrosion of Al_2O_3 coated evaporated copper film at 90 °C after 75 hours in water. Capping layers of ALD TiO_2 were needed for sufficient durability, as will be elaborated below.

Compared to Al_2O_3, TiO_2 coatings are expected to have better chemical durability. Matero et al.[26] observed pitting of stainless steel samples coated with TiO_2 during immersion in 1 M HCl solution. However, the coatings themselves were found stable even in aggressive H_2SO_4 solutions. Marin et al.[118] showed changes in a 20 nm TiO_2 coated stainless steel in 0.2 M NaCl during the first 24 h of a 500 h immersion. After the first 24 h the system was stabilised for the remaining duration of the test. This indicated slight reduction of the protective properties of the TiO_2 coatings, but no dissolution was observed. It can be concluded that the chemical durability of ALD TiO_2 would appear to be sufficient against a range of aggressive chemicals, but it also contains pinhole defects endangering the long-term durability of the protected material.

Similar to TiO_2, Ta_2O_5 is expected to be chemically more stable than Al_2O_3,[35] and therefore a possible alternative to TiO_2. The Ta_2O_5 coatings deposited from $Ta(OCH_2CH_3)_5$ and H_2O are amorphous.[8,26,113] Thus the problem of pinhole defects formed at the grain boundaries of polycrystalline coatings is avoided. Unfortunately, the long-term stability tests of Ta_2O_5 coatings on metal substrates are limited. Matero et al.[26] showed that stainless steel coated with 150–300 nm Ta_2O_5 suffer from pitting corrosion in 0.1 M HCl solutions. Slight solubility of Ta_2O_5 was indicated. On the other hand, Sammelselg et al.[47] have shown that Ta_2O_5 on silicon is etched at a very low rate of <0.1 nm/s in 80% H_2SO_4 solution at 110 °C.

Systematic electrochemical studies on corrosion protection properties of ALD SiO_2 coatings on metals have not been done. The existing papers have been focused on proving the viability of protection with ALD for specific applications.[49,132-135] On Al-mirrors the SiO_2 coatings were grown from $[(CH_3)_3CO]_3SiOH$ with $Al(CH_3)_3$ catalyst at 300 °C.[49] The protection afforded by a 10 nm ALD coating was better than that achieved with 30 nm e-beam evaporated SiO_2 and 100 nm commercial SiO_2 coatings. The testing was done in 24 wt.% KOH solutions. The protective properties further improved with increasing coating thickness. Al mirrors coated with 120 nm SiO_2 were shown to withstand 6 wt.% hydrochloric acid, 70 wt.% nitric acid, 40 wt.% sulphuric acid, 24 wt.% KOH, acetone, isopropanol and 0.77 M NaCl solutions for 2 hours without noticeable changes.

Adequate protection of the electrodes used in attaching and detaching proteins on surfaces with nanonewton dielectrophoretic forces has been realised with 10 nm ALD SiO_2.[133-135] The electrolyte solution was deionised water. The coating was deposited from

tris(dimethylamino)silane ($[(CH_3)_2N]_3SiH$) and O_2 plasma at 200 °C. On stainless steel substrates aimed as biological implants 15 nm SiO_2 coatings were electrochemically determined to completely cover the surface.[132] The SiO_2 coatings were grown from bis(tertiarybutylamino)silane ($[(CH_3)_3CNH]_2SiH_2$) and O_2 plasma at 300 °C. The testing was done in 2mM $Ru(NH_3)_6Cl_3$ - 0.1 M KCl solution. In both applications only the viability of using the protective ALD coating was demonstrated without additional work on optimizing the coating properties.

2.2.3.4 Multilayer and mixture coatings

Coatings combining two or more ALD grown materials have been used to protect stainless steel,[19, 26, 114, 115, 117] silver and sterling silver,[19,97,124] copper,[19,53] magnesium alloy,[19,119] cobalt alloy[19] and aluminium alloy.[19] The most common material combination is Al_2O_3 and TiO_2: Al_2O_3 layers have been used to improve the adhesion/nucleation of the subsequent TiO_2 layer,[53,124] and provide adequate sealing properties.[53] TiO_2 layers in turn have been used to protect the chemically unstable Al_2O_3 from the environment thus preventing its corrosion.[53,138] Also nanolaminate and mixture coatings have been used to combine the sealing properties of Al_2O_3 and chemical durability of TiO_2 in more complex coating systems.[19,26,51,97,114,115,117,119,131]

Nucleation of ALD Al_2O_3 from $Al(CH_3)_3$ and H_2O is known to occur well on a variety of substrate materials.[22-25] Thus it can be used even as a very thin layer beneath other ALD materials to ensure good nucleation. Abdulagatov et al.[53] studied in detail the nucleation of Al_2O_3 and TiO_2 on copper. While nucleation of Al_2O_3 was observed to occur in 15–20 cycles, the TiO_2 coatings had significant porosity still at 20 nm thicknesses and showed increased roughnesses compared to the bare substrate implying an island-like growth mechanism. Sufficient corrosion protection properties were only observed with coatings utilizing an Al_2O_3 nucleation layer beneath TiO_2. Ultra-thin 0.2 nm Al_2O_3 layers have also been shown to decrease the necessary thickness of an ALD TiO_2 coating on plasmonic silver nanoparticles in DSSCs from 7.7 to 5.8 nm.[124]

Abdulagatov et al.[53] have shown that the durability of ALD Al_2O_3 on copper can be improved with TiO_2 capping (Figure 6). Al_2O_3 on copper lost its protective properties almost immediately in H_2O at 90 °C, but the ALD TiO_2 capped Al_2O_3 protected the substrate for nearly 90 days.

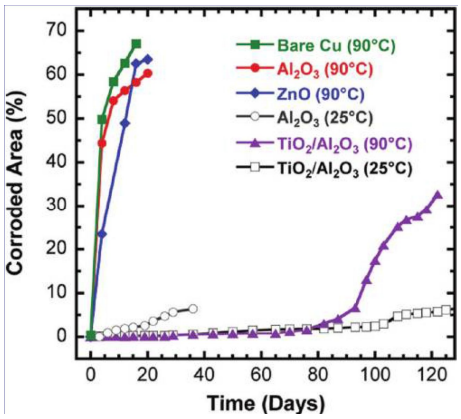

Figure 6 *Corrosion durability of ALD Al_2O_3, ZnO and Al_2O_3-TiO_2 nanolaminate coated copper during immersion in H_2O at 25 and 90 °C temperatures. Reprinted with permissions from [53]. Copyright (2011) American Chemical Society.*

Nanolaminate coatings of Al_2O_3 with TiO_2 or HfO_2 have been shown to have better protective properties than single layers.[19,26,51,97,114,117,119,131] Both the electrochemical barrier properties and long-term durability were improved. Furthermore, Al_2O_3-TiO_2 nanolaminate coatings were observed to have better adhesion to stainless steel than the corresponding single layers of similar thickness.[114,117] The adhesion also improved with the decreasing bilayer thickness. As with single layers, the protective properties of the nanolaminate coatings improved with increasing total thickness.[26,114,117,119] The electrical insulating properties of ALD nanolaminates for instance in thin film capacitor structures have been shown to improve with increasing number of bilayers within a certain total nanolaminate thickness.[151] However, in corrosion protection coatings no great differences for varying number of bilayers have been observed. Matero et al.[26] showed that a 400 nm Al_2O_3-TiO_2 laminate with 20 bilayers had only slightly better sealing properties and durability in 3.5 wt.% NaCl solution during a 12 weeks immersion than laminates with 2–8 bilayers. No differences between the 2–8 bilayer coatings could be discerned. Also Marin et al.[114,117,119] achieved almost identical electrochemical barrier properties with 100 nm Al_2O_3-TiO_2 nanolaminates consisting of 2–4 bilayers on stainless steel and magnesium alloy (Figure 7). For Al_2O_3-HfO_2 nanolaminates on electrical aluminium contacts only the improved protective properties of the nanolaminates compared to the single layers was shown.[51,131]

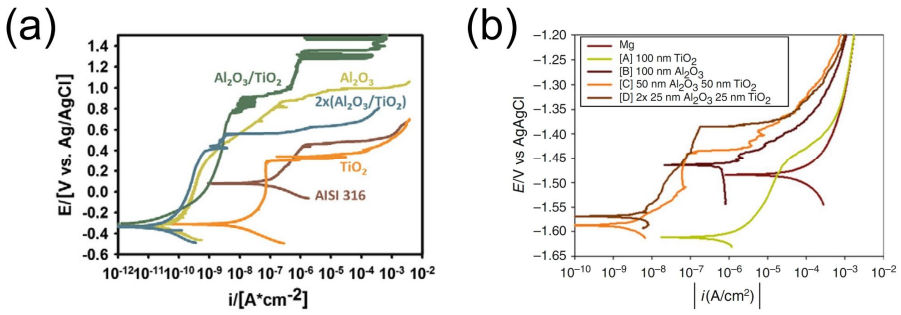

Figure 7 *Polarisation results on ALD Al_2O_3, TiO_2 and Al_2O_3-TiO_2 nanolaminate coatings on (a) stainless steel, and (b) magnesium alloy. Figure (a) reprinted from [114] with permissions from Elsevier. Figure (b) reprinted from [119] with permissions from Springer.*

Mixture coatings are less studied than nanolaminates. However, $Al_xTi_yO_z$ mixtures have been shown to have better electrochemical barrier properties than the corresponding single ALD layers.[114] As the mixture coatings were significantly thinner than the corresponding nanolaminates, their comparison was not possible.

2.2.3.5 Duplex coatings

Two classes of duplex coatings have been studied for protection of metals from liquid corrosives. A thin PVD layer can act as a buffer between the substrate and the ALD coating,[140] or ALD can be used to block pinholes in hard PVD coatings or CVD graphene.[137-139] Wang et al.[140] studied the effect of a sputtered Al-interlayer on the corrosion resistance of ALD Al_2O_3 coatings on a Mg-Li-Zn alloy. Significant improvements in electrical barrier properties were observed and attributed to a blocking of Li diffusion into the ALD Al_2O_3 coating.

Hard PVD coatings have gained significant attention due to their resistance to wear, good thermal stability, and low friction coefficient.[154] Unfortunately, they contain through-coating pores, which has rendered them unsuitable for use in corrosive environments. Sealing these pinholes with ALD has been shown to be a viable option for improving the electrochemical barrier properties.[138,139] Shan et al.[139] obtained an order of magnitude decrease in corrosion current density of CrN coated stainless steel with a 90 nm ALD TiO_2 sealing layer (Figure 8). Marin et al.[138] showed an impressive two orders of magnitude decrease in the corrosion current density of TiCN coated mild steel with a 4 nm ALD Al_2O_3 layer. However, on a less defected TiAlN/TiN nanolaminate the same Al_2O_3 coating decreased the corrosion current density only by one order of magnitude.

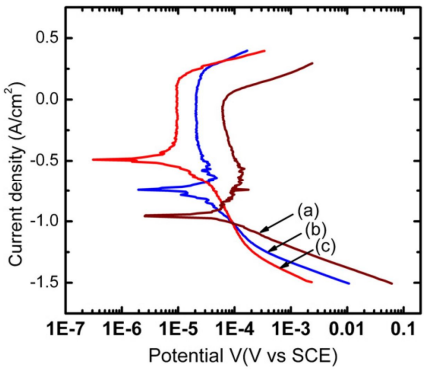

Figure 8 *Polarisation results on (a) stainless steel, (b) CrN coated stainless steel and (c) ALD TiO_2 sealing on CrN coated stainless steel in 3 wt.% NaCl solution. Reprinted from [139] with permissions from Elsevier.*

Graphene was initially expected to be an excellent protective coating due to its impermeability to gases and oxidisers.[155,156] However, in electrochemical tests graphene was found to contain nanometre-sized structural defects, and the layers gave short-term protection at best and accelerated the corrosion at worst. Hsieh et al.[137] have shown that ALD Al_2O_3 can improve the protective properties of graphene on copper. The ALD film grows preferentially on defects thus blocking the most vulnerable sites. The performance was improved with increasing the ALD layer thickness.

2.2.4 Diffusion prevention

A comprehensive review on all ALD materials and processes for diffusion barrier applications is beyond the scope of this work. Therefore the reader is directed to reviews for more specific overview on the following applications: TFEL displays,[5,12,157,158] interconnects in microelectronics,[159,160] and Li-ion batteries.[14,161] In addition, some papers present ALD diffusion barriers in CIGS solar cells on flexible stainless steel substrates.[162,163]

2.2.4.1 Applications

The TFEL displays are deposited on glass substrates.[157] Commonly a non-alkaline containing glass is used. However, a good sodium diffusion barrier enables the use of a less expensive soda lime glass.[5] The literature on the subject has remained scarce, but a 50 nm ALD Al_2O_3 appeared to be sufficient.[157,164]

Incorporation of Cu interconnects in the ultra large-scale integration microelectronics has generated a need for a suitable barrier layer.[159,160] The barriers are required to prevent diffusion of Cu into the surrounding materials and impurities from the surroundings into Cu during both the manufacturing and operation of the device. In addition, the barrier

should have excellent adhesion to Cu and the other surrounding materials, low resistivity, good electromigration and stress resistance, and preferentially amorphous or nanocrystalline structure to limit diffusion through voids, dislocations and grain boundaries. The deposition of the barrier should be done within the thermal budget (<400 °C) of the back-end-of-line microelectronics processing. As ALD thin films are conformal and can be controlled down to sub-nanometre thicknesses, they are predicted to become the predominant solution in the future when the currently used PVD techniques reach their limits.[165] The research on ALD barriers has been mainly focused on transition metal nitrides like TiN,[56-58,61,66,166] TaN,[54,55,62,64,66,167] WN,[65,166] NbN,[68] MoN[67] and VN.[69] However, also transition metal carbides,[168] ternary materials like TaCN and WCN,[169-173] oxides[174-176] and metals[177] have been considered. Also Ru containing mixtures and nanolaminates have been studied to enable direct electroplating of copper on the diffusion barrier.[178-183]

In all-solid-state batteries one envisioned device architecture is based on 3D structure on a silicon substrate. To ensure stable long-term performance, the diffusion of Li out of the active layers and into the substrate has to be prevented. The barrier layer should serve also as the current collector thus requiring good conductivity. From the ALD grown materials the main focus has been on TiN and TaN, but also Pt has been used.[66,184-187]

Chalcopyrite Cu(In,Ga)Se_2 (CIGS) solar cells are made from thin films and thus have the distinctive advantage over the traditional silicon wafer based solar cells that they can be made flexible.[188] However, to exploit this property also a flexible substrate is needed. Some device structures have been grown on polymers, but the thermal budget of polymers restricts the conditions for depositing the active layers. Therefore metal foils have been considered as an alternative. Stainless steel foils require a barrier layer for inhibiting out-diffusion of Fe, Ni, Cr, Mn and Mg, and an insulator to enable monolithic integration. The most detrimental of the out-diffusing elements in regards of performance stability is Fe.[189] ALD Al_2O_3 films have been considered as possible combined diffusion barriers and insulators.[162,163]

2.2.2.4 Influence of deposition parameters

As for coatings against gaseous and liquid corrosives, the most important parameters affecting the diffusion barrier properties of ALD thin films are the choice of precursors,[54-58,61,62,64,166,167] deposition temperature[54,58,61,62,67,68,168,187] and film thickness.[55,62,64,172,174-176] Because research in this area has been primarily application oriented, simply preventing diffusion is not enough. The influences of deposition parameters to other film properties have to be additionally considered. In Cu interconnects and Li-ion batteries the film resistivity is especially important.[159,184] For instance, the pulse lengths,[54,56,62,66,168,170,171,187] precursor sequence,[54,58] and plasma power,[66,171] have been shown to have an effect on the purity and resistivity of ALD nitride barrier films.

First the choice between thermal ALD and PEALD must be considered. Thermal ALD has the advantage that conformal films can be deposited in very demanding high aspect ratio structures,[20,54,61,65,166,169] which will be progressively required in the future devices. However, good conformalities have also been reported for some materials deposited with PEALD.[40,55,62,168,171,178,190] The advantages of PEALD lie in the precursor reactivities. For instance, the most widely researched diffusion barrier material in Cu interconnects, TaN, is challenging to deposit with thermal ALD,[54,59] as elaborated in chapter 2.2.1.2. More parameters for optimisation are available in PEALD (plasma conditions and gas mixtures), and thus TaN can be formed more easily from both halide and metalorganic precursors.[55,62,66] However, with PEALD the possible damage to the existing layers by the reactive plasma species should be considered. The PEALD processes are also hard to apply in batch mode, which limits their industrial scale-up.[11]

The effects of the deposition temperature have been found twofold. The impurity content is usually decreased with increasing temperature,[5] which results in decreased resistivity.[54,58,67,68,168,187] For instance, in a ALD Ta(Al)N(C) film ($TaCl_5$-$Al(CH_3)_3$-NH_3) an increased deposition temperature from 250 to 400 °C led to a decrease of resistivity from ~22 000 to 1300 μΩcm.[54] This was mainly attributed to the decreased chloride impurities from 14 to 4 at.%. On the other hand, the decreased resistivity with deposition temperature has also been correlated to a higher degree of crystallinity and increased crystallite size. This has been shown for several barrier materials including TiN,[58] TaN,[54] NbN,[68] MoN[67] and TaC.[168] However, as the diffusion along grain boundaries is increased with increasing crystallinity, amorphous or nanocrystalline barriers would be preferred. This has led to a need to optimise the deposition temperature with respect to film purity, crystallinity, resistivity, and barrier performance.

Also thickness has been shown to have a conflicting influence on the diffusion barriers. The barrier properties were significantly improved [55,62,64,66,172,174-176] and the resistivity decreased with increasing thickness.[56,69] However, the crystallinity of ALD films is known to increase with thickness.[8,64] For instance, <10 nm TaN is amorphous when deposited from $Ta[N(CH_2H_3)(CH_3)]_5$ and NH_3 at 250 °C.[64] When the thickness is increased to 30 nm the film is clearly polycrystalline. Furthermore, in Cu interconnects the industry is aspiring for thin barriers (≤5 nm).[165] Slightly less strict demands in regards of film thickness are enforced for Li-ion barriers.[66]

A complex thickness dependence has been observed for ALD Al_2O_3 barriers in preventing out-diffusion of elements from the stainless steel substrates into the CIGS solar cells. The diffusion barrier properties of Al_2O_3 against Fe, Cr and Mg were improved with increasing barrier thickness from 30 to 300 nm.[162,163] However, for Ni and Mn no clear effect of thickness could be determined. The reason for this difference was unknown. Fortunately, the inhibition of out-diffusion of Ni was already very effective with the thinnest 30 nm barrier tested.[162]

2.2.4.3 Comparison of barrier materials

The most actively studied materials for diffusion barriers for Cu in interconnects and Li-ions in batteries have been TiN and TaN.[54-58,61,62,64,66,166,167] Both materials have high thermal stabilities, low bulk electrical resistivities and are stable in contact with Cu.[35,191,192] In regards of the Cu interconnects the barrier properties of TaN are usually reported to be slightly better than those of TiN (Table 4).[54-58,61,62,64,66,166,167] This has been attributed to the smaller crystallite size or even amorphous structure of TaN compared to TiN.[54,55,57,62,64] Furthermore, the HCl by-product of the $TiCl_4$-NH_3 process has been shown to cause pitting corrosion on Cu thus making direct deposition of TiN on Cu challenging.[166] Unfortunately, ALD TaN films are not as easy as TiN to deposit with the desired oxidation state (chapter 2.2.1.2.).[59] Both TiN and TaN have been reported to have poor adhesion to Cu.[181,183]

Table 4. *Copper diffusion barrier performance of selected ALD materials.*

ALD barrier (material / deposition temperature / thickness)	**Resistivity** (μΩcm)	**Testing** (method / atmosphere / time)	**Failure temp.** (°C)	**Ref**
TiN (ALD) / 450 °C / 36 nm	120	XRD / vacuum / 60 min	600	57
Ti(Al)N (ALD) / 400 °C / 10 nm	140	XRD / N_2 / 15 min	650	58
TiN (PEALD) / 350 °C / 30 nm	200	XRD / vacuum / 30 min	>700	66
Ta(Al)N(C) (ALD) / 400 °C / 10 nm	1300	XRD / N_2 / 15 min	600	54
TaN (ALD) / 250 °C / 5 nm	NA	Sheet resistance / N_2 / 30 min	600	64
TaN (PEALD) / 225 °C / 30 nm	1550	XRD / vacuum / 30 min	600	66
TaN (PEALD) / 250 °C / 2–15 nm	300–500	XRD / He / continuous heating	700–800	62
WN (ALD) / 250–350 °C / 1.5 nm	1500–4000	SEM-RBS / H_2-N_2 / 30 min	600	65
VN (PEALD) / 150 °C / 5 nm	~300	XRD / NA / continuous heating	720	69
NbN (ALD) / 400 °C / 10 nm	750	XRD / N_2 / 15 min	600	68
MoN (ALD) / 400 °C / 10 nm	490	XRD / N_2 / 15 min	650	67
TaC (PEALD) / 300 °C / 5 nm	600	XRD / vacuum / 30 min	650	168
WNC (ALD) / 313 °C / 12 nm	350	XRD / vacuum / 30 min	700	169
TaCN (PEALD) / 200 °C / 5 nm	230	XRD / NA / 60 min	550	170
Al_2O_3 (ALD) / 250 °C / 1–3 nm	NA	XRD / N_2 / 5 min	675–750	175, 176
TiO_2 (ALD) / 240 °C / 1–3 nm	NA	XRD / N_2 / 15 min	650-700	174
Ta_2O_5 (ALD) / 240 / 1–4 nm	NA	XRD / N_2 / 15 min	650	174
HfO_2 (ALD) / 250 / 1-3 nm	NA	XRD / N_2 / 5 min	650–700	175, 176

Excellent results have been obtained with TiN in inhibiting Li-ion diffusion into the silicon substrate in battery applications.[66,184-187] Very little intercalation of Li into TiN was observed, and the samples remained stable during 50 galvanostatic cycles in a $LiClO_4$ and

$LiPF_6$ containing electrolyte. TaN has been found to be much more reactive towards Li than TiN.[66,186]

Other potential diffusion barrier materials for Cu interconnects include several binary nitrides,[65,67-69,166,173] TaC,[168] WCN,[169,172,173] TaCN,[170,171] a few oxides[174-176] and Ru.[177] Similar to TiN and TaN, the other nitrides and carbides have been found to be relatively good barriers (Table 4).[65,67-69,168] However, they share some of the challenges observed for TiN and TaN. For instance, the HF formed in the ALD WN process from WF_6 and NH_3 has been found to etch Cu, Si and SiO_2.[166] Most of the materials are polycrystalline thus enabling diffusion along grain boundaries.[67-69,166,168,173] The ternary WCN and TaCN seem to lack some issues related to the corresponding binary nitrides. No etching of Cu, Si or SiO_2 has been observed for WNC deposited from WF_6, NH_3 and triethylboron,[173] and the carbon in TaCN has been shown to significantly decrease the resistivity.[171] The oxides have excellent barrier properties already at very low thicknesses (1–3 nm) (Table 4).[174-176] Their insulating nature is suggested to become less significant when the diffusion barrier thickness diminishes. Ru is polycrystalline with columnar structure as deposited impeding its barrier properties.[177] Furthermore, it has poor adhesion to Si and SiO_2.[181,183]

Prevention of out-diffusion of elements from stainless steel into the active layers of a CIGS solar cell has only been studied for Al_2O_3 by ALD.[162,163] Comparison of coating material properties is therefore impossible. With a 300 nm thick Al_2O_3, Fe diffusion could be decreased by 95 %. Furthermore, almost all Ni diffusion was inhibited already with a 30 nm film. Unfortunately, significant Cr, Mn and Mg diffusion could be detected even through a 300 nm film.

2.2.4.4 Multilayer and mixture coatings

Nanolaminates and mixtures have not been studied for prevention of diffusion in Li-ion batteries or CIGS solar cells. The main objective in using complex structures in diffusion barriers for Cu interconnects has been to allow direct electroplating of Cu onto the barrier.[178-181,183] Currently, PVD copper seed layers have to be deposited on the barrier for the electroplating.[62] This approach has the same challenge as PVD barriers: the conformality is not sufficient for the future devices. Direct electroplating of Cu on ALD Ru has been shown,[179,182] but the barrier properties of Ru are poor.[177] Therefore, the work on laminates and mixtures as diffusion barriers for Cu interconnects has focused on combining the direct electroplating properties of Ru with materials that have better barrier properties. Some examples include Ru-TiN,[183] Ru-TaN,[181,182] Ru-WCN,[178] Ru-TaCN[180] and Ru-Al_2O_3.[179] Because the nanolaminate or mixture structures disrupt the crystallites in the films, the barrier properties have been shown to be even better than those observed for the corresponding single layers. Also direct plating has been proven.[178-180,193] Furthermore, as Ru has excellent adhesion to Cu and the nitrides have good adhesion to Si and SiO_2, the adhesion issues encountered with the single layers could be simultaneously solved.[181,183]

Nanolaminates made of two materials with different sized crystallites can form coatings through which the diffusion path is more tortuous, and thus improve the barrier properties. Limited research has been focused on simply inhibiting diffusion along grain boundaries with nanolaminate structures, but this has been demonstrated with TiN-WN and TiN-WNC nanolaminates.[173]

2.2.5 Summary on protective ALD coatings

Coatings deposited by ALD have been studied for protection of metals, metal alloys and metallic components in multimaterial structures against gaseous and liquid corrosives for a number of applications. The application areas encompass for instance gas permeation barriers, nanoparticles and nanostructures in general and in/on substrates for analytical tools, DSSCs and heterogeneous catalysis, biomedical devices, prevention of tarnishing in silver jewels and historical artefacts, optical components and electrodes in Li-ion batteries, MCFCs and PECs for water splitting. In addition, there has been increasing activity in fundamental research on the protection of metals and metal alloys in liquid corrosives.

The most common protective ALD coating material has been Al_2O_3. It has an almost ideal ALD process that enables deposition in a broad temperature range, excellent sealing properties, and it has been shown to nucleate well on a variety of substrates. The main challenge with Al_2O_3 is the limited chemical stability. Some susceptibility has been observed even to water and water vapour. The other widely studied material for protective ALD coatings has been TiO_2. Unlike Al_2O_3, it is chemically stable. However, depending on the deposition temperature, it has either a high impurity content or a polycrystalline structure. Therefore, it also has limited sealing properties. The other studied protective ALD materials include Ta_2O_5, SiO_2, ZnO, ZrO_2, HfO_2, AlN and TiN. Best protective properties have been achieved with coatings consisting of two or more materials instead of single layers. These coatings enable combination of beneficial properties of two materials into a single coating and disrupt through-coating defects. The most effective, and studied, combination has been Al_2O_3 and TiO_2. Al_2O_3 is used to ensure good nucleation and sealing properties, and TiO_2 to gain chemical stability.

The main parameters affecting the protective performance of ALD coatings against both gaseous and liquid corrosives have been shown to be the deposition temperature, the coating thickness and the oxygen precursor. The quality of the coatings is improved with increasing deposition temperature due to decreased impurity contents. However, with ALD materials that can become deposited in polycrystalline form, careful optimisation should be conducted between the purity and crystallinity of the coatings. Grain boundaries offer an easy route to the protected surface. The purity and adhesion of ALD coatings have been shown to improve when a more aggressive oxygen precursor than H_2O is used. However, care should be taken to ensure that the properties of the substrate are preserved. The protective properties of ALD coatings have been observed to significantly improve with increasing thickness. This has been attributed to increased coverage, closure of

defects and decreased impurity content. Furthermore, in liquid corrosives the role of the substrate pre-treatment has been raised. Only a few studies have concentrated on the topic, but it would appear that at least decreasing substrate roughness and most probably also improved cleanliness are beneficial.

Duplex coatings comprising of layers deposited by ALD and another method have been studied in protection against liquid corrosives. Two main goals have been focused on. A thin PVD layer has been used to separate the substrate and the ALD coating in order to prevent Li diffusion from the substrate to the protective layer. Also blocking of pinholes in PVD and graphene coatings with ALD has been considered.

ALD diffusion barriers have mainly been studied for Cu interconnects in microelectronics, but attention has also been given to Li-ions in batteries and diffusion of substrate species into active layers in TFEL displays and CIGS solar cells. The most studied ALD diffusion barriers for Cu interconnects and Li-ion batteries include nitrides like TiN and TaN, transition metal carbides, ternary materials like TaCN and WCN, oxides and metals. Generally similar dependencies with deposition parameters and single layers vs. multilayer and mixture structures were reported as for the corrosion protection coatings. However, the research was mostly focused on specific applications, and therefore also other material properties in addition to the diffusion barrier properties were critical. For inhibiting diffusion of substrate species into active layers in TFEL and CIGS solar cells, ALD Al_2O_3 has been studied. Only few papers exist on the topics, and thus drawing clear conclusions is challenging. It would appear that already 30–50 nm Al_2O_3 can prevent diffusion of some metals, like Na and Fe. However, even 300 nm is not enough for some metals, like Cr, Mn and Mg.

3 Experimental

A low alloy steel (AISI 52100, DIN 100Cr6) was used as the substrate. The steel was tempered at 180 °C and hardened to 805 HV hardness. The temperature range for processing the steel was limited to 160 °C for maintaining the mechanical properties. The composition of the steel was in wt.% C (0.95-1.1), Cr (1.5), Ni (max. 0.30), Mn (0.25-0.45), Cu (max. 0.30), Si (0.15-0.35), P (max. 0.030), S (max. 0.025) and Fe (balance).

3.1 Pre-treatment of the substrate

Substrate surfaces were polished using two methods: lapping and brushing. All the samples were first ground by planar grinding and then lapped. The lapping was conducted in a water based diamond suspension (6 μm). Thereafter, mechanical brushing for 1 min with Vitax polishing lathes (rotation speed 2800 rpm) using a Luxor polishing agent with a grain size of 0.1 μm was conducted for the brushed samples. The surface conditioning is indicated separately for each sample.

After mechanical surface conditioning the samples were covered with silicone oil (Sigma-Aldrich GmbH, No. 85409) to prevent corrosion prior to applying the protective coating. Then the samples were packed in plastic boxes between two polyurethane membranes and shipped to another location for coating. At the coating location the samples were degreased. Two degreasing recipes were used. In the short recipe the samples were wiped with an acetone soaked precision wipe, ultrasonicated in isopropanol for 5 min, rinsed with ethanol and blow-dried with compressed air. In the longer recipe the samples were additionally ultrasonicated in acetone for 5 min prior to ultrasonication in isopropanol.

Some of the samples were *in situ* or *ex situ* H_2-Ar plasma pre-treated prior to coating with ALD. The aim of the plasma pre-treatment was to more completely clean the sample surface from organic residues. The pre-treatments were done with a Beneq TFS-200 ALD reactor presented in detail in reference [194]. The plasma was generated with a capacitively coupled rf power source at 13.56 MHz. The reactor was operated in remote plasma configuration with a grid separating the active plasma from the substrate. The pressure and temperature in the reactor were approximately 500 Pa and 160 °C. The plasma gases, hydrogen (>99.999 %) and argon (>99.999 %), were purified on site with Aeronex Gatekeeper and Entergris Gatekeeper purifiers prior to mixing in the reactor. The short pre-treatments (5 min) were conducted with a continuous plasma exposure and the longer pre-treatments (30 min) with ALD-type pulsing to avoid excessive heating of the reaction chamber and samples. A sequence of 5 s on-pulse and 10 s off-pulse was repeated until the desired treatment time was reached. Between the *in situ* pre-treatment and the ALD process the reaction chamber was purged for 15 min with nitrogen (>99.999 %). The *ex situ* treatment additionally involved cooling the reactor to 100 °C, venting to laboratory air and moving the samples to another reactor for coating. The samples were exposed to

laboratory air (non-cleanroom conditions) for 2–3 min. The pre-treatment details and sample coding are presented in Table 5.

Table 5. *H_2-Ar plasma pre-treatment conditions.*

Code	**In situ/ex situ**	**Time** (min)	**Power** (W)	**Gas flow rates** (sccm)	
				H_2	**Ar**
In-5	In situ	5	300	30	130
In-30	In situ	30[a]	100	15	130
Ex-30	Ex situ	30[a]	170	15	130

[a]The pre-treatment was done by ALD-type pulsing (5 s on and 10 s off) and the cycle was repeated 360 times to reach the desired treatment time.

3.2 Coating deposition

In this work, three coating types were studied: ALD coatings alone, ALD coatings on thin sublayers deposited with filtered cathodic arc deposition (FCAD), and ALD films on thick PVD coatings. The ALD films were grown in Picosun SUNALE R-150 and Beneq TFS-200 ALD reactors. Most of the films were grown in R-150 and, if not otherwise stated, this is assumed in the text. The FCAD layers were grown with the DIARC-Technology Inc. equipment, and the hard PVD coatings were sputtered with the Hauzer Techno Coating BV equipment (Hauzer Flexicoat 1200).

3.2.1 Atomic layer deposition

In R-150 the deposition temperature was 160 °C and the pressure approximately 500 Pa. The inert pulsing and purging gas was nitrogen (>99.999 %). Two ALD materials were studied as protective coatings, Al_2O_3 and Ta_2O_5. The precursors for Al_2O_3 were trimethyl aluminium ($Al(CH_3)_3$, Chemtura AXION® PA 1300) and ultrapure water (resistivity > 18 MΩ cm), and the pulsing sequence was 0.1 s $Al(CH_3)_3$ pulse – 5 s purge – 0.1 s H_2O pulse – 5 s purge. The precursors for Ta_2O_5 were tantalum pentaethoxide ($Ta(OC_2H_5)_5$, SAFC Hitech™) and ultrapure water, and the pulsing sequence was 0.4 s $Ta(OC_2H_5)_5$ pulse – 5 s purge – 0.4 s H_2O pulse – 5 s purge. $Ta(OC_2H_5)_5$ was evaporated at 140 °C, and $Al(CH_3)_3$ and H_2O at room temperature (~25 °C). The growth rates of Al_2O_3 and Ta_2O_5, as measured from silicon wafers, were 0.09 and 0.04 nm/cycle. The number of cycles was chosen to reach a nominal desired thickness.

In TFS-200, the deposition temperature and pressure were the same as in R-150. The inert purging gas was argon (>99.999 %). Only Al_2O_3 coatings were grown, and the precursors and evaporation temperatures were the same as in R-150. The pulsing sequence was 0.3 s

$Al(CH_3)_3$ pulse – 1 s purge – 0.35 s H_2O pulse – 1 s purge. The Al_2O_3 growth rate was 0.10 nm/cycle, as measured from silicon wafers.

All the ALD coatings discussed in the present overview, reactors used to deposit them, coding and nominal thicknesses are presented in Table 6.

Table 6. *ALD coatings deposited on low alloy steel.*

Code	ALD reactor	Coating material	Nominal thickness
A10	R-150	Al_2O_3	10 nm
A50	R-150	Al_2O_3	50 nm
A100	R-150	Al_2O_3	100 nm
TFS-A50	TFS-200	Al_2O_3	50 nm
T10	R-150	Ta_2O_5	10 nm
T50	R-150	Ta_2O_5	50 nm
A5-T5_40	R-150	Al_2O_3-Ta_2O_5 nanolaminate	4 × (5 + 5) nm
A10-T10_40	R-150	Al_2O_3-Ta_2O_5 nanolaminate	2 × (10 + 10) nm
A20-T20_40	R-150	Al_2O_3-Ta_2O_5 nanolaminate	1 × (20 + 20) nm
A12.5-T12.5_50	R-150	Al_2O_3-Ta_2O_5 nanolaminate	2 × (12.5 + 12.5) nm
A10-T10_80	R-150	Al_2O_3-Ta_2O_5 nanolaminate	4 × (10 + 10) nm
A20-T20_80	R-150	Al_2O_3-Ta_2O_5 nanolaminate	2 × (20 + 20) nm
AT11_50	R-150	$Al_xTa_yO_z$ mixture (Al_2O_3:Ta_2O_5 cycling 1:1)	50 nm
AT13_50	R-150	$Al_xTa_yO_z$ mixture (Al_2O_3:Ta_2O_5 cycling 1:3)	50 nm
AT15_50	R-150	$Al_xTa_yO_z$ mixture (Al_2O_3:Ta_2O_5 cycling 1:5)	50 nm

3.2.2 Duplex coatings

Two types of duplex coatings were studied. Thin FCAD Ta:O sub-layers were used as a buffer to separate the ALD process from the steel surface. A more precise control of the substrate-coating interface was targeted. The FCAD films were grown as described in reference [195]. First the samples were etched *in situ* with 350 eV Ar^+ ions at 0.5 $mAcm^{-2}$ current density for 30 min. Then the Ta:O films were grown by vaporizing tantalum from a cathode target with an arc in the presence of low partial pressure of oxygen. The formed plasma expanded away from the cathode target at high velocity, and thus the coating species collided with the substrate with high ion energies. The deposition temperature was <100 °C. The duplex coatings with FCAD sublayers are presented in Table 7.

Table 7. *Duplex FCAD-ALD coatings grown on low alloy steel.*

Code	FCAD Ta:O nominal thickness	ALD layer
F-T10	10 nm	-
F-T50	50 nm	-
F-T10-laminate	10 nm	A12.5-T12.5_50
F-T10-mixture	10 nm	AT13_50

ALD films were also used to block pinholes in unbalanced magnetron (UBM) sputtered CrN coatings. The deposition temperature was 180 °C. The duplex coatings with the UBM sputtered CrN are presented in Table 8.

Table 8. *ALD sealed PVD CrN coatings on low alloy steel.*

Code	UBM sputtered CrN nominal thickness	ALD layer
CrN	2.44 µm	-
CrN-laminate	2.44 µm	A12.5-T12.5_50
CrN-mixture	2.44 µm	AT13_50

3.3 Characterisation

Thicknesses of the ALD coatings were determined from silicon wafers coated simultaneously with the steel samples. The thicknesses of <50 nm single layers and nanolaminate and mixture coatings were determined with X-ray reflection (XRR, Bruker AXS D8 Advance) and modelled with Leptos 7.03. or 7.05. The structure used for modelling consisted of a Si substrate, 1.5 nm SiO_2 native oxide, and the ALD film. The thicknesses of the ≥50 nm single layer coatings were measured with ultraviolet-visible (UV-Vis) reflectance spectrophotometry (Hitachi U-2000) and modelled with the software by Ylilammi and Ranta-aho.[196] The structure used for modelling consisted of a Si substrate and the ALD film.

Morphology of selected samples was studied with field emission scanning electron microscope (FESEM, Hitachi S-4800) and transmission electron microscope (TEM, Philips CM20 analytical TEM). The sample thinning for TEM consisted of the following steps: cutting the samples, embedding into a Ti-holder, mechanically grinding and polishing, milling with 10 keV Ar^+ ions, and finally milling with 3 keV Ar^+ ions.

Composition of selected samples was studied with time-of-flight elastic recoil detection analysis (ToF-ERDA) and time-of-flight secondary ion mass spectrometry (ToF-SIMS). The ToF-ERDA measurements were done with a 1.7 MV Pelletron accelerator using 5.0 MeV ^{35}Cl and 9.9 MeV ^{35}Cl ions. An Iontof 5 spectrometer was used for the ToF-SIMS measurements. The analysis was done with a pulsed 25 keV Bi^+ primary ion source and the depth profiling by sputtering with 1–2 keV Cs^+ beam. The pressure was 10^{-7} Pa. Ion-

Spec software was used for the data acquisition and post-processing analysis. Negative ion profiles were recorded due to their sensitivity to fragments originating from oxide matrixes.

Energy dispersive X-ray spectrometry (EDS) was used for elemental mapping of the cross section of a defect site. The cross section was prepared by focused ion beam (FIB) milling. A FEI Quanta 3D 200i Dual-Beam FIB/SEM microscope equipped with an Omniprobe nanomanipulator was used for lift-out preparation and cross section imaging. For the analysis an Oxford Instruments X-max 50 mm^2 SSD Detector with INCA 350 Analyzer was used. The spatial resolution and surface sensitivity were improved by using a 5 kV electron beam.

The electrochemical responses of all uncoated and coated low alloy steel samples were studied with LSV. Additionally, a number of samples were studied with open circuit potential (OCP) and electrochemical impedance spectroscopy (EIS) measurements. The electrochemical measurements were done with an Autolab PGSTAT30 potentiostat/galvanostat in a conventional three-electrode cell with a saturated calomel electrode (SCE) as the reference and a platinum counter electrode. The working electrode area was restricted to 0.44 cm^2 with a Viton o-ring. The solution was 0.2 M NaCl (Analar Normapur analytical reagent, VWR® BDH Prolabo®) at pH 7.2±0.2. For testing the long-term performance of the coatings in acidic solutions, the pH was decreased to 2 with HCl (HCl 37 % Analar Normapur analytical reagent, VWR® BDH Prolabo®). The solutions were deaerated by bubbling with argon for 30 min before starting the measurements and the bubbling was continued throughout the measurements. The LSV measurement range was from -0.9 to 0 V or until the current density exceeded 0.01 $mAcm^{-2}$. The scan rate was 1 mVs^{-1}. If OCP and EIS measurements were done, they always preceded the more destructive LSV measurement. First the OCP measurement was conducted to reach a stable potential. Thereafter the EIS measurement was performed at OCP in the frequency range of 10^5 and 10^{-2} Hz with a 10 mV exciting signal.

The corrosion durability of the samples was studied with neutral salt spray (NSS) testing. The testing was conducted according to the standard DIN 50021 (ISO 9227) with the exception that the samples were removed from the testing chamber for photographing after regular intervals. The testing was continued after photographing if complete bleeding of the sample was not observed. The temperature, pH, and NaCl concentration were kept constant throughout the experiments at 35±0.2 °C, 6.5–7.2 and 50±5 g/l, respectively.

4 Results and discussion

The main experimental results are presented in this section. Detailed results on all studied coatings and more thorough discussion on the results can be found in the corresponding publications.[I-IX]

The thicknesses of all ALD coatings reported in this work were within 8 % of the nominal thicknesses as determined by UV-Vis spectrophotometry and XRR from films grown on silicon simultaneously with the steel.[I-IX] However, it should be noted that the actual thicknesses of the coatings on steel might slightly differ due to issues related to reactive surface groups and nucleation.[22-24]

4.1 Pre-treatment of the substrate

The influence of the substrate surface on the properties of ALD films is well established in the literature.[22-24,122,123] On metals and metal alloys the surface roughness has been proposed as one of the most influential parameters.[24,122,123] In addition, we considered the purity of the surface vital. Therefore, the effects of the mechanical surface conditioning and substrate cleaning with the H_2-Ar plasma pre-treatment on the protective properties of the ALD coatings were studied.

4.1.1 Mechanical surface conditioning

The mechanical surface conditioning prior to ALD was done by either lapping or brushing. In FESEM the lapped steel surface appeared significantly rougher than the brushed one (Figure 9). In addition, on the lapped surface some scratches seemed to be partially covered over resulting in a 'pocket' formation. These types of structures were not seen on the brushed samples. Both lapped and brushed surfaces contained some unidentified foreign particles (not shown here).

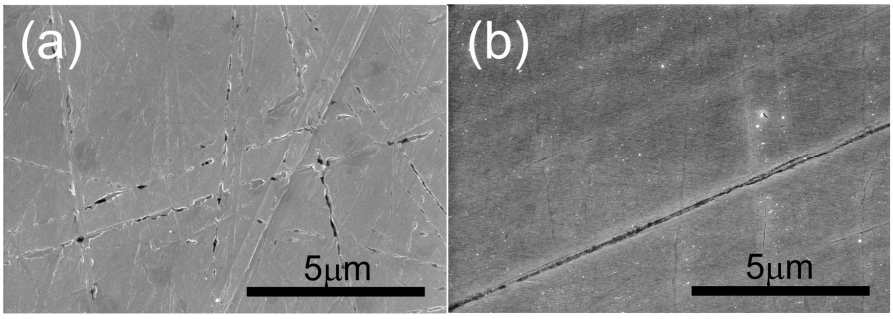

Figure 9 *FESEM images of uncoated (a) lapped and (b) brushed low alloy steel.*

In the LSV measurements the uncoated lapped and brushed surfaces had slightly differing properties (Figure 10a). The corrosion potential of the brushed steel was higher than that of the lapped steel. Also the composition of the native oxides was seen to differ at the ALD coating-steel interfaces in ToF-SIMS depth profiles.[VII] On both samples, the interface contained iron and chromium oxide species accumulated under ambient exposure and possibly also during the first ALD cycles. However, on the brushed steel a bilayer interface was formed consisting of an inner iron-rich Fe and Cr oxide and an outer Fe oxide layer. The bilayer formation was attributed to overheating of the steel surface during brushing, and it could account for the difference in the LSV response of the uncoated steels. However, the corrosion current densities of the lapped and brushed steels were close to each other indicating similar corrosion rates.[1]

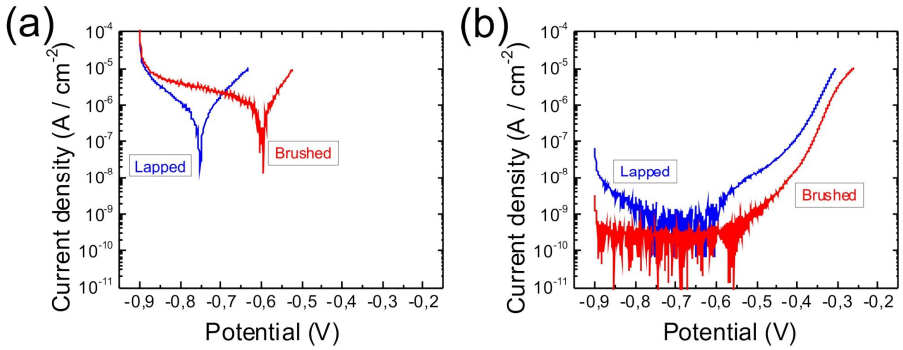

Figure 10 *LSV results in neutral 0.2 M NaCl solution on (a) uncoated and (b) ALD Al_2O_3 coated (A50) lapped and brushed low alloy steel.*

A 50 nm ALD Al_2O_3 coating significantly decreased the current density of both lapped and brushed steel in the measured potential range (Figure 10b). Lower current density, i.e. lower corrosion rate,[1] was achieved with Al_2O_3 on the brushed steel surface. The more protective nature of the ALD coatings on brushed steel was verified also with EIS measurements.[VII] On brushed steel the coatings had higher charge transfer and pitting resistances than the corresponding coatings on the lapped steel. In addition, the coating capacitance was more stable during immersion in an aggressive solution indicating better resistance to pit formation and enlargement. The better performance of the coatings on the brushed surface was mainly attributed to decrease in the number of mechanically fragile sites, which can promote defect formation after the ALD growth by detachment of conformally coated particles and/or steel flakes.

4.1.2 Plasma pre-treatment

In the literature the metal plates are commonly polished and thereafter degreased in organic solvents prior to growing protective ALD coatings on them.[37,49,113,114,116-119,122,123,130] This type of treatment can leave organic contamination on the metal surface, which may lead to unideal ALD film nucleation. In order to evaluate the effect of the

chemical purity of the substrate on the protective properties of the ALD coatings, the pre-treatment of steel surfaces with H_2-Ar plasma was studied.[I] The aim was to decrease the amount of carbon contamination and possibly reduce the native oxide of the steel.[197-199] The work was done on the lapped steel surfaces degreased with the longer recipe. The *in situ* depositions were made with the TFS-200 reactor and the *ex situ* depositions with the R-150 reactor.

ToF-SIMS depth profiles of OH^-, C^- and FeO_2^- species in 50 nm ALD Al_2O_3 coatings on low alloy steel are presented in Figure 11.[I] The purities of the ALD coatings can be qualitatively compared by considering the OH^- and C^- intensities.[32] The FeO_2^- represents the interfacial steel oxide layer. The effects of 5 and 30 min *in situ* and 30 min *ex situ* H_2-Ar plasma pre-treatments to the compositions of the ALD coatings and the coating-steel interfaces were evaluated. The interface was identified to start at the point where the FeO_2^- intensity rapidly increased. This is marked with a dashed line. In the untreated sample a homogeneous in-depth composition was observed for the OH^- impurities in the bulk of the Al_2O_3 coating (Figure 11). A rapid increase occurred at the outer surface indicating that water from the ambient penetrated into the ALD coating.[150] The C^- content seemed to increase when approaching the interface. This might be due to a more defective film growth in the early stages of the deposition and/or film growth on a rough carbon-contaminated surface. In the interface clear peaking of OH^- and FeO_2^- were seen, and the C^- content rose to a higher level. This indicated that the steel surface was oxidised during ambient exposure and/or during the first ALD cycles, and that carbon contamination was found at the steel surface.

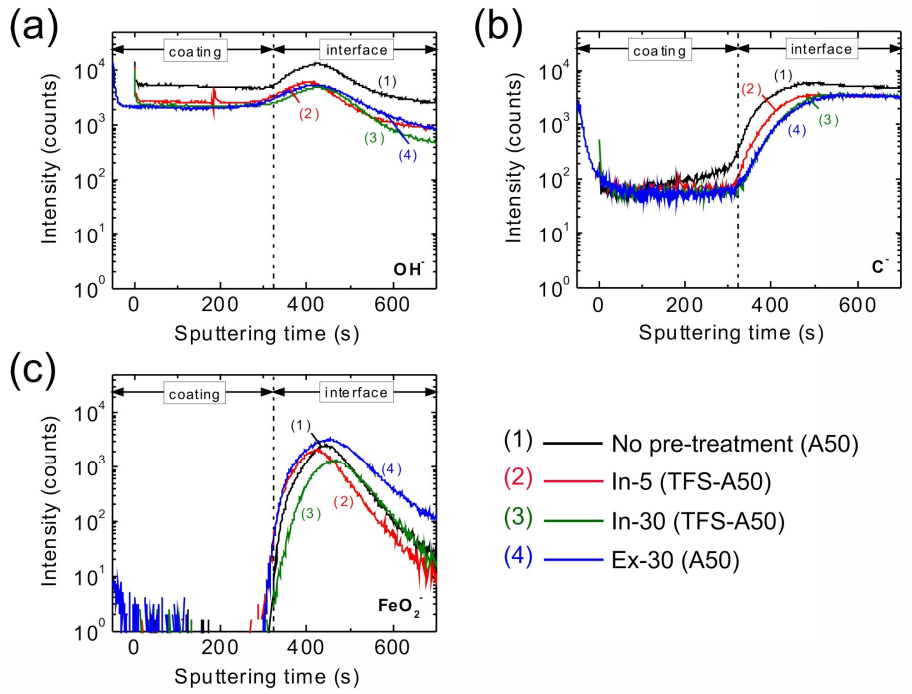

Figure 11 *ToF-SIMS depth profiles of (a) OH^-, (b) C^- and (c) FeO_2^- in a low alloy steel coated with ALD Al_2O_3 (A50 and TFS-A50) after different H_2-Ar plasma pre-treatments.*

In the H_2-Ar plasma pre-treated samples the OH^- content was significantly lower in the bulk of the ALD coatings (Figure 11).[I] Usually this would indicate more complete deposition reactions leading to a lower impurity content.[5] However, as it is quite difficult to understand how the plasma pre-treatment could affect the growth steadily throughout the film depth, the cause of the lower hydroxyl content was suggested to be decreased water absorption from the ambient.[150] This implies that the ALD coatings on the plasma pre-treated steel were denser and therefore inhibited water penetration more effectively. No clear differences in the OH^- profiles could be observed between the different pre-treatment procedures.

The C^- impurity content in the H_2-Ar plasma pre-treated samples had a homogeneous in-depth composition (Figure 11).[I] This implied that either the growth in the beginning of deposition was improved and/or that the carbon contamination at the steel surface was effectively decreased by the pre-treatment. Regardless of the exact mechanism, the ALD coating purity was clearly improved. A decrease of the C^- intensity in the interface region could also be observed indicating that at least some carbon contamination left of the steel surface after degreasing could be removed with the plasma pre-treatment. A slight enhancement of the C^- impurity removal could be achieved with increasing pre-treatment time. No difference could be seen between the *in situ* and *ex situ* procedures, which was slightly surprising considering that the *ex situ* pre-treated samples were exposed to laboratory air and handled prior to coating.

The FeO_2^- peak at the interface was not significantly changed by the H_2-Ar pre-treatment (Figure 11).[I] This indicated either that the native oxide was not reduced by the pre-treatment, that the oxide layer was regrown before the ALD growth or both. Because a continuous plasma pre-treatment without a waiting time in between the pre-treatment and ALD growth in another reactor clearly decreased the Fe and Cr oxide peaks at the interface, at least partial reduction of the native oxide was indicated.[I] After the continuous plasma pre-treatment the interfacial oxide layer was regrown when the *ex situ* procedure with a short air exposure was applied. Furthermore, the thickness of the interfacial oxide layer in the pulsed plasma pre-treatment presented here appeared slightly wider with the *ex situ* procedure (Figure 11).

The *in situ* H_2-Ar plasma pre-treatment clearly improved the electrochemical protective properties of 50 nm ALD Al_2O_3 coatings (Figure 12).[I] In the LSV measurement the current density was decreased by one order of magnitude over the whole tested potential range. A slightly better performance was achieved with the longer 30 min pre-treatment compared to the 5 min one. The Al_2O_3 coating on the *ex situ* pre-treated steel appeared to have similar protective properties as the Al_2O_3 coating on the untreated steel. However, clearly improved durability during immersion in an aggressive solution was shown with EIS for an ALD Al_2O_3-Ta_2O_5 nanolaminate on an *ex situ* H_2-Ar plasma pre-treated steel compared to steel without pre-treatment.[VII] The initial resistance to corrosion was improved, and the protective properties were degraded less during the immersion.

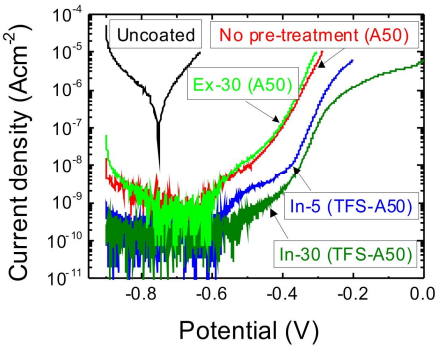

Figure 12 *LSV results in neutral 0.2 M NaCl solution on a low alloy steel coated with ALD Al_2O_3 (A50 and TFS-A50) after different H_2-Ar plasma pre-treatments.*

It would appear that the H_2-Ar plasma pre-treatment cleaned some of the carbonaceous contamination from the steel surface.[I] This led to lower impurity contents in the ALD films, and thus a denser coating structure.[32] Both the barrier properties and durability of the ALD coatings were enhanced. The shown reduction of carbonaceous contamination from the interface and C^- and OH^- impurities from the bulk of the ALD coatings would seem to be the main attributing factors. The chemically cleaner surface was suggested to allow more ideal nucleation paths and therefore result in better quality ALD films. The adhesion of the ALD coatings on the steel surface was also qualitatively shown to be improved.[I]

4.2 Atomic layer deposited coatings

4.2.1 Aluminium and tantalum oxide

Al_2O_3 and Ta_2O_5 were chosen as the ALD coating materials because both materials are amorphous as deposited,[8,9,200] Al_2O_3 is known to be a good insulator,[151] and Ta_2O_5 has good chemical stability.[35,47] Additionally, well-known ALD processes exist for both materials.[8,9,200] Single layer Al_2O_3 and Ta_2O_5 coatings on low alloy steel were deposited with the R-150 reactor (Table 6). The mechanical surface conditioning was done by lapping and prior to ALD the samples were degreased with the short recipe without plasma pre-treatment.

The composition of the ALD Al_2O_3 and Ta_2O_5 films on silicon deposited at 160 °C were studied with ToF-ERDA (Table 9).[V] The stoichiometries of the films were close to nominal: O/Al=1.6 for Al_2O_3 and O/Ta=2.5 for Ta_2O_5. Carbon, hydrogen and nitrogen impurities were found. The carbon impurities are usually attributed to incorporation of partially unreacted metal precursor ($Al(CH_3)_3$ and $Ta(OCH_2CH_3)_5$) species into the growing film.[5] The hydrogen can be similarly incorporated from the unreacted metal precursors, but water is another possible source. The origin of the nitrogen impurity in Ta_2O_5 is hitherto unknown. The Al_2O_3 film was purer than Ta_2O_5. This was expected, as a similar trend has also been observed previously at 250–300 °C.[32] Also the increase in impurity content with decreasing deposition temperature was significantly higher for Ta_2O_5 than Al_2O_3. This is most likely due to the very reactive nature of $Al(CH_3)_3$,[9] leading to more complete reactions even at the relatively low deposition temperature adopted in this work.

Table 9. *ToF-ERDA results on ALD Al_2O_3 and Ta_2O_5 coatings deposited on silicon at 160 °C.*

Material	**Al** (at.%)	**Ta** (at.%)	**O** (at.%)	**H** (at.%)	**C** (at.%)	**N** (at.%)
Al_2O_3	36 ± 3	–	59 ± 4	5 ± 1	0.5 ± 0.1	–
Ta_2O_5	–	23 ± 3	57 ± 6	15 ± 3	5 ± 2	1.0 ± 0.5

The depth profiles of the pristine 50 nm ALD Al_2O_3 and Ta_2O_5 coatings on low alloy steel were studied with ToF-SIMS (Figure 13).[II-IV] In both samples the ALD coating was clearly distinguishable from the interface and steel substrate. The bulk ALD coatings were characterised by the AlO_2^-, Al^-, TaO_2^-, Ta^- and O^- signals. On the other hand, the substrate was characterised by the FeO_2^-, Fe^-, CrO_2^- and Cr^- signals. The sputtering time at which the signals of the most prominent substrate species (Fe^- and FeO_2^-) increased, i.e. the start of the interface region, is marked with a dashed line across the images.

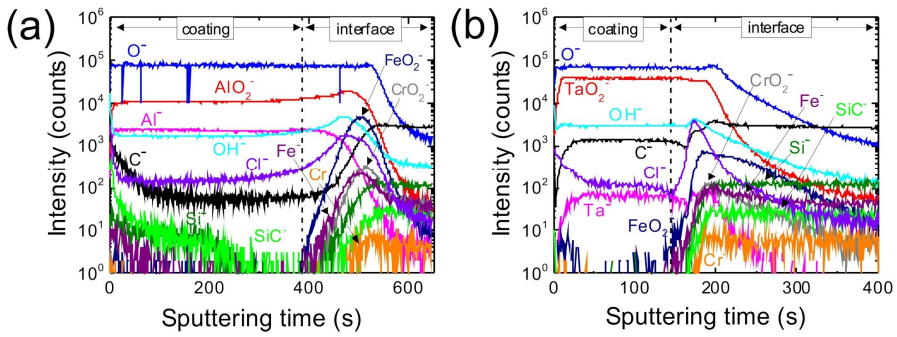

Figure 13 *ToF-SIMS depth profiles of pristine ALD (a) Al_2O_3 (A50) and (b) Ta_2O_5 (T50) coated low alloy steel.*

The ALD coatings had homogeneous in-depth composition (Figure 13).[II-IV] In the ALD coating regions C^-, OH^- and Cl^- impurities were observed in addition to the film species. Observation of the C^- and OH^- impurities corroborates with the ToF-ERDA results. Observation of the Cl^- impurities was surprising and is expected to be low as only small amounts of chlorine can be found in the used precursors (≤0.01 wt.% in $Al(CH_3)_3$, 0 wt.% in $Ta(OCH_2CH_3)_5$). The technique would appear to be extremely sensitive to chloride as in both Al_2O_3 and Ta_2O_5 on steel the Cl^- content has been found to be below the detection limit of x-ray photoelectron spectroscopy (<0.5 at.%).[II,IV] Small amounts of Si^- and SiC^- were found in the ALD coating-steel interfaces and in the bulk ALD coatings. This implies that the silicone oil used for protecting the steel surfaces during shipping was not adequately removed by the shortened degreasing without plasma pre-treatment. The clear peaking of FeO_2^- and CrO_2^- at the interface indicated that the steel surface was oxidised during exposure to ambient and/or the first ALD cycles.

The sealing properties of ALD Al_2O_3 coatings on low alloy steel were excellent (Figure 14).[II] The corrosion current density was decreased by one to four orders of magnitude with 10 to 100 nm thick coatings, and the corrosion potential was slightly increased. This indicated a decreased corrosion rate, and an ennoblement of the coating-substrate system.[1] These results were expected based on previous results on corrosion protection of metals[26,113,114,117-119] and the generally excellent insulating properties of ALD Al_2O_3.[151] Similar to what was observed previously on stainless steel, the sealing properties of ALD Ta_2O_5 were less impressive.[113] This can be partly attributed to the intrinsically poorer insulating properties of Ta_2O_5.[151] However, the effects of the higher impurity contents and challenges in nucleation of Ta_2O_5 compared to Al_2O_3 at the quite low deposition temperature cannot be excluded.[II-V] Both 10 and 50 nm Ta_2O_5 coatings afforded an approximately one order of magnitude decrease in the corrosion current density.[IV] Contrary to what was previously observed on stainless steel,[113] the protective properties were not significantly affected by the increased coating thickness. The exact cause for this is not known, but it is possible that the impure 50 nm ALD Ta_2O_5 coating deposited at 160 °C was still too thin to sufficiently seal the steel surface. Better results could possibly be obtained by further increasing the coating thickness.

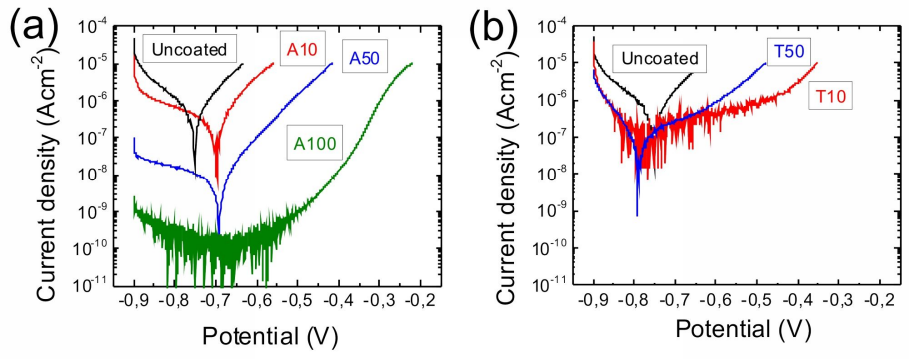

Figure 14 *LSV results on ALD (a) Al_2O_3 and (b) Ta_2O_5 coated low alloy steel in neutral 0.2 M NaCl solution.*

In order to study the corrosion durability of the ALD coated steel during exposure to aggressive conditions the samples were immersed in neutral and acidic 0.2 M NaCl solutions.[III,IV] The corrosion development was monitored with ToF-SIMS and EIS. The ToF-SIMS measurements were conducted prior to (Figure 13) and after testing (Figure 15) and the EIS measurements during the last 10 min of every hour of immersion up to six hours (Figure 17).

The ToF-SIMS depth profile of 50 nm ALD Al_2O_3 coated low alloy steel after immersion in neutral 0.2 M NaCl solution for 6 hours is presented in Figure 15a.[III] The sputtering time needed to reach the substrate appeared to be significantly shorter than before the immersion (cf. Figures 13a and 15a). Although the actual coating thickness cannot be reliably determined from the ToF-SIMS data, a comparative analysis between the depth profiles before and after immersion suggested that the Al_2O_3 coating dissolved during the immersion. The composition of the ALD coating was quite similar before and after the immersion. The most notable difference was the increase of the Cl^- content in the bulk coating and especially at the coating-steel interface, which indicated that chloride from the solution penetrated through the ALD coating. A simultaneous decrease of OH^- suggested substitution of hydroxyls with chloride. This is a typically suggested mechanism for passive film breakdown and inhibition of repassivation.[201,202] We have found that ALD Al_2O_3 on silicon with a native oxide is quite stable in a neutral 0.2 M NaCl solution (Figure 16). Furthermore, Marin et al.[118] have shown a good long-term stability for ALD Al_2O_3 on stainless steel in a 0.2 M NaCl solution. Therefore, it is suggested that the reduction of oxygen at the active and non-passivating low alloy steel surface resulted in a local increase of pH at defected sites of the ALD coating, and led to the observed dissolution of Al_2O_3. The interface and substrate appeared almost unchanged after the immersion. Only a slight enrichment of iron compared to chromium oxides was observed at the interface.

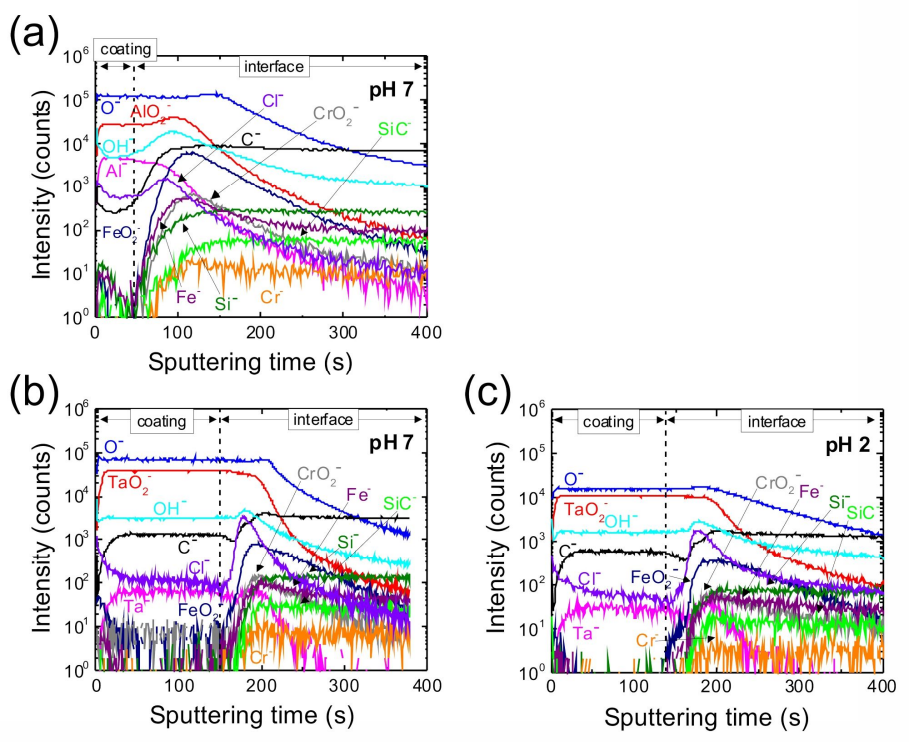

Figure 15 *ToF-SIMS depth profiles of ALD (a) Al_2O_3 (A50) and (b and c) Ta_2O_5 (T50) coated low alloy steel after immersion for 6 h in (a and b) neutral and (c) acidic 0.2 M NaCl solutions.*

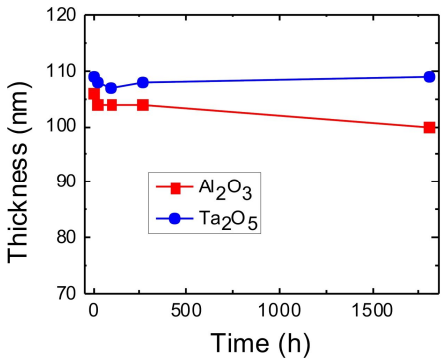

Figure 16 *Change of thickness in ALD Al_2O_3 and Ta_2O_5 films on undoped silicon during immersion in neutral 0.2 M NaCl solution.*

In the ToF-SIMS depth profiles the ALD Ta_2O_5 coated low alloy steel appeared almost unchanged during immersion in neutral and acidic 0.2 M NaCl solutions (cf. Figures 13b and 15b and c).[IV] The sputtering time needed for reaching the interface and substrate regions were similar indicating chemical stability. In the neutral solution the only change was the appearance of some FeO_2^- and CrO_2^- in the bulk Ta_2O_5 region. This suggested that aggressive species reached the interface and accumulation of corrosion products occurred at defected sites. However, the intensities of the steel oxide signals in the Ta_2O_5 coating region were very low. In the acidic solution no corrosion products of steel were seen in the

Ta_2O_5 coating region, which suggested that any oxidised species were dissolved. This conclusion was supported by the fact that the interfacial region appeared to extend deeper into the steel substrate implying an increased roughness due to active corrosion.

Bode plots of the EIS results measured during the immersion of the uncoated and ALD coated low alloy steel samples are presented in Figure 17.[III,IV] The initial and changed protective properties of the coatings and the corrosion process on the exposed steel surface can be quite specifically modelled from the EIS results with equivalent circuits. Details on this type of analysis on the corrosion of Al_2O_3 and Ta_2O_5 coated steels is given in publications [III] and [IV]. Here only the most prominent conclusions are presented.

In the beginning of the immersion in neutral 0.2 M NaCl solution the 50 nm ALD Al_2O_3 coating appeared to protect the steel very efficiently.[III] The global impedance was very high as evidenced in the Bode plot by the low frequency range (Figures 17a). Furthermore, the capacitive range with phase angles nearly equal to 90° extended almost through the whole measured frequency range, which is characteristic for good quality coatings.[26] The excellent initial protective properties exhibited by the ALD Al_2O_3 coatings corroborated the results obtained in literature[26,113,114,117-119] and with LSV (Figure 14). However, the Bode plots changed drastically during immersion (Figure 17a). The global impedance at low frequencies was decreased, and the phase angle at high and middle frequencies deviated from the capacitive response. These changes were attributed to decreased charge transfer resistance (middle frequencies) and to decreased resistance against redox reactions at the bottom of pinholes exposing the steel surface (high frequencies).[203] The decrease of charge transfer resistance has been shown to correlate with increased porosity.[II] Furthermore, the coating capacitance was increased, which indicated decreased coating thickness. The decrease in coating thickness during immersion was also observed with ToF-SIMS (Figure 15). Thus initially the ALD Al_2O_3 coating protected the steel well, but the protective properties were rapidly decreased by both local and general dissolution of the coating. An average dissolution rate of 7 nm/h was calculated for ALD Al_2O_3 on low alloy steel from the ToF-SIMS and EIS results.[III]

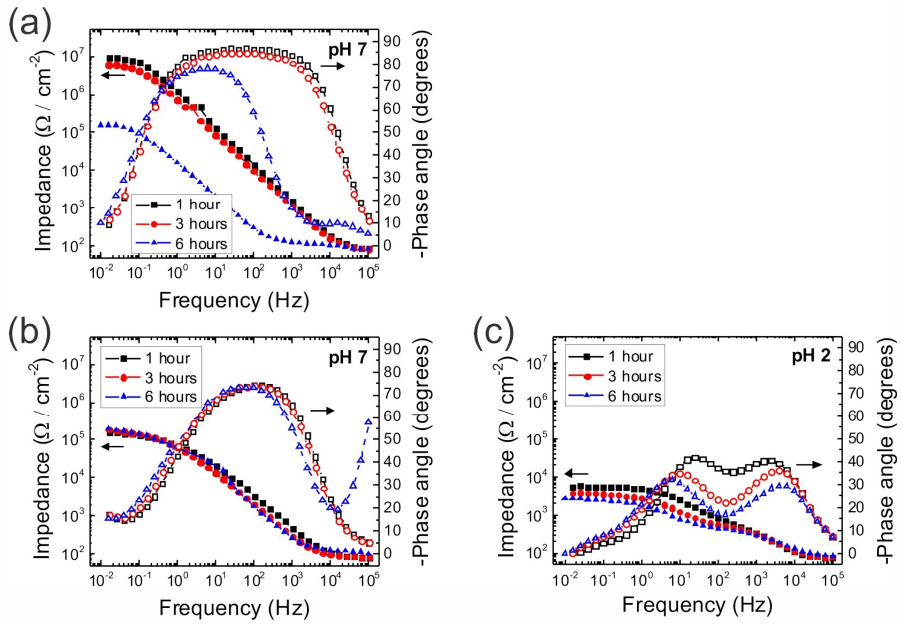

Figure 17 *EIS results as Bode plots for ALD (a) Al_2O_3 (A50) and (b and c) Ta_2O_5 (T50) during immersion in (a and b) neutral and (c) acidic 0.2 M NaCl solutions.*

The initial protective properties of the 50 nm ALD Ta_2O_5 coatings were slightly less impressive than those achieved with the Al_2O_3 coatings (Figure 17b).[IV] This is in agreement with literature[113] and the LSV results (Figure 14). However, different from the Al_2O_3 coated steel, the Ta_2O_5 coated steel appeared more stable during the immersion. Only a slight increase of the global impedance and changes in the phase angle at high frequencies could be seen. The increased global impedance was attributed to the accumulation of corrosion products on the steel surface at the defected sites of the Ta_2O_5 coating, as corroborated by the oxide species of steel observed with ToF-SIMS (Figure 15). However, a slight increase of capacitance, which included the combined contribution from both the Ta_2O_5 coating and double layer capacitance, implied a local breakdown of the Ta_2O_5 coating and increased porosity. Thus, it was concluded that the ALD Ta_2O_5 coating was generally stable in the neutral NaCl solution, but the porosity of the coating was increased leading to increased local corrosion.

In the acidic NaCl solution, the ALD Ta_2O_5 coating (Figure 17c) protected the low alloy steel significantly less efficiently than in the neutral solution.[IV] The global impedance was lower, and it was further decreased throughout the immersion. The phase angle changed over the whole frequency range. The Bode plots could be roughly divided into three frequency ranges, from which contributions of different processes could be determined:[204-206] the changes at low frequencies (mHz) were attributed to adsorption of intermediate corrosion products at the bottom of pinholes, the changes in the middle frequencies (Hz) to the global corrosion rate, and the changes in the high frequencies (kHz) to local corrosion by pitting. The contributions from the adsorption of corrosion products were exempted from the modelling. However, the relatively fast onset of corrosion product

accumulation indicated significant local corrosion. The significant decrease of the global impedance, and the changes in the middle and high frequencies indicated increased global corrosion rate and pitting. The increased pitting was confirmed by the decrease of the coating capacitance and increase of the double layer capacitance, which were attributed to a significant increase of the exposed steel surface fraction by formation of new pits and/or enlargement of existing ones. The steel surface was concluded to be under significant local corrosion although the Ta_2O_5 coating itself was stable.

Marin et al.[118] have reported stable corrosion protection performance for ALD Al_2O_3 and TiO_2 coated stainless steel during immersion in neutral 0.2 M NaCl solutions. They tested the electrochemical performance up to 500–2000 h. Almost no changes were seen on the Al_2O_3 coated stainless steel. On the TiO_2 coated stainless steel some changes were seen during the first 24 h, but thereafter the system stabilised for the remaining time. The stable performance of ALD Al_2O_3 and TiO_2 was similar to what was observed in this work for the ALD films on the silicon substrate (Figure 16). As explained above, the differences to the present results on low alloy steel are attributed to the characteristics of the substrates. The absence of available electrons on the passive native oxides films on silicon and stainless steel[1] may prevent the cathodic reduction of oxygen. The pH at the bottom of pinholes is therefore probably not increased similarly as on the low alloy steel, and the Al_2O_3 coating is stable, as expected in the neutral NaCl conditions.[35]

The NSS durability of the 50 nm ALD Al_2O_3 and Ta_2O_5 coated low alloy steel corroborated the LSV and immersion test results (Figure 18).[V,VI] The Al_2O_3 coating protected the steel initially very effectively. However, after 24 h the whole steel surface was bleeding indicating severe corrosion. In the light of the immersion test results it is likely that all or almost all of the ALD Al_2O_3 had dissolved from the steel surface at this point. The Ta_2O_5 coated steel had some corrosion spots already after 2 h, but the coating clearly protected the surface still after 24 h. This is in agreement with the poorer sealing properties and higher chemical stability of ALD Ta_2O_5 compared to Al_2O_3.[35,47,113,151]

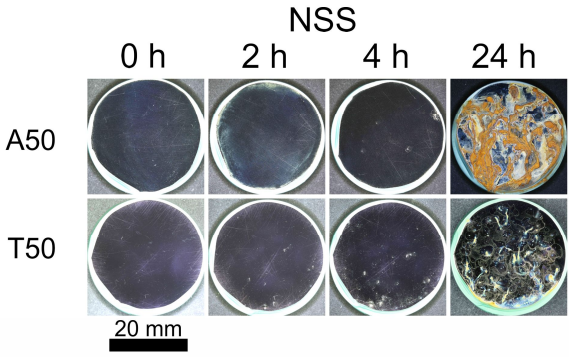

Figure 18 *NSS test results on low alloy steel coated with 50 nm ALD Al_2O_3 (A50) and 50 nm Ta_2O_5 (T50).*

4.2.2 Multilayer and mixture coatings

Improvement of the long-term performance of protective ALD coatings on low alloy steel was studied by combining the sealing properties of Al_2O_3 with the chemical stability of Ta_2O_5.[V,VI,VII] In literature, similar studies can be found for coatings combining Al_2O_3 and TiO_2.[19,26,97,114,117,119] Both Al_2O_3-Ta_2O_5 nanolaminates and $Al_xTa_yO_z$ mixtures were prepared and their architecture was optimised for the best protective properties.[V,VI] The performance was evaluated with LSV measurements and NSS testing. The nanolaminate structure optimisation was done on the lapped steel surfaces degreased with the short recipe without plasma pre-treatment. For the optimisation of the mixture composition, brushed steel surfaces cleaned with the longer recipe and *ex situ* plasma pre-treatment (Ex-30) were applied. The studied structures are presented in Table 6.

The sealing performance of the Al_2O_3-Ta_2O_5 nanolaminates was found to be dependent on both the total laminate thickness and the number of bilayers (Figure 19a).[V] This is different from what was observed previously with Al_2O_3-TiO_2 nanolaminates, for which no clear dependencies with the number of bilayers could be determined.[19,26,97,114,117,119] Here, the sealing performance improved with increasing total laminate thickness as expected.[V] However, the dependence on the number of bilayers was found more complex. For nanolaminates with 40 nm total thicknesses the performance improved when increasing the number of bilayers from one to two, i.e. changing the structure from 20 nm Al_2O_3–20 nm Ta_2O_5 (A20-T20_40) to 2×(10 nm Al_2O_3–10 nm Ta_2O_5) (A10-T10_40). Further increase of the number of bilayers to four (A5-T5_40) was not beneficial. For the nanolaminates with 80 nm total thickness the performance was also better with two bilayers (A20-T20_80) compared to four (A10-T10_80). A similar trend has been observed for the leakage current densities and breakdown potentials of Al_2O_3-Ta_2O_5 nanolaminates on indium-tin-oxide electrodes.[151] The performance improved with increasing number of bilayers down to 5 nm thick single layers, but a further decrease of the single layer thicknesses to 2.5 nm was not beneficial. This suggested that two main factors, namely the integrity of the single layers in the nanolaminate and the number of defect interrupting interfaces, must be optimised. Those factors are however, oppositely affected by the single layer thickness: the integrity of the single layers is improved with increasing thickness,[113] but the number of interfaces for a given total thickness is increased with decreasing single layer thickness. No clear conclusions on the optimum number of bilayers could be drawn from the NSS testing.[V] Thus, based on the LSV results the optimum structure was concluded to consist of two Al_2O_3-Ta_2O_5 bilayers, i.e. A10-T10_40 for the 40 nm and A20-A20_80 for the 80 nm total thickness.

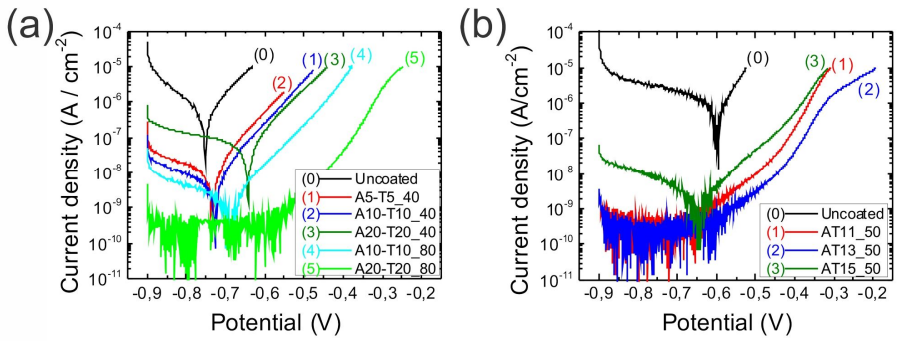

Figure 19 *LSV results on low alloy steel coated with ALD (a) Al_2O_3-Ta_2O_5 nanolaminates and (b) $Al_xTa_yO_z$ mixtures in neutral 0.2 M NaCl solution.*

According to LSV the sealing performance of the $Al_xTa_yO_z$ mixture improved with increasing Al_2O_3 content (Figure 19b).[VI] The improvement was attributed to the better intrinsic insulating properties and higher purity of ALD Al_2O_3 compared to Ta_2O_5.[32,151] However, in the NSS testing the best long-term durability was obtained with the mixture containing the highest content of Ta_2O_5.[VI] This is in agreement with the higher chemical stability of Ta_2O_5 than Al_2O_3.[35,47] The optimum mixture composition was concluded to be an approximately 1:1 mixture of Al_2O_3 and Ta_2O_5 (AT13_50).[VI]

No previous studies on ALD Al_2O_3-Ta_2O_5 nanolaminates and $Al_xTa_yO_z$ mixtures as corrosion protection coatings on metals have been done. With 100 nm ALD Al_2O_3-TiO_2 nanolaminates the corrosion current density of bare stainless steel and magnesium alloy could be decreased over three and four orders of magnitude.[114,119] The decrease of over three orders of magnitude achieved in this work with the 40 nm nanolaminate and the 50 nm mixture were comparable to the literature values.[V,VI] However, direct comparison is challenging as the substrates, coating thicknesses and testing conditions differed.

The protective performance of the optimised Al_2O_3-Ta_2O_5 nanolaminate and $Al_xTa_yO_z$ mixture was compared.[VI,VII] To ensure reliable comparison, the thicknesses of all 10 nm layers in the optimised 40 nm nanolaminate were increased by 2.5 nm so that the total thickness was increased to 50 nm similar to the mixture coating. The performance was evaluated with LSV measurements, immersion durability experiments and NSS testing. The immersion experiments were similar to those conducted for Ta_2O_5 in the acidic 0.2 M NaCl solution. The corrosion development was followed with ToF-SIMS before and after immersion and EIS measurements at the end of every hour up to six hours. All steel samples were brushed, degreased with the longer recipe and *ex situ* plasma pre-treated (Ex-30) prior to coating with ALD.

In the LSV measurements the 50 nm $Al_xTa_yO_z$ mixture appeared to have slightly better sealing properties than the corresponding Al_2O_3-Ta_2O_5 nanolaminate (Figure 20).[VI] Especially the current density at the cathodic potential range was lower. This was unexpected, as interfaces are usually thought to interrupt defects extending through the film, thereby for instance lowering leakage current densities and increasing the breakdown

potentials in thin film capacitor structures.[151] Therefore, the nanolaminate was anticipated to provide better sealing properties. A possible purifying effect of the Al_2O_3 precursor $Al(CH_3)_3$ on the rather impure Ta_2O_5 was suggested, but not verified by compositional analysis.[VI] Increased coating purity is known to result in lower corrosion current densities, i.e. reduced defect density and corrosion rate.[1,113]

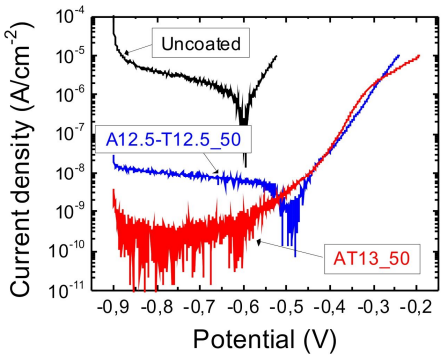

Figure 20 *LSV results on low alloy steel coated with an optimised Al_2O_3-Ta_2O_5 nanolaminate (A12.5-T12.5_50) and $Al_xTa_yO_z$ mixture (AT13_50) in neutral 0.2 M NaCl solution.*

The ToF-SIMS depth profiles of 50 nm Al_2O_3-Ta_2O_5 nanolaminate and $Al_xTa_yO_z$ mixture coated steels before and after immersion in acidic NaCl are presented in Figure 21.[VII] Before immersion the depth profiles (Figure 21a and c) appeared as expected based on the depth profiles obtained for Al_2O_3 and Ta_2O_5 coated steels (Figure 13). The coating species were clearly distinguishable from the interface and substrate, some C^-, OH^- and Cl^- impurities were seen, and a native oxide layer was observed at the interface. In the nanolaminate the different layers were distinguishable, while the mixture appeared to have a homogeneous composition. The sputtering time needed for reaching the interface was shorter for the mixture compared to the nanolaminate. This was suggested to indicate a slightly less compact film structure of the mixture,[VI] but could also have been a result of matrix effects resulting from depth profiling films with differing compositions.[207] No great changes were seen in the depth profiles after immersion (Figure 21b and d).[VII] The sputtering times needed for reaching the interface and substrate were the same implying that neither coating was generally dissolved. Also the compositions were almost identical. Slight increase of Cl^- in the outermost Ta_2O_5 layer in the ALD nanolaminate was seen, which was attributed to the higher porosity of the ALD Ta_2O_5 compared to Al_2O_3.[113] For the mixture low signals of FeO_2^- and CrO_2^- were seen in the coating region indicating some local coating breakdown and accumulation of corrosion products at the bottom of defects.

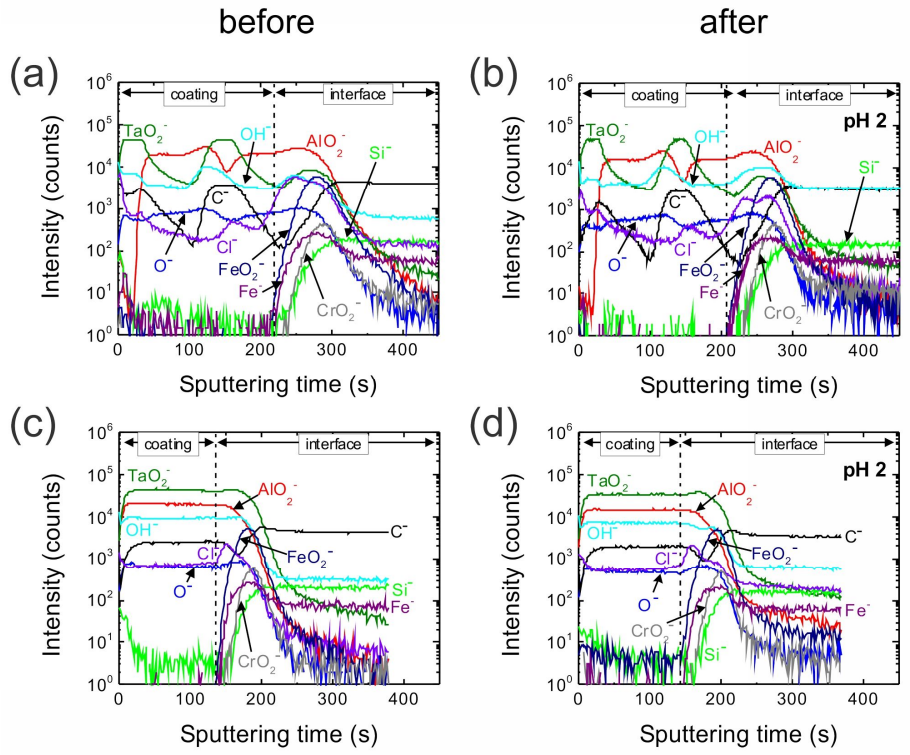

Figure 21 *ToF-SIMS depth profiles of ALD (a and b) Al_2O_3-Ta_2O_5 nanolaminate (A12.5-T12.5_50) and (c and d) $Al_xTa_yO_z$ mixture (AT13_50) coated low alloy steel (a and c) before and (b and d) after immersion for 6 h in acidic 0.2 M NaCl solutions.*

Different from the LSV results, based on EIS results the Al_2O_3-Ta_2O_5 nanolaminate appeared to have better protective properties than the $Al_xTa_yO_z$ mixture (Figure 22).[VII] The initial global impedance was higher, the capacitive range extended over a wider frequency range and fewer changes were observed during the immersion. The underlying reason for the difference between the LSV and EIS results is not known. However, as mentioned above, based on the literature the nanolaminate was expected to have better protective properties.[151] A detailed discussion including modelling of the EIS results with equivalent circuits is given in publication [VII]. As for the Ta_2O_5 coated steel, the changes in EIS at low frequencies (mHz) were attributed to adsorption of intermediate corrosion products, and the changes at the middle (Hz) and high (kHz) frequencies to the global and pitting corrosion.[204-206] The nanolaminate appeared to be significantly more resistant to pitting corrosion than the mixture: the pitting resistance was decreased less and the double layer capacitance increased less for the nanolaminate. Furthermore, the capacitance of the nanolaminate coating remained constant whereas the capacitance of the mixture coating decreased. The more prominently changed capacitances of the mixture coating were indicative of an increased uncoated surface fraction. This corroborated the observation of steel oxide species in the coating region in the ToF-SIMS depth profile of the mixture coating (Figure 21). Also the global corrosion rate evidenced by the changes in the middle frequencies was higher in the mixture than the nanolaminate coated steel. No general dissolution of either the nanolaminate or the mixture coating was observed.

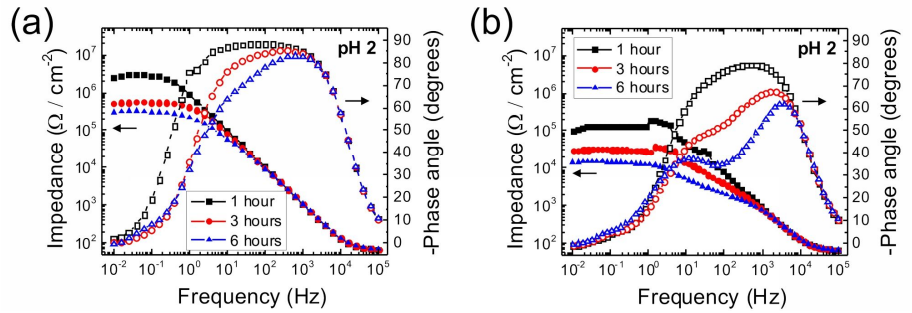

Figure 22 *EIS Bode plots for low alloy steel coated with ALD (a) Al_2O_3-Ta_2O_5 nanolaminate (A12.5-T12.5_50) and (b) $Al_xTa_yO_z$ (AT13_50) mixture during immersion in acidic 0.2 M NaCl solution.*

The NSS performances of the Al_2O_3-Ta_2O_5 nanolaminate and $Al_xTa_yO_z$ mixture coated steel were similar (Figure 23).[VI] Both coatings protected the steel surface well for four hours, but after 24 hours several distinct corrosion spots were seen. Thus no clear conclusions could be drawn on the superiority of either structure. It is possible that the long continuous NSS exposure from four to 24 h without observation of the samples in between masked the differences seen in the immersion tests. Different from the steel samples protected with single layer coatings, no bleeding was observed and the majority of the steel surfaces were still intact after 24 hours. Thus the concept of improving long-term durability by combining Al_2O_3 and Ta_2O_5 in nanolaminate and mixture coatings was further confirmed.

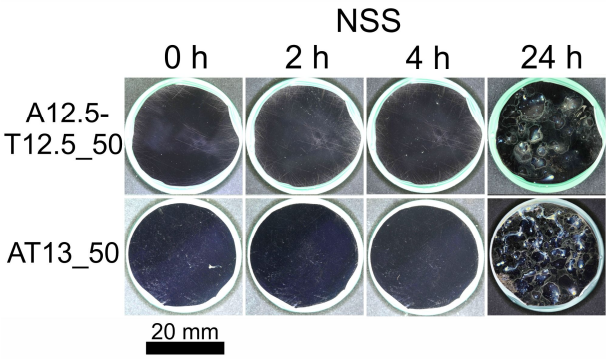

Figure 23 *NSS test results on low alloy steel coated with ALD Al_2O_3-Ta_2O_5 nanolaminate (A12.5-T12.5_50) and $Al_xTa_yO_z$ mixture (AT13_50).*

4.3 Duplex coatings

Combination of ALD with coatings deposited by PVD and plasma-enhanced CVD (PECVD) were studied in order to improve the protective properties and widen the range of applications utilizing ALD based protection.[VIII,IX] Two routes were envisioned. Firstly, the challenges in the ALD coating-steel interface were targeted.[VIII] Thin FCAD Ta:O and

Cr:O-Ta:O nanolaminate sub-layers were deposited in between the ALD coating and steel to control the interface properties, to ensure a surface with appropriate reactive sites for good ALD film nucleation, and to suppress the steel surface oxidation. The FCAD films are denoted as Ta:O and Cr:O-Ta:O because they are not stoichiometric oxides. Secondly, pinhole defects in thicker UBM sputtered CrN and PECVD diamond like carbon (DLC) coatings were sealed with conformal ALD films.[IX] The aim was to combine the proven mechanical protection of the CrN and DLC coatings with the chemical protection from ALD. The duplex coatings were composed of the optimised ALD layers containing Al_2O_3 and Ta_2O_5 presented in the section above. This overview focuses on the Al_2O_3-Ta_2O_5 nanolaminate, because it appeared to have better long-term performance than the $Al_xTa_yO_z$ mixture.[VII] All samples were brushed and degreased with the short recipe before growing the FCAD, PVD and PECVD layers. Before ALD the samples were degreased again with the longer recipe and *ex situ* plasma pre-treated (Ex-30).

4.3.1 Interface control with filtered cathodic arc deposited sublayers

It is shown in Chapter 4.1. and literature[22-24,122,123] that the ALD film properties are highly dependent on the substrate surface. Therefore controlling and providing a compositionally homogeneous starting surface for growing protective ALD coatings was studied with FCAD sublayers.[VIII] Thin 10 nm Ta:O and 50 nm Cr:O-Ta:O nanolaminate films were studied. Because only a minimal improvement compared to the 10 nm Ta:O was achieved with the more complex Cr:O-Ta:O nanolaminate, this overview is focused only on the Ta:O sublayer (Table 7). Detailed results on all studied coatings can be found in publication [VIII].

The top surface and cross sectional appearance of low alloy steel coated with the FCAD Ta:O sublayer and ALD coating are presented in Figure 24.[VIII] The FCAD coated low alloy steel appeared similar to the uncoated steel (cf. Figures 9 and 24a). Some of the scratches and holes were marginally more pronounced. This might be due to the directionality of the coating method.[208] The ALD coating did not significantly change the appearance of the Ta:O coated steel, and no defects could be observed (Figure 24b). In the cross sectional image both the FCAD sublayer and ALD coating closely followed the substrate morphology (Figure 24c). No defects or delamination could be seen in either layer. The FCAD Ta:O appeared to be slightly thicker than the nominal value suggested (15 vs. 10 nm). The interfacial oxidised steel layer that could be seen under the single ALD layers (Figures 15 and 21) was not seen. This suggested that the *in situ* Ar^+ ion sputtering prior to the FCAD removed the native oxide of steel and the FCAD sublayer prevented the formation of a new oxide layer during the ambient exposure and first ALD cycles.

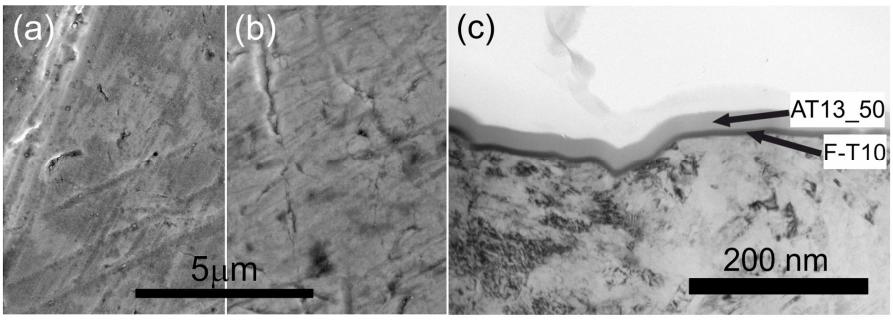

Figure 24 *The appearance of low alloy steel coated with FCAD Ta:O sublayer (a) without (F-T10) and (b and c) with ALD coating (F-T10-mixture). The top surface images (a and b) were taken with FESEM and the cross sectional image (c) with TEM.*

The corrosion protection properties of the duplex FCAD-ALD coatings were studied with LSV measurements, immersion experiments, and NSS testing.[VIII] In LSV the FCAD Ta:O appeared to increase the corrosion potential of the bare steel, but the corrosion current density was only slightly decreased (Figure 25). The increased corrosion potential implied ennoblement, and was attributed to the removal of the native oxide layer of steel.[195,IV] The duplex coating had lower current density than either the single FCAD or ALD coating over the whole potential range. The current density in the cathodic range was even below the resolution of the equipment thus preventing further analysis. As only a minimal decrease of corrosion current density was achieved with the single FCAD Ta:O film, the sealing properties were in a major part attributed to the ALD nanolaminate.[VIII]

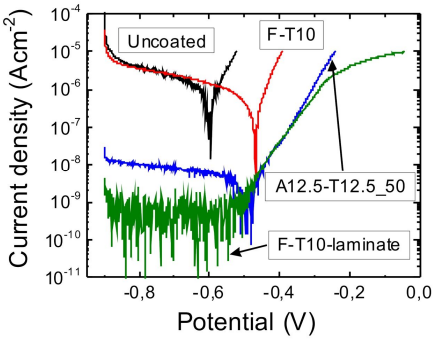

Figure 25 *LSV results on low alloy steel coated with FCAD Ta:O (F-T10), ALD Al_2O_3-Ta_2O_5 nanolaminate (A12.5-T12.5_50) and a corresponding FCAD-ALD duplex (F-T10-laminate) in neutral 0.2 M NaCl solutions.*

The immersion durability testing of the FCAD-ALD duplex coatings was done with the same procedure as for single Ta_2O_5, Al_2O_3-Ta_2O_5 nanolaminate and $Al_xTa_yO_z$ mixture ALD coatings.[VIII] An acidic 0.2 M NaCl solution was used. The ToF-SIMS depth profiles of duplex 10 nm FCAD Ta:O and 50 nm ALD Al_2O_3-Ta_2O_5 nanolaminate coated steel are presented in Figure 26. Before immersion, the sputtering time to the interface and composition of the ALD coatings were the same as observed for the corresponding single

coatings on steel (cf. Figures 21 and 26). In the FCAD layer the Ta:O species expectedly peaked, and the OH^- and Cl^- impurity intensities dropped (Figure 26). The C^- and TaC^- impurities peaked at the steel-FCAD interface. Similar results have been obtained for single FCAD coatings on steel.[195] The peaking of C^- and TaC^- at the interface were attributed to the growth of the FCAD layer on a carbon-contaminated surface. The most significant difference of the duplex coating compared to the single ALD coatings was that no peaking of FeO_2^- or CrO_2^- could be seen in the interfacial region. Therefore, as speculated based on the TEM images, the FCAD process completely removed the native oxide of steel and suppressed its reformation.

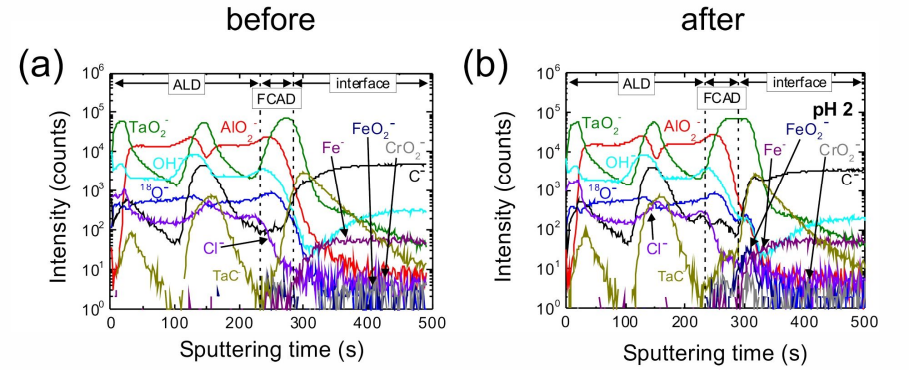

Figure 26 *ToF-SIMS depth profiles of the FCAD-ALD duplex coatings (F-T10-laminate) (a) before and (b) after immersion in acidic 0.2 M NaCl solution for 6 hours.*

Almost identical ToF-SIMS depth profiles were recorded for the FCAD-ALD duplex coatings before and after immersion for 6 hours in acidic NaCl solutions (Figure 26).[VIII] The sputtering time needed for reaching the interface was the same. The only difference in composition was the slight increase of Cl^- content in the outermost Ta_2O_5 layer of the ALD nanolaminate after the immersion. As for the ALD nanolaminate, the increase of Cl^- was attributed to the higher porosity of the ALD Ta_2O_5 compared to Al_2O_3.[113] The absence of any other changes indicated that the duplex coating was globally stable.

The corrosion development during the immersion was followed with the EIS measurements.[VIII] Bode plots of the 60 nm FCAD-ALD nanolaminate duplex coating are presented in Figure 27. A detailed analysis on the EIS results is given in publication [VIII]. The interpretation of the results was done along the same lines as used for the ALD Ta_2O_5, Al_2O_5-Ta_2O_5 nanolaminate and $Al_xTa_yO_z$ mixture coatings. Initially the global impedance was higher and the capacitive frequency range wider in the Bode plot of the duplex than in the ALD nanolaminate coated steel (cf. Figures 22 and 27). Also a more stable performance was achieved with the duplex-coated sample. For both the FCAD-ALD duplex and the ALD nanolaminate coated steel changes could be seen in the middle frequencies, i.e. the global corrosion rate was increased. However, the protection afforded by the duplex coating was initially more effective and decreased less compared to the ALD nanolaminate. Furthermore, resistance to the pitting corrosion was especially improved with the FCAD sublayers, as evidenced by the almost unchanged high

frequency domain. Because the ALD film properties have been seen to be dependent on the substrate surface morphology and cleanliness (Chapter 4.1.),[22-24,122,123] the FCAD sublayer was concluded to improve nucleation of the ALD growth.[VIII] Thus a better quality ALD coating, i.e. a better barrier and chemically more stable, could be grown on the controlled FCAD sublayer. This most markedly improved the protection against local corrosion by pitting.

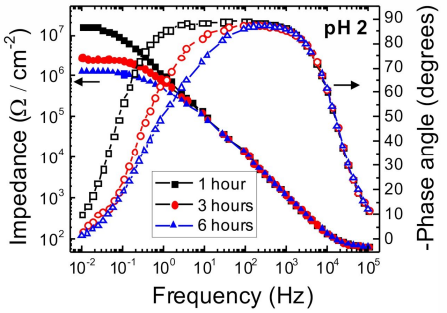

Figure 27 *Evolution of the EIS Bode plots of a FCAD-ALD duplex coating (F-T10-laminate) during immersion in acidic 0.2 M NaCl solution.*

In the NSS protective properties of the duplex FCAD-ALD coatings was better than those of the single FCAD or ALD coatings (Figures 23 and 28).[VIII] A 50 nm FCAD Ta:O coated steel had a number of corrosion spots covering a significant fraction of the substrate already after two hours. After four hours the number of corrosion spots appeared unchanged, but the size had increased. On the 50 nm ALD nanolaminate coated steel first corrosion spots appeared after 4 hours (Figure 23).[VI] The 60 nm duplex coatings were almost completely free of corrosion after 24 hours and only some single spots were seen after 48 and 96 h (Figure 28). This confirmed the LSV measurement and immersion test results. Because even the 50 nm thick FCAD did not protect the steel for two hours, the effect of the 10 nm FCAD layer on the protective properties was assumed negligible. Thus it was concluded that the FCAD sublayer significantly improved the ALD coating quality.

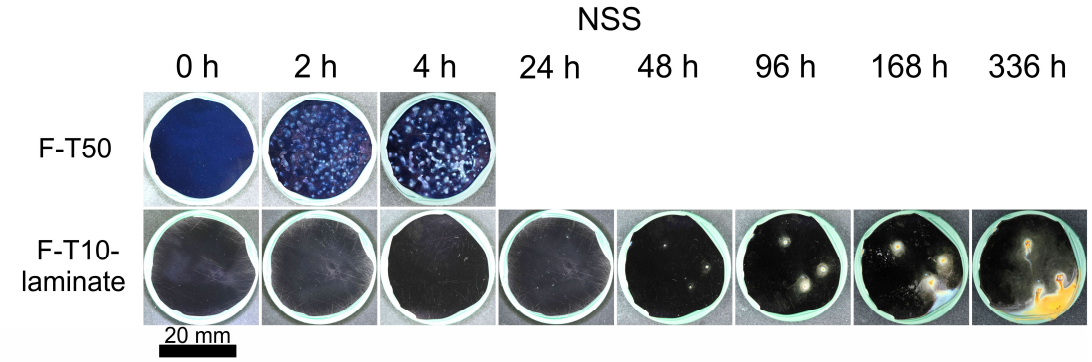

Figure 28 *NSS durability of low alloy steel coated with FCAD Ta:O (F-T50) and FCAD-ALD nanolaminate duplex (F-T10-laminate).*

4.3.2 Blocking of pinholes in hard coatings

PVD and CVD hard coatings are known for their excellent chemical durability and resistance against mechanical degradation.[154,209,210] They are widely used for increasing the lifetime of tools, especially in applications where mechanical protection is needed. However, the corrosion protection properties of the coatings are limited by the existence of through-coating pinholes.[154] The pinholes render the protected surface especially vulnerable, because often the PVD and CVD coatings are electrochemically active and nobler than the protected surface. Therefore, local corrosion at the exposed sites is accelerated. Sealing of these pinholes with conformal insulating ALD films has been proposed as one solution (Figure 29).[137-139] Even if the thin ALD layer may be relatively rapidly eroded away from the top surface under mechanical load in use, the coating in the pinholes survives and provides corrosion protection. In the present work the sealing of UBM sputtered CrN and PECVD DLC coatings with ALD were studied. However, the overview is focused on the CrN coating, because of the more comprehensive analysis conducted on it (Table 8). Detailed results and discussion on all studied coatings are given in publication [IX].

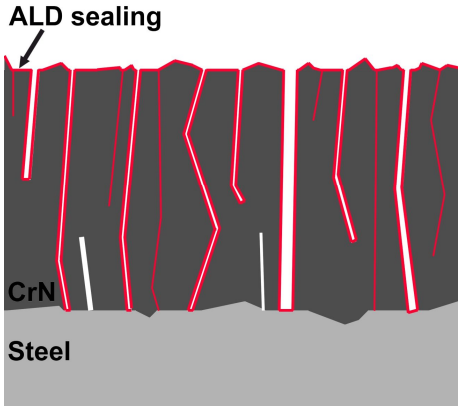

Figure 29 *Schematic presentation of sealing pinholes in PVD CrN coatings with ALD.*

The top surface and cross sectional appearance of low alloy steel coated with CrN and ALD sealed CrN coatings are presented in Figure 30.[IX] When imaged from the top the CrN coating appeared to consist of tightly packed columns. Between the columns some pinhole defects could be observed (Figure 30a), as expected.[154] The ALD films closely followed the surface morphology of the CrN coatings and no defects could be observed in the ALD layers (Figure 30b). The largest pinholes in the CrN coating were still visible after the ALD sealing, because the ALD coating was too thin to completely block them. However, ALD coating is expected to cover the walls and steel surfaces possibly exposed at the bottom of the pinholes. No delamination of the CrN coating or the ALD film could be observed (Figure 30c). Thus, the adhesion of the layers appeared to be sufficient. No through-coating defects were seen in the TEM image of the CrN layer, most probably due to the very local nature of the analysis.

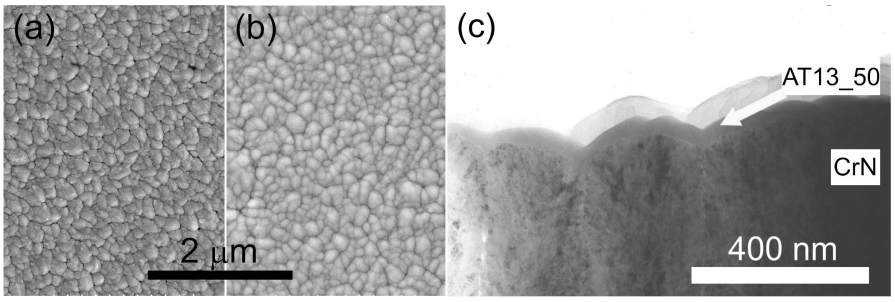

Figure 30 *The appearance of low alloy steel coated with (a) CrN and (b and c) ALD sealed CrN coating (CrN-mixture). The top surface images (a and b) were taken with FESEM and the cross sectional image (c) with TEM.*

The sealing of pinholes in CrN was verified with a combined SEM and EDS analysis (Figure 31).[IX] A defected site was selected from the SEM top view. This defect was cross-sectioned with FIB, and the cross section surface was mapped with EDS. The SEM cross section clearly showed a pinhole defect extending along the right-side particle edge to the steel surface. In the Cr and N EDS maps the intensity at the pinhole site was notably lower, and in the corresponding Al and Ta maps penetration into the CrN layer was seen. The Al signal appeared stronger and extended deeper into the pinhole. The difference can be attributed to the higher vapour pressure of $Al(CH_3)_3$ compared to $Ta(OCH_2CH_3)_5$.[211,212] This type of high aspect ratio structures are challenging even for ALD, and a continuously growing film further increases the aspect ratio towards infinity as the pinhole is filled. Gordon et al.[20] have shown that conformality of ALD films in high aspect ratio structures is a product of the exposure time, i.e. pulse length, and the vapour pressure of the precursors, thus explaining why the Al_2O_3 coating penetrated deeper than Ta_2O_5.

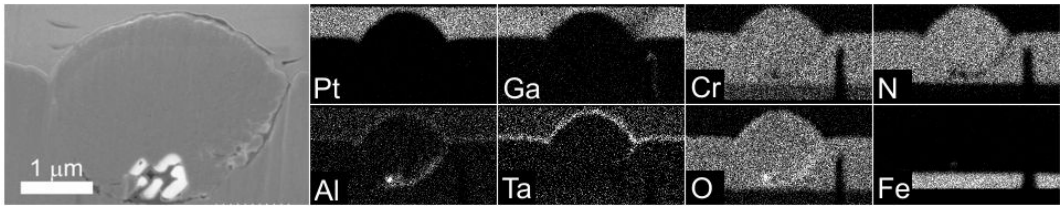

Figure 31 *SEM image and EDS elemental maps on ALD sealed pinhole defect in an UBM sputtered CrN (CrN-mixture) on low alloy steel.*

The sealing performance and effect of the ALD films on corrosion protection properties were evaluated with LSV measurements and NSS testing.[IX] In LSV the CrN coating slightly decreased the corrosion current density and increased the corrosion potential of the bare steel (Figure 32). The increase of the corrosion potential was too small to indicate a simple CrN response, and thus a combined effect of the CrN and steel exposed due to pinholes was most likely seen.[213,214] However, as CrN was chemically inert in the analysis conditions,[213] the anodic corrosion reactions were mostly occurring on the steel surface. This further confirms the literature[154] and SEM results (Figures 29 and 30) that pinhole

defects existed in the sputtered CrN coating. The insulating 50 nm ALD nanolaminates decreased the current density in the whole measured potential range (Figure 32), and the decrease was more than two orders of magnitude. In fact, the current density was so low that the detection limit of the equipment was reached. This proved excellent sealing behaviour, but prevented any further analysis. In literature a more modest sealing performance has been achieved with ALD TiO_2 films on sputtered CrN.[139] With ALD Al_2O_3 sealing on reactive arc evaporated TiCN the results were comparable to those obtained in this work.[138]

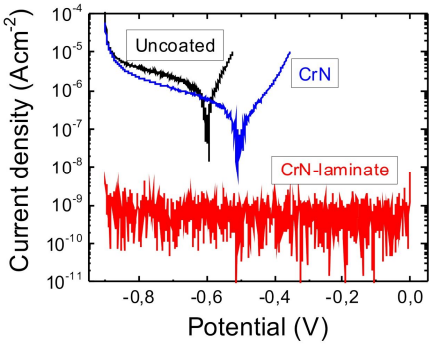

Figure 32 *LSV results on low alloy steel coated with CrN and ALD nanolaminate sealed CrN (CrN-laminate) in neutral 0.2 M NaCl solutions.*

The NSS durability of CrN coated low alloy steel was greatly improved with the ALD sealing (Figure 33).[IX] Different from the other samples, the unsealed CrN coated steel samples tested with NSS were only fine ground. The CrN coated steel suffered from significant corrosion already after two hours of testing. On the 50 nm ALD nanolaminate sealed samples no corrosion was observed after 72 hours and some corrosion free areas could be seen still after 336 hours. This showed that the ALD nanolaminate sealed CrN had excellent chemical durability and long-term protective properties, which was mainly attributed to the optimised ALD coating composition and structure. Compared to the previous literature utilizing single Al_2O_3 or TiO_2 films,[138,139] these ALD films combined the best properties of Al_2O_3 and Ta_2O_5 resulting in all-around better barrier properties and long-term durability.

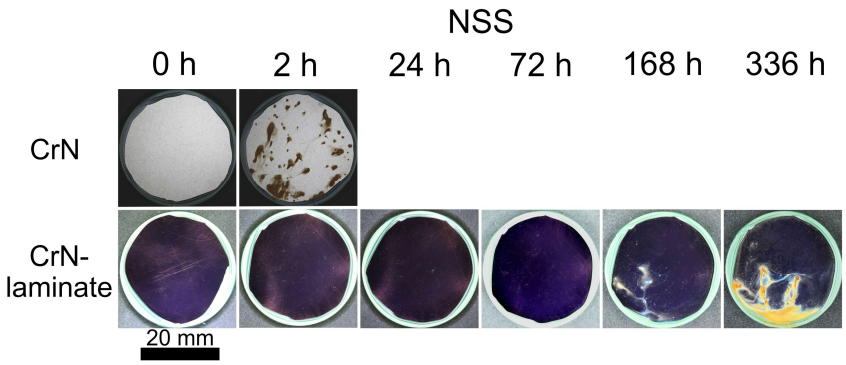

Figure 33 *NSS durability of low alloy steel coated with CrN and ALD nanolaminate sealed CrN (CrN-laminate).*

5 Conclusions

In this thesis the protection of metals, metal alloys and metallic constituents in multimaterial structures with ALD coatings was evaluated. The objective was to study the applicability of ALD coatings alone and ALD coatings in duplex structures with layers deposited by other methods for corrosion protection. The effects of the substrate pre-treatment, ALD coating material and deposition parameters to the protective properties and the improvement obtained with more complex nanolaminate and mixture coatings compared to single layers were explored. In the literature review, protection from both gaseous and liquid corrosives was evaluated. In addition, ALD barriers against metal diffusion were shortly overviewed. The experimental work was focused on optimizing the substrate pre-treatment, the protective properties of ALD coatings based on Al_2O_3 and Ta_2O_5 and studying the failure mechanisms. The optimised structures were combined with PVD and PECVD grown coatings for synergistically enhanced protection.

A low alloy steel was selected as the material to be protected. The mechanical conditioning and pre-treatment of the steel surface were found critical for achieving optimal protection with ALD coatings. Both decreasing the surface roughness and efficient cleaning of the surface with H_2-Ar plasma were found beneficial. The improvements were attributed to improved ALD nucleation on the smoother and cleaner surface, and lowered defect formation after the deposition due to detachment of foreign particles or steel flakes.

When optimising the protective properties of the ALD coatings, Al_2O_3 was found to have superior sealing properties, but also to dissolve from the low alloy steel surface even in neutral NaCl solutions. The dissolution was attributed to local increase of pH due to the cathodic reduction of O_2 at the bottom of pinholes exposing the steel surface. Ta_2O_5 was found chemically more stable, but inherently less protective due to impurities and moderate insulating properties. The best corrosion protection was achieved when nanolaminates and mixtures were used, with nanolaminates providing better long-term protection. The optimum protective properties required a balanced composition of Al_2O_3 and Ta_2O_5 in the mixture coatings, and an optimised bilayer structure in the nanolaminates.

A further improvement in the long-term protective properties of ALD coatings could be achieved with duplex PVD-ALD and PECVD-ALD coatings. A thin Ta:O FCAD sublayer effectively separated the ALD process from the steel surface and provided a compositionally controlled starting surface for the ALD growth. This led to improved sealing properties and better long-term durability. ALD sealing could also be used to block pinholes in thick PVD and PECVD coatings. Significant improvement in the corrosion protection properties of hard CrN and DLC coatings was achieved. The ALD sealed hard coatings had a combination of good mechanical durability provided by the CrN or DLC coating and excellent corrosion protection properties provided by the ALD sealing of pinholes, a challenging combination to achieve by either method alone.

ALD based protective coatings could be used to achieve effective corrosion protection of steel. The coatings themselves had good sealing properties and stability when Al_2O_3 was combined with Ta_2O_5. However, a good substrate-coating interface was challenging to produce, and both the mechanical conditioning and chemical pre-treatment of the substrate were found critical for producing the proper starting surface for ALD to achieve optimum long-term protection. Separation of the ALD process from the steel surface was also beneficial. Further improvement of the protective properties of ALD coatings on metallurgical surfaces is likely to require additional consideration on the substrate conditioning and cleaning.

References

1. ASM International, ASM International Handbook Committee. *Metals Handbook*, 9th ed.; Metals Park, Ohio, 1987; Vol. 13.
2. G. Schmitt, *Global Needs for Knowledge Dissemination, Research, and Development in Materials Degradation and Corrosion Control*, World Corrosion Organization, 2009.
3. Data calculated from the GDP published in Wikipedia: The Free Encyclopedia, List of countries by GDP (PPP), International Monetary Fund (2014). http://en.wikipedia.org/wiki/List_of_countries_by_GDP_(nominal) (accessed April 9, 2015)
4. A. W. Batchelor, L. N. Lam and M. Chandrasekaran, *Materials Degradation and Its Control by Surface Engineering*, 3rd ed.; Imperial College Press: London, 2011.
5. M. Ritala and M. Leskelä, Atomic layer deposition. In *Handbook of Thin Film Materials*; H. S. Nalwa Ed.; Academic Press: San Diego, CA, 2002, Vol. 1, pp. 103-159.
6. M. Ritala and J. Niinistö, Atomic Layer Deposition. In *Chemical Vapour Deposition: Precursors, Processes and Applications*, A. C. J. Jones and M. L. Hitchman, Eds.; Royal Society of Chemistry: Cambridge, U.K., 2009, pp. 158-206.
7. S. M. George, B. Yoon and A. A. Dameron, *Accounts Chem. Res.*, **42** (2009) 498-508.
8. V. Miikkulainen, M. Leskelä, M. Ritala and R. L. Puurunen, *J. Appl. Phys.*, **113** (2013) 021301.
9. R. L. Puurunen, *J. Appl. Phys.*, **97** (2005) 121301.
10. S. E. Potts and W. M. M. Kessels, *Coordin. Chem. Rev.*, **257** (2013) 3254-3270.
11. H. B. Profijt, S. E. Potts, M. C. M. van de Sanden and W. M. M. Kessels, *J. Vac. Sci. Technol. A*, **29** (2011) 050801.
12. T. Suntola and J. Hyvärinen, *Annu. Rev. Mater. Sci.*, **15** (1985) 177-195.
13. J. Niinistö, K. Kukli, M. Heikkilä, M. Ritala and M. Leskelä, *Adv. Eng. Mater.*, **11** (2009) 223-234.
14. X. B. Meng, X. Q. Yang and X. L. Sun, *Adv. Mater.*, **24** (2012) 3589-3615.
15. C. Marichy, M. Bechelany and N. Pinna, *Adv. Mater.*, **24** (2012) 1017-1032.
16. J. A. van Delft, D. Garcia-Alonso and W. M. M. Kessels, *Semicond. Sci. Technol.*, **27** (2012) 074002.
17. T. Wang, Z. B. Luo, C. C. Li and J. L. Gong, *Chem. Soc. Rev.*, **43** (2014) 7469-7484.
18. M. Cassir, A. Ringuede and L. Niinistö, *J. Mater. Chem.*, **20** (2010) 8987-8993.
19. E. Marin, A. Lanzutti, F. Andreatta, M. Lekka, L. Guzman and L. Fedrizzi, *Corros. Rev.*, **29** (2011) 191-208.
20. R. G. Gordon, D. Hausmann, E. Kim and J. Shepard, *Chem. Vapor Deposition*, **9** (2003) 73-78.
21. A. Niskanen, Radical Enhanced Atomic Layer Deposition of Metals and Oxides. PhD. Dissertation, University of Helsinki, Helsinki, Finland, 2006.

22. Y. D. Zhang, J. A. Bertrand, R. G. Yang, S. M. George and Y. C. Lee, *Thin Solid Films*, **517** (2009) 3269-3272.

23. Y. D. Zhang, D. Seghete, A. Abdulagatov, Z. Gibbs, A. Cavanagh, R. G. Yang, S. George and Y. C. Lee, *Surf. Coat. Technol.*, **205** (2011) 3334-3339.

24. M. D. Groner, J. W. Elam, F. H. Fabreguette and S. M. George, *Thin Solid Films*, **413** (2002) 186-197.

25. G. N. Parsons, S. E. Atanasov, E. C. Dandley, C. K. Devine, B. Gong, J. S. Jur, K. Lee, C. J. Oldham, Q. Peng, J. C. Spagnola and P. S. Williams, *Coordin. Chem. Rev.*, **257** (2013) 3323-3331.

26. R. Matero, M. Ritala, M. Leskelä, T. Salo, J. Aromaa and O. Forsen, *J. Phys. IV France*, **9** (1999) Pr8-493–Pr8-499.

27. H. Im, N. J. Wittenberg, N. C. Lindquist and S. H. Oh, *J. Mater. Res.*, **27** (2012) 663-671.

28. D. M. King, J. A. Spencer, X. Liang, L. F. Hakim and A. W. Weimer, *Surf. Coat. Technol.*, **201** (2007) 9163-9171.

29. P. F. Carcia, R. S. McLean, M. H. Reilly, M. D. Groner and S. M. George, *Appl. Phys. Lett.*, **89** (2006) 031915.

30. A. A. Dameron, S. D. Davidson, B. B. Burton, P. F. Carcia, R. S. McLean and S. M. George, *J. Phys. Chem. C*, **112** (2008) 4573-4580.

31. M. D. Groner, F. H. Fabreguette, J. W. Elam and S. M. George, *Chem. Mater.*, **16** (2004) 639-645.

32. R. Matero, A. Rahtu, M. Ritala, M. Leskelä and T. Sajavaara, *Thin Solid Films*, **368** (2000) 1-7.

33. S. Jakschik, U. Schroeder, T. Hecht, M. Gutsche, H. Seidl and J. W. Bartha, *Thin Solid Films*, **425** (2003) 216-220.

34. O. M. E. Ylivaara, X. W. Liu, L. Kilpi, J. Lyytinen, D. Schneider, M. Laitinen, J. Julin, S. Ali, S. Sintonen, M. Berdova, E. Haimi, T. Sajavaara, H. Ronkainen, H. Lipsanen, J. Koskinen, S. P. Hannula and R. L. Puurunen, *Thin Solid Films*, **552** (2014) 124-135.

35. *CRC Handbook of Chemistry and Physics*, 95th edn. [Online]; CRC Press/Taylor and Francis: Boca Raton, FL, 2015; http://www.hbcpnetbase.com/ (accessed January 13, 2015).

36. R. L. Puurunen, J. Kiihamäki and H. Kattelus, Poster: Controlling the solubility of ALD aluminium oxide in deionised water, In *AVS Atomic Layer Deposition*, 2005.

37. S. E. Potts, L. Schmalz, M. Fenker, B. Diaz, J. Swiatowska, V. Maurice, A. Seyeux, P. Marcus, G. Radnoczi, L. Toth and W. M. M. Kessels, *J. Electrochem. Soc.*, **158** (2011) C132-C138.

38. Y. Q. Yang, Y. Duan, P. Chen, F. B. Sun, Y. H. Duan, X. Wang and D. Yang, *J. Phys. Chem. C*, **117** (2013) 20308-20312.

39. S.-H. Ha, E. Choi, S.-H. Kim and J. S. Roh, *Thin Solid Films*, **476** (2005) 252-257.

40. H. C. M. Knoops, E. Langereis, M. C. M. van de Sanden and W. M. M. Kessels, *J. Electrochem. Soc.*, **157** (2010) G241-G249.

41. D. M. King, Y. Zhou, L. F. Hakim, X. H. Liang, P. Li and A. W. Weimer, *Ind. Eng. Chem. Res.*, **48** (2009) 352-360.

42. S. W. Seo, E. Jung, C. Lim, H. Chae and S. M. Cho, *Appl. Phys. Express*, **5** (2012) 035701.

43. C. X. Shan, X. H. Hou and K. L. Choy, *Surf. Coat. Technol.*, **202** (2008) 2399-2402.

44. T. O. Kääriäinen, P. Maydannik, D. C. Cameron, K. Lahtinen, P. Johansson and J. Kuusipalo, *Thin Solid Films*, **519** (2011) 3146-3154.

45. M. Ritala, M. Leskelä, L. Niinistö and P. Haussalo, *Chem. Mater.*, **5** (1993) 1174-1181.

46. M. Ritala, M. Leskelä, E. Nykänen, P. Soininen and L. Niinistö, *Thin Solid Films*, **225** (1993) 288-295.

47. V. Sammelselg, I. Netsipailo, A. Aidla, A. Tarre, L. Aarik, J. Asari, P. Ritslaid and J. Aarik, *Thin Solid Films*, **542** (2013) 219-224.

48. H.-B. Wang, D.-Y. Ma, F. Ma and K.-W. Xu, *J. Vac. Sci. Technol. B*, **30** (2012) 040601.

49. X. H. Du, K. Zhang, K. Holland, T. Tombler and M. Moskovits, *Appl. Optics*, **48** (2009) 6470-6474.

50. Y. Duan, F. B. Sun, Y. Q. Yang, P. Chen, D. Yang, Y. H. Duan and X. Wang, *ACS Appl. Mater. Inter.*, **6** (2014) 3799-3804.

51. A. J. Haemmerli, J. C. Doll, J. Provine, R. T. Howe, D. Goldhaber-Gordon and B. L. Pruitt, 2013 Transducers & Eurosensors XXVII: The 17th International Conference on Solid-State Sensors, Actuators and Microsystems, Barcelona, Spain, June 16-20, 2013, IEEE: Barcelona, 2013.

52. P. C. Hsu, H. Wu, T. J. Carney, M. T. McDowell, Y. Yang, E. C. Garnett, M. Li, L. B. Hu and Y. Cui, *ACS Nano*, **6** (2012) 5150-5156.

53. A. I. Abdulagatov, Y. Yan, J. R. Cooper, Y. Zhang, Z. M. Gibbs, A. S. Cavanagh, R. G. Yang, Y. C. Lee and S. M. George, *ACS Appl. Mater. Inter.*, **3** (2011) 4593-4601.

54. P. Alen, M. Juppo, M. Ritala, T. Sajavaara, J. Keinonen and M. Leskelä, *J. Electrochem. Soc.*, **148** (2001) G566-G571.

55. H. Kim, C. Detavernier, O. van der Straten, S. M. Rossnagel, A. J. Kellock and D. G. Park, *J. Appl. Phys.*, **98** (2005) 014308.

56. J. Musschoot, Q. Xie, D. Deduytsche, S. Van den Berghe, R. L. Van Meirhaeghe and C. Detavernier, *Microelectron. Eng.*, **86** (2009) 72-77.

57. J. Uhm and H. Jeon, *Jpn. J. Appl. Phys. 1*, **40** (2001) 4657-4660.

58. M. Juppo, P. Alen, M. Ritala and M. Leskela, *Chem. Vapor Deposition*, **7** (2001) 211-217.

59. M. Ritala, P. Kalsi, D. Riihelä, K. Kukli, M. Leskelä and J. Jokinen, *Chem. Mater.*, **11** (1999) 1712-1718.

60. M. Juppo, M. Ritala and M. Leskelä, *J. Electrochem. Soc.*, **147** (2000) 3377-3381.

61. D.-J. Kim, Y.-B. Jung, M.-B. Lee, Y.-H. Lee, J.-H. Lee and J.-H. Lee, *Thin Solid Films*, **372** (2000) 276-283.

62. H. Kim, *Surf. Coat. Technol.*, **200** (2006) 3104-3111.

63. G. Cho and S. W. Rhee, *J. Vac. Sci. Technol. A*, **31** (2013) 01A117.

64. N. J. Bae, K. I. Na, H. I. Cho, K. Y. Park, E. Boo, J. H. Bae and J. H. Lee, *Jpn. J. Appl. Phys. 1*, **45** (2006) 9072-9074.

65. J. S. Becker and R. G. Gordon, *Appl. Phys. Lett.*, **82** (2003) 2239-2241.

66. H. C. M. Knoops, L. Baggetto, E. Langereis, M. C. M. van de Sanden, J. H. Klootwijk, F. Roozeboom, R. A. H. Niessen, P. H. L. Notten and W. M. M. Kessels, *J. Electrochem. Soc.*, **155** (2008) G287-G294.

67. P. Alen, M. Ritala, K. Arstila, J. Keinonen and M. Leskelä, *J. Electrochem. Soc.*, **152** (2005) G361-G366.

68. P. Alen, M. Ritala, K. Arstila, J. Keinonen and M. Leskelä, *Thin Solid Films*, **491** (2005) 235-241.

69. G. Rampelberg, K. Devloo-Casier, D. Deduytsche, M. Schaekers, N. Blasco and C. Detavernier, *Appl. Phys. Lett.*, **102** (2013) 111910.

70. P. F. Carcia, R. S. McLean and M. H. Reilly, *Appl. Phys. Lett.*, **97** (2010) 221901.

71. M. D. Groner, S. M. George, R. S. McLean and P. F. Carcia, *Appl. Phys. Lett.*, **88** (2006) 015907.

72. H. Klumbies, P. Schmidt, M. Hähnel, A. Singh, U. Schroeder, C. Richter, T. Mikolajick, C. Hoßbach, M. Albert, J. W. Bartha, K. Leo and L. Müller-Meskamp, *Org. Electron.*, **17** (2015) 138-143.

73. E. Langereis, M. Creatore, S. B. S. Heil, M. C. M. Van de Sanden and W. M. M. Kessels, *Appl. Phys. Lett.*, **89** (2006) 081915.

74. H. Jeon, K. Shin, C. Yang, C. E. Park and S. H. K. Park, *Appl. Phys. Lett.*, **93** (2008) 163304.

75. P. Görrn, T. Riedl and W. Kowalsky, *J. Phys. Chem. C*, **113** (2009) 11126-11130.

76. L. F. Hakim, C. L. Vaughn, H. J. Dunsheath, C. S. Carney, X. Liang, P. Li and A. W. Weimer, *Nanotechnology*, **18** (2007) 345603.

77. B. Moghtaderi, I. Shames and E. Doroodchi, *Chem Eng Technol*, 2006, **29**, 97-103.

78. Y. Zhou, D. M. King, J. H. Li, K. S. Barrett, R. B. Goldfarb and A. W. Weimer, *Ind. Eng. Chem. Res.*, **49** (2010) 6964-6971.

79. E. V. Formo, S. M. Mahurin and S. Dai, *ACS Appl. Mater. Inter.*, **2** (2010) 1987-1991.

80. H. Im, S. H. Lee, N. J. Wittenberg, T. W. Johnson, N. C. Lindquist, P. Nagpal, D. J. Norris and S. H. Oh, *ACS Nano*, **5** (2011) 6244-6253.

81. H. Im, N. C. Lindquist, A. Lesuffleur and S. H. Oh, *ACS Nano*, **4** (2010) 947-954.

82. H. Im and S.-H. Oh, *small*, **10** (2014) 680-684.

83. J. F. John, S. Mahurin, S. Dai and M. J. Sepaniak, *J. Raman Spectrosc.*, **41** (2010) 4-11.

84. Q. C. Sun, Y. C. Ding, S. M. Goodman, H. H. Funke and P. Nagpal, *Nanoscale*, **6** (2014) 12450-12457.

85. J. Sung, K. M. Kosuda, J. Zhao, J. W. Elam, K. G. Spears and R. P. Van Duyne, *J. Phys. Chem. C*, **112** (2008) 5707-5714.

86. A. V. Whitney, J. W. Elam, P. C. Stair and R. P. Van Duyne, *J. Phys. Chem. C*, **111** (2007) 16827-16832.

87. X. Y. Zhang, J. Zhao, A. V. Whitney, J. W. Elam and R. P. Van Duyne, *J. Am. Chem. Soc.*, **128** (2006) 10304-10309.

88. M. L. Chang, T. C. Cheng, M. C. Lin, H. C. Lin and M. J. Chen, *Appl. Surf. Sci.*, **258** (2012) 10128-10134.

89. O. M. Hahtela, A. F. Satrapinski, P. H. Sievilä and N. Chekurov, *IEEE Trans. Instrum. Meas.*, **58** (2009) 1183-1187.

90. M. J. M. Mies, E. V. Rebrov, M. H. J. M. de Croon and J. C. Schouten, *Chem. Eng. J.*, **101** (2004) 225-235.

91. M. Muoth, S. W. Lee, K. Chikkadi, M. Mattmann, T. Helbling, A. Intlekofer and C. Hierold, *Phys. Status Solidi B*, **247** (2010) 2997-3001.

92. M. J. Pellin, J. W. Elam and J. F. Moore, *ECS Transactions*, **11** (2007) 23-28.

93. D. Schmidt, E. Schubert and M. Schubert, *Appl. Phys. Lett.*, **100** (2012) 011912.

94. H. G. Yeo and S. Trolier-McKinstry, *J. Appl. Phys.*, **116** (2014) 014105.

95. M. J. M. Mies, E. Rebrov, J. C. Jansen, M. H. J. M. Croon and J. C. Schouten, *J. Catal.*, **247** (2007) 328-338.

96. V. Rinnerbauer, Y. X. Yeng, W. R. Chan, J. J. Senkevich, J. D. Joannopoulos, M. Soljacic and I. Celanovic, *Opt. Express*, **21** (2013) 11482-11491.

97. L. Paussa, L. Guzman, E. Marin, N. Isomaki and L. Fedrizzi, *Surf. Coat. Technol.*, **206** (2011) 976-980.

98. The University of Maryland Home Page, *Materials Scientists, Conservators Join Forces to Preserve Silver Artifacts and Art.* http://www.mse.umd.edu/news/news_story.php?id=5270 (accessed March 2, 2015).

99. Science Daily Home Page, *Nanotechnology Helps Scientists Keep Silver Shiny*, http://www.newswise.com/articles/nanotechnology-helps-scientists-keep-silver-shiny (accessed May 3, 2015).

100. M. Mäkelä, P. Soininen and S. Sneck, Protective coating of silver, U.S. Patent 8,883,258, November 11, 2014.

101. K. Ali, K.-H. Choi, J. Jo and Y. W. Lee, *Mater. Lett.*, **136** (2014) 90-94.

102. C. Y. Chang and F. Y. Tsai, *J. Mater. Chem.*, **21** (2011) 5710-5715.

103. C. T. Chou, P. W. Yu, M. H. Tseng, C. C. Hsu, J. J. Shyue, C. C. Wang and F. Y. Tsai, *Adv. Mater.*, **25** (2013) 1750-1754.

104. S. H. Jen, B. H. Lee, S. M. George, R. S. McLean and P. F. Carcia, *Appl. Phys. Lett.*, **101** (2012) 234103.

105. J. Meyer, P. Görrn, F. Bertram, S. Hamwi, T. Winkler, H. H. Johannes, T. Weimann, P. Hinze, T. Riedl and W. Kowalsky, *Adv. Mater.*, **21** (2009) 1845-1849.

106. D. C. Miller, R. R. Foster, Y. D. Zhang, S. H. Jen, J. A. Bertrand, Z. X. Lu, D. Seghete, J. L. O'Patchen, R. G. Yang, Y. C. Lee, S. M. George and M. L. Dunn, *J. Appl. Phys.*, **105** (2009) 093527.

107. S. W. Seo, E. Jung, C. Lim, H. Chae and S. M. Cho, *Thin Solid Films*, **520** (2012) 6690-6694.

108. A. Singh, F. Nehm, L. Muller-Meskamp, C. Hossbach, M. Albert, U. Schroeder, K. Leo and T. Mikolajick, *Org. Electron.*, **15** (2014) 2587-2592.

109. W. M. Yun, J. Jang, S. Nam, L. H. Kim, S. J. Seo and C. E. Park, *ACS Appl. Mater. Inter.*, **4** (2012) 3247-3253.

110. S. H. K. Park, J. Oh, C. S. Hwang, J. I. Lee, Y. S. Yang and H. Y. Chu, *Electrochem. Solid-State Lett.*, **8** (2005) H21-H23.

111. H. Chatham, *Surf. Coat. Technol.*, **78** (1996) 1-9.

112. A. Perrotta, E. R. J. van Beekum, G. Aresta, A. Jagia, W. Keuning, R. M. C. M. van de Sanden, E. W. M. M. Kessels and M. Creatore, *Micropor. Mesopor. Mater.*, **188** (2014) 163-171.

113. B. Diaz, J. Swiatowska, V. Maurice, A. Seyeux, B. Normand, E. Härkönen, M. Ritala and P. Marcus, *Electrochim. Acta*, **56** (2011) 10516-10523.

114. E. Marin, L. Guzman, A. Lanzutti, W. Ensinger and L. Fedrizzi, *Thin Solid Films*, **522** (2012) 283-288.

115. E. Marin, A. Lanzutti, L. Guzman and L. Fedrizzi, *J. Coat. Technol. Res.*, **8** (2011) 655-659.

116. E. Marin, A. Lanzutti, L. Guzman and L. Fedrizzi, *Metallogr. Microstr. Anal.*, **2** (2013) 313-320.

117. E. Marin, A. Lanzutti, M. Lekka, L. Guzman, W. Ensinger and L. Fedrizzi, *Surf. Coat. Technol.*, **211** (2012) 84-88.

118. E. Marin, A. Lanzutti, L. Paussa, L. Guzman and L. Fedrizzi, *Mater. Corros.*, **66** (2015) 907-914.

119. E. Marin, A. Lanzutti, L. Guzman and L. Fedrizzi, *J. Coat. Technol. Res.*, **9** (2012) 347-355.

120. P. C. Wang, Y. T. Shih, M. C. Lin, H. C. Lin, M. J. Chen and K. M. Lin, *Thin Solid Films*, **518** (2010) 7501-7504.

121. P. C. Wang, Y. T. Shih, M. C. Lin, H. C. Lin, M. J. Chen and K. M. Lin, *Surf. Coat. Technol.*, **204** (2010) 3707-3712.

122. Z. Chai, J. Li, X. Lu and D. He, *RCS Adv.*, **4** (2014) 39365-39371.

123. Z. Chai, Y. Liu, J. Li, X. Lu and D. He, *RCS Adv.*, **4** (2014) 50503-50509.

124. S. D. Standridge, G. C. Schatz and J. T. Hupp, *Langmuir*, **25** (2009) 2596-2600.

125. S. D. Standridge, G. C. Schatz and J. T. Hupp, *J. Am. Chem. Soc.*, **131** (2009) 8407-8409.

126. A. C. Alba-Rubio, B. J. O'Neill, F. Y. Shi, C. Akatay, C. Canlas, T. Li, R. Winans, J. W. Elam, E. A. Stach, P. M. Voyles and J. A. Dumesic, *ACS Catal.*, **4** (2014) 1554-1557.

127. J. C. Lee, D. H. K. Jackson, T. Li, R. E. Winans, J. A. Dumesic, T. F. Kuech and G. W. Huber, *Energ. Environ. Sci.*, **7** (2014) 1657-1660.

128. B. J. O'Neill, D. H. K. Jackson, A. J. Crisci, C. A. Farberow, F. Y. Shi, A. C. Alba-Rubio, J. L. Lu, P. J. Dietrich, X. K. Gu, C. L. Marshall, P. C. Stair, J. W. Elam, J. T. Miller, F. H. Ribeiro, P. M. Voyles, J. Greeley, M. Mavrikakis, S. L. Scott, T. F. Kuech and J. A. Dumesic, *Angew. Chem. Int. Edit.*, **52** (2013) 13808-13812.

129. B. J. O'Neill, C. Sener, D. H. K. Jackson, T. F. Kuech and J. A. Dumesic, *ChemSusChem*, **7** (2014) 3247-3251.

130. C. C. Kei, Y. S. Yu, J. Racek, D. Vokoun and P. Sittner, *J. Mater. Eng. Perform.*, **23** (2014) 2641-2649.

131. M. Schindler, S. K. Kim, C. S. Hwang, C. Schindler, A. Offenhausser and S. Ingebrandt, *Phys. Status Solidi R*, **2** (2008) 4-6.

132. A. M. Slaney, V. A. Wright, P. J. Meloncelli, K. D. Harris, L. J. West, T. L. Lowary and J. M. Buriak, *ACS Appl. Mater. Inter.*, **3** (2011) 1601-1612.

133. S. Emaminejad, M. Javanmard, R. W. Dutton and R. W. Davis, *Anal. Chem.*, **84** (2012) 10793-10801.

134. S. Emaminejad, M. Javanmard, R. W. Dutton and R. W. Davis, *ECS Transactions*, **58** (2013) 67-72.

135. S. Emaminejad, M. Javanmard, C. Gupta, R. W. Dutton, R. W. Davis and R. T. Howe, 2013 Transducers & Eurosensors XXVII: The 17th International Conference on Solid-State Sensors, Actuators and Microsystems, Barcelona, Spain, June 16-20, 2013, IEEE: Barcelona, 2013.

136. M. Fedel, C. Zanella, S. Rossi and F. Deflorian, *Solar. Energy*, **101** (2014) 167-175.

137. Y. P. Hsieh, M. Hofmann, K. W. Chang, J. G. Jhu, Y. Y. Li, K. Y. Chen, C. C. Yang, W. S. Chang and L. C. Chen, *ACS Nano*, **8** (2014) 443-448.

138. E. Marin, L. Guzman, A. Lanzutti, L. Fedrizzi and M. Saikkonen, *Electrochem. Commun.*, **11** (2009) 2060-2063.

139. C. X. Shan, X. Hou, K. L. Choy and P. Choquet, *Surf. Coat. Technol.*, **202** (2008) 2147-2151.

140. P. C. Wang, T. C. Cheng, H. C. Lin, M. J. Chen, K. M. Lin and M. T. Yeh, *Appl. Surf. Sci.*, **270** (2013) 452-456.

141. Z. H. Chen, Y. Qin, K. Amine and Y. K. Sun, *J. Mater. Chem.*, 2010, **20**, 7606-7612.

142. A. Mauger and C. Julien, *Ionics*, **20** (2014) 751-787.

143. A. Melendez-Ceballos, V. Albin, S. M. Fernandez-Valverde, A. Ringuede and M. Cassir, *Electrochim. Acta*, **140** (2014) 174-181.

144. A. Melendez-Ceballos, V. Albin, A. Ringuede, S. M. Fernandez-Valverde and M. Cassir, *Int. J. Hydrogen Energy*, **39** (2014) 12233-12241.

145. A. Melendez-Ceballos, S. M. Fernandez-Valverde, C. Barrera-Diaz, V. Albin, V. Lair, A. Ringuede and M. Cassir, *Int. J. Hydrogen Energy*, **38** (2013) 13443-13452.

146. J. Q. Zhao and Y. Wang, *J. Solid State Electr.*, **17** (2013) 1049-1058.

147. Y. W. Chen, J. D. Prange, S. Duhnen, Y. Park, M. Gunji, C. E. D. Chidsey and P. C. McIntyre, *Nat. Mater.*, **10** (2011) 539-544.

148. S. Hu, M. R. Shaner, J. A. Beardslee, M. Lichterman, B. S. Brunschwig and N. S. Lewis, *Science*, **344** (2014) 1005-1009.

149. A. Paracchino, V. Laporte, K. Sivula, M. Gratzel and E. Thimsen, *Nat. Mater.*, **10** (2011) 456-461.

150. C. R. Ottermann, K. Bange, W. Wagner, M. Laube and F. Rauch, *Surf. Inter. Anal.*, **19** (1992) 435-438.

151. K. Kukli, J. Ihanus, M. Ritala and M. Leskelä, *J. Electrochem. Soc.*, **144** (1997) 300-306.

152. I. Jogi, K. Kukli, M. Kemell, M. Ritala and M. Leskelä, *J. Appl. Phys.*, **102** (2007) 114114.

153. W. Tato and D. Landolt, *J. Electrochem. Soc.*, **145** (1998) 4173-4181.

154. M. Fenker, M. Balzer and H. Kappl, *Surf. Coat. Technol.*, **257** (2014) 182-205.

155. J. S. Bunch, S. S. Verbridge, J. S. Alden, A. M. van der Zande, J. M. Parpia, H. G. Craighead and P. L. McEuen, *Nano Lett.*, **8** (2008) 2458-2462.

156. S. S. Chen, L. Brown, M. Levendorf, W. W. Cai, S. Y. Ju, J. Edgeworth, X. S. Li, C. W. Magnuson, A. Velamakanni, R. D. Piner, J. Y. Kang, J. Park and R. S. Ruoff, *ACS Nano*, **5** (2011) 1321-1327.

157. Y. A. Ono, *Electroluminescent Displays*, Series on Information Display; World Scientific: Singapore, Japan, 1995; Vol. 1.

158. P. D. Rack and P. H. Holloway, *Mat. Sci. Eng. R*, **21** (1998) 171-219.

159. A. E. Kaloyeros and E. Eisenbraun, *Annu. Rev. Mater. Sci.*, **30** (2000) 363-385.

160. H. Kim, *J. Vac. Sci. Technol. B*, **21** (2003) 2231-2261.

161. J. F. M. Oudenhoven, L. Baggetto and P. H. L. Notten, *Adv. Energy Mater.*, **1** (2011) 10-33.

162. D. Bae, S. Kwon, J. Oh, W. K. Kim and H. Park, *Renew. Energ.*, **55** (2013) 62-68.

163. H. Park, S. C. Kim, H. C. Bae, T. Cheon, S. H. Kim and W. K. Kim, *Mol. Cryst. Liq. Cryst.*, **551** (2011) 147-153.

164. H. Antson, M. Grasserbauer, M. Hamilo, L. Hiltunen, T. Koskinen, M. Leskelä, L. Niinistö, G. Stingeder and M. Tammenmaa, *Fresenius Z. Anal. Chem.*, **322** (1985) 175-180.

165. P. Cogez, M. Graef, B. Huizing, R. Mahnkopf, H. Ishiuchi, N. Ikumi, S. Choi, J. H. Choi, C. H. Diaz, Y. C. See, P. Gargini, T. Kingscott and I. Steff, *The 2013 International Technology Roadmap for Semiconductors (ITRS)*, http://www.itrs.net/home.html (accessed February 11, 2015).

166. K. E. Elers, V. Saanila, P. J. Soininen, W. M. Li, J. T. Kostamo, S. Haukka, J. Juhanoja and W. F. A. Besling, *Chem. Vapor Deposition*, **8** (2002) 149-153.

167. Q. Xie, J. Musschoot, C. Detavernier, D. Deduytsche, R. L. Van Meirhaeghe, S. Van den Berghe, Y. L. Jiang, G. P. Ru, B. Z. Li and X. P. Qu, *Microelectron. Eng.*, **85** (2008) 2059-2063.

168. T. E. Hong, T. H. Kim, J. H. Jung, S. H. Kim and H. Kim, *J. Am. Ceram. Soc.*, **97** (2014) 127-134.

169. S. H. Kim, S. S. Oh, H. M. Kim, D. H. Kang, K. B. Kim, W. M. Li, S. Haukka and M. Tuominen, *J. Electrochem. Soc.*, **151** (2004) C272-C282.

170. Q. Xie, D. Deduytsche, J. Musschoot, R. L. Van Meirhaeghe, C. Detavernier, S. F. Ding and X. P. Qu, *Microelectron. Eng.*, **88** (2011) 646-650.

171. C. Hossbach, S. Teichert, J. Thomas, L. Wilde, H. Wojcik, D. Schmidt, B. Adolphi, M. Bertram, U. Muhle, M. Albert, S. Menzel, B. Hintze and J. W. Bartha, *J. Electrochem. Soc.*, **156** (2009) H852-H859.

172. S. H. Kim, S. S. Oh, K. B. Kim, D. H. Kang, W. M. Li, S. Haukka and M. Tuominen, *Appl. Phys. Lett.*, **82** (2003) 4486-4488.

173. K. E. Elers, V. Saanila, W. M. Li, P. J. Soininen, J. T. Kostamo, S. Haukka, J. Juhanoja and W. F. A. Besling, *Thin Solid Films*, **434** (2003) 94-99.

174. P. Alen, M. Vehkamaki, M. Ritala and M. Leskelä, *J. Electrochem. Soc.*, **153** (2006) G304-G308.

175. P. Majumder, R. Katamreddy and C. Takoudis, *J. Cryst. Growth*, **309** (2007) 12-17.

176. P. Majumder, R. Katamreddy and C. Takoudis, *Electrochem. Solid-State Lett.*, **10** (2007) H291-H295.

177. H. Wojcik, U. Merkel, A. Jahn, K. Richter, M. Junige, C. Klein, J. Gluch, M. Albert, F. Munnik, C. Wenzel and J. W. Bartha, *Microelectron. Eng.*, **88** (2011) 641-645.

178. D. Greenslit, S. Kumar, T. Chakraborty and E. Eisenbraun, *ECS Transactions*, **13** (2008) 63-70.

179. T. E. Hong, T. Cheon, S. H. Kim, J. K. Kim, Y. B. Park, O. J. Kwon, M. J. Kim and J. J. Kim, *J. Alloy Compd.*, **580** (2013) 72-81.

180. S. H. Kim, H. T. Kim, S. S. Yim, D. J. Lee, K. S. Kim, H. M. Kim, K. B. Kim and H. Sohn, *J. Electrochem. Soc.*, **155** (2008) H589-H594.

181. S. W. Kim, S. H. Kwon, S. J. Jeong and S. W. Kang, *J. Electrochem. Soc.*, **155** (2008) H885-H888.

182. S. Kumar, D. Greenslit, T. Chakraborty and E. T. Eisenbraun, *J. Vac. Sci. Technol. A*, **27** (2009) 572-576.

183. S. H. Kwon, O. K. Kwon, J. S. Min and S. W. Kang, *J. Electrochem. Soc.*, **153** (2006) G578-G581.

184. L. Baggetto, H. C. M. Knoops, R. A. H. Niessen, W. M. M. Kessels and P. H. L. Notten, *J. Mater. Chem.*, **20** (2010) 3703-3708.

185. L. Baggetto, J. F. M. Oudenhoven, T. van Dongen, J. H. Klootwijk, M. Mulder, R. A. H. Niessen, M. H. J. M. de Croon and P. H. L. Notten, *J. Power Sources*, **189** (2009) 402-410.

186. H. C. M. Knoops, L. Baggetto, E. Langereis, M. C. M. Van de Sanden, J. H. Klootwijk, F. Roozeboom, R. A. H. Niessen, P. H. L. Notten and W. M. M. Kessels, *ECS Transactions*, **11** (2007) 45-54.

187. H. C. M. Knoops, M. E. Donders, L. Baggetto, M. C. M. van de Sanden, P. H. L. Notten and W. M. M. Kessels, *ECS Transactions*, **25** (2009) 333-344.

188. F. Kessler and D. Rudmann, *Solar Energy*, **77** (2004) 685-695.

189. R. Wuerz, A. Eicke, M. Frankenfeld, F. Kessler, M. Powalla, P. Rogin and O. Yazdani-Assl, *Thin Solid Films*, **517** (2009) 2415-2418.

190. M. Kariniemi, J. Niinisto, M. Vehkamaki, M. Kemell, M. Ritala, M. Leskela and M. Putkonen, *J. Vac. Sci. Technol. A*, **30** (2012) 01A115.

191. C. E. Ramberg, E. Blanquet, M. Pons, C. Bernard and R. Madar, *Microelectron. Eng.*, **50** (2000) 357-368.

192. *CRC Materials Science and Engineering Handbook,* 3rd edn.; J. F. Shackelford and W. Alexander, Eds.; CRC Press: Boca Raton, FL, 2001.

193. T. Cheon, S. H. Choi, S. H. Kim and D. H. Kang, *Electrochem. Solid-State Lett.*, **14** (2011) D57-D61.

194. M. Kariniemi, J. Niinistö, T. Hatanpaa, M. Kemell, T. Sajavaara, M. Ritala and M. Leskelä, *Chem. Mater.*, **23** (2011) 2901-2907.

195. B. Diaz, J. Swiatowska, V. Maurice, M. Pisarek, A. Seyeux, S. Zanna, S. Tervakangas, J. Kolehmainen and P. Marcus, *Surf. Coat. Technol.*, **206** (2012) 3903-3910.

196. M. Ylilammi and T. Ranta-aho, *Thin Solid Films*, **232** (1993) 56-62.

197. T. J. Lin, J. A. Antonelli, D. J. Yang, H. K. Yasuda and F. T. Wang, *Prog. Org. Coat.*, **31** (1997) 351-361.

198. M. Mozetic, *Vacuum*, **61** (2001) 367-371.

199. H. Steffen, J. Schwarz, H. Kersten, J. F. Behnke and C. Eggs, *Thin Solid Films*, **283** (1996) 158-164.

200. K. Kukli, M. Ritala and M. Leskelä, *J. Electrochem. Soc.*, **142** (1995) 1670-1675.

201. G. S. Frankel, *J. Electrochem. Soc.*, **145** (1998) 2186-2198.

202. P. Marcus, V. Maurice and H. H. Strehblow, *Corros. Sci.*, **50** (2008) 2698-2704.

203. A. Bonnel, F. Dabosi, C. Deslouis, M. Duprat, M. Keddam and B. Tribollet, *J. Electrochem. Soc.*, **130** (1983) 753-761.

204. I. Epelboin, M. Keddam and J. C. Lestrade, *Farad. Discuss.*, **56** (1973) 264-275.

205. P. Li, T. C. Tan and J. Y. Lee, *Corros. Sci.*, **38** (1996) 1935-1955.

206. F. Wenger, S. Cheriet, B. Talhi and J. Galland, *Corros. Sci.*, **39** (1997) 1239-1252.

207. A. M. Belu, D. J. Graham and D. G. Castner, *Biomaterials*, **24** (2003) 3635-3653.

208. I. G. Brown, *Annu. Rev. Mater. Sci.*, **28** (1998) 243-269.

209. P. J. Kelly and R. D. Arnell, *Vacuum*, **56** (2000) 159-172.

210. W. D. Sproul, *Surf. Coat. Technol.*, **81** (1996) 1-7.

211. M. Fulem, K. Ruzicka, V. Ruzicka, E. Hulicius, T. Simecek, K. Melichar, J. Pangrac, S. A. Rushworth and L. M. Smith, *J. Cryst. Growth*, **248** (2003) 99-107.

212. T. Li, W.-W. Zhuang, S. T. Hsu, MOCVD precursors in mixed solvents. U.S. Patent 6,503,314, June 7, 2003.

213. J. Creus, H. Mazille and H. Idrissi, *Surf. Coat. Technol.*, **130** (2000) 224-232.

214. C. Mendibide, P. Steyer and J. P. Millet, *Surf. Coat. Technol.*, **200** (2005) 109-112.